NEOHELOS STIRTONI, A NEW SPECIES OF ZYGOMATURINAE (DIPROTODONTA: MARSUPIALIA) FROM THE MID-TERTIARY OF THE NORTHERN TERRITORY, AUSTRALIA

Peter Murray, Dirk Megirian, Thomas Rich, Michael Plane and Patricia Vickers-Rich

The abundanee and exeellent preservation of the Bullock Creek Local Fauna *Neohelos stirtoni* n. sp. material provides an opportunity to deseribe a member of the genus in greater detail than previously possible, as no other named or unnamed speeies of the genus is so completely represented. *Neohelos stirtoni* is an excellent structural intermediate between the most plesiomorphic mid-Tertiary zygomaturines and the late Miocene–early Pliocene genus *Kolopsis*. This provides useful insights for interpretation of highly derived anatomieal features of late Miocene–Pleistocene *Zygomaturus* speeies, and for identifying those structures potentially useful for stage-of-evolution biochronology.

Keywords: Zygomaturinae, Miocene, Australia morphology, variability, new genus, new speeies.

NEOHELOS Stirton, 1967a, was deseribed from five isolated teeth collected in 1962 from the Wipajiri Formation (formerly known as the Wipajiri Channel Sand) on the eastern shore of Lake Ngapakaldi, South Australia. Although the diagnostie speeimen, a permanent upper third premolar (P^3) was missing its anterior half, Stirton inferred the presenee of a parastyle on the type and then only known speeies, *Neohelos tirarensis*, from the basie similarity of its posterior half to those of complete specimens belonging to the diprotodontid genera *Plaisiodon* Woodburne, 1967, *Kolopsis* Woodburne, 1967, *Kolopsoides* Plane, 1967, and *Zygomaturus* Owen, 1859.

Stirton, Woodburne and Plane (1967) went on to analyse a representative collection of diprotodontids from all of the Australian and New Guinean localities known at that time, resulting in the formulation of the basie outline of diprotodontid phylogeny in current use. While they were unable to provide any details about the overall appearance of *Neohelos tirarensis*, their 'stage-of-evolution' analysis of the morphology of the cheek teeth of the various diprotodontid species established the phylogenetie position of *Neohelos* within the subfamily Zygomaturinae, newly erected by the authors to aecommodate the genera possessing a large parastyle and posterolingual cusp or hypoeone on the P^3.

The zygomaturines thus became established as one of the most useful lineages for stage-of-evolution correlation of fossiliferous deposits in Australia. In 1967 *Neohelos* fossils represented the oldest and most structurally primitive forms within the subfamily. The generic name *Neohelos* is derived from Greek equivalents meaning 'new' (*neo*) + 'wart' (*helos*), referring to the presenee of a hypoeone on the P^3, speeifically alluding to the evolutionary appearanee of the structure. The remaining genera of diprotodontids that charaeteristically laeked a parastyle and a hypoeone were assigned to either the Diprotodontinae (speeies with lophodont P^3 and divided parametaeone) or the Nototheriinae (speeies with simple, bieuspid P^3 and an undivided parametaeone).

The only subsequent change in the elassifieation of the diprotodontids proposed by Stirton et al. (1967) has been the inelusion of the nototheres with the Diprotodontinae by Archer (1977). Reeent work on the Diprotodontidae has eoneentrated on filling in the details of the established higher systematie construet. Although several new diprotodontid genera and speeies (some yet to be named) have been found sinee Stirton et al. (1967) (i.e. Rieh et al. 1978, Flannery & Plane 1986, Murray 1990a-b, Flannery 1992, Hand et al. 1993, Murray et al. 1993, Blaek 1997) the genus *Neohelos*, whieh was originally eentral to our understanding of the phylogeny of the Zygomaturinae, has remained more or less in obseurity until now.

The initial reason for the laek of additional doeumentation for *Neohelos* was the rarity and fragmentary condition of *Neohelos* material from the type loeality. In 1966, not long before Stirton et al. (1967) went to print, a new source of *Neohelos* fossil material was diseovered at Bullock Creek, Northern Territory by C. Gatehouse (Plane & Gatehouse 1968). The newly found *Neohelos* material fully eonfirmed Stirton's diagnosis, whieh he was unable to appreeiate due to his death in 1966. M. Plane, then of the Bureau of Mineral Resources, prepared a draft manuscript deseribing the Bullock Creek *Neohelos* as a new speeies named in honour of his colleague and mentor.

In addition to the type speeies *Neohelos tirarensis* Stirton (1967) and *Neohelos stirtoni* n. sp., two other speeies of *Neohelos* are deseribed in *Museums and Art Galleries of the Northern Territory Research Report 6*. This unpublished report, 'Morphology, systematies and evolution of the marsupial genus *Neohelos* Stirton (Diprotodontidae, Zygomaturinae)' is the body of a manuseript submitted for publieation in 1995. Subsequent to peer review, certain aspeets of the paper had already been published elsewhere and at the point of going to press, some eo-authors felt that signifieant parts of the manuseript had been largely superseded. Rather than reeireulate the manuseript for another lengthy round of editorial revision (a process that had already spanned the greater part of a deeade), we deeided to forgo journal publieation and simply make the original manuseript

available on request from the Northern Territory Museum and the Queen Victoria Museum and Art Gallery.

This unpublished report examines the geology, systematics, phylogeny, and biochronology of *Neohelos*, and includes statistical and phylogenetic appendices. The description of *Neohelos stirtoni* n. sp. published here is an extract from the original manuscript devoid of references to material from other localities over which dissenting co-authors have priority.

Neohelos is the most common element among the taxa contained in the Bullock Creek Local Fauna (Murray & Megirian 1992), and is now represented by hundreds of specimens including complete crania, dentaries and most of the postcranial skeleton. The Bullock Creek form provides many anatomical details necessary for the understanding of the evolution of the group, and because of its abundance, provides a rare opportunity for the assessment of the individual variability within a fossil population.

Following Luckett (1993), the molars are numbered M1-4. The anatomical terminology follows the appendix in Stirton, Woodburne and Plane (1967). Additional terms are listed in the key to abbreviations (appendix).

PHYSICAL AND GEOLOGICAL SETTING

The Camfield Beds, which crop out along the Bullock Creek and Cattle Creek tributaries of the Camfield River consist of calcareous siltstone, sandy siltstones, and silty sandstones; conglomeratic limestone, calcimudstone, chalcedonic limestone and gypsiferous siltstone (fig. 1). Vertebrate fossils are concentrated in the limestone facies which Murray and Megirian (1992) interpret to have been deposited in fluviatile channels and associated billabongs: Randal and Brown (1967) postulated a normally saline lacustrine, lagoonal or estuarine environment of deposition, occasionally flooded by freshwater inflow.

SYSTEMATICS

Superorder MARSUPIALIA Illiger, 1811
Order DIPROTODONTIA Owen, 1866
Family DIPROTODONTIDAE Gill, 1872
Subfamily ZYGOMATURINAE Stirton, Woodburne and Plane, 1967

The extinct Family Diprotodontidae to which *Neohelos* belongs, is a diverse group of vombatomorphian marsupials united by the possession of relatively simple bilophodont molars, a transversely lobate, minimally bicuspid, oval to triangular P^3 and three upper and one lower incisor per quadrant (fig. 2). Although subfamilial divisions of the Diprotodontidae were proposed in the late 1800s, the affinities of the various genera remained ambiguous until Stirton, Woodburne and Plane (1967) revised the family, recognising the Subfamily Zygomaturinae as distinct from two newly ranked subfamilies, the Nototheriinae and the Diprotodontinae.

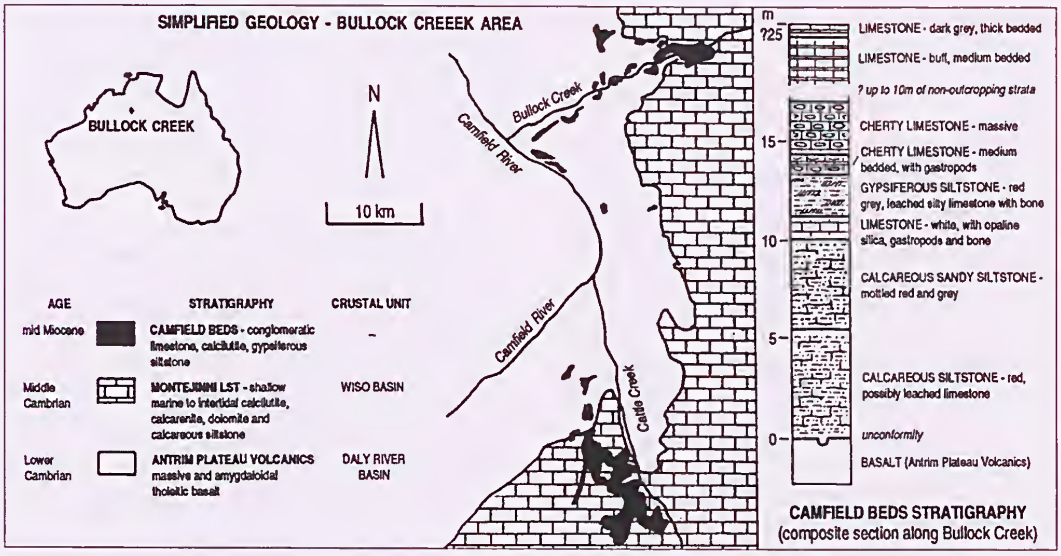

Figure 1. Bullock Creek area, Northern Territory. Camfield Beds contain *N. stirtoni* only. (Bullock Creek geology after Murray and Megirian 1992. Fig. 1; composite stratigraphic section along Bullock Creek after Randal and Brown 1967, 47).

Stirton et al. (1967) considered the Nototheriinae to represent an intercalary lineage that gave rise to the Zygomaturinae through the addition of a large conical parastyle to the P^3. The Diprotodontinae were distinguished from the Nototheriinae by the differentiation of the paracone and metacone from a single large buccal cusp on the P^3, giving rise to a horse-shoe-shaped lophodont pattern when the crown was worn. Because the P^3 of *Euryzygoma dunense*, a 'notothere', was structurally intermediate between the diprotodontine, *Diprotodon* and other nototheriines, Archer (1977) recommended suppression of the Subfamily Nototheriinae.

Other than the inclusion of the Nototheriinae within the Diprotodontinae, Stirton et al.'s original diagnoses remain valid; but to which we append the following observations. Unknown to Stirton at the time, an epitympanic fenestra in the superficies meatus area similar to that in *Ngapkaldia tedfordi* Stirton is present among the more primitive genera of both subfamilies. The structure is diminished and eventually lost in the later, more derived species of which he was aware and upon which he based his observation. In addition to the presence of a parastyle on the P^3 (fig. 3) the Zygomaturinae are also distinguished apomorphically from the Diprotodontinae by the development of the ventral surface of the tympanic process within the alisphenoid. In the Diprotodontinae, the tympanic process is formed entirely within the squamosal, as in the Vombatidae (fig. 4).

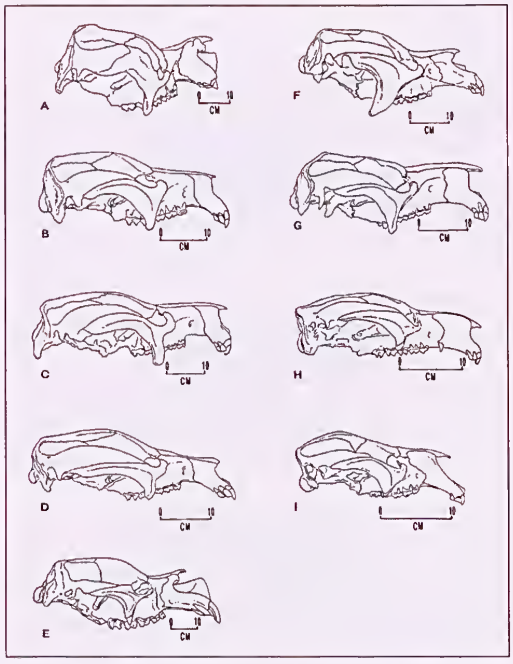

Figure 2. Outline drawings of representative diprotodontid marsupials (restored) for comparison of overall form; **A**, *Zygomaturus trilobus*; **B**, *Kolopsis torus*; **C**, *Plaisodon centralis*; **D**, *Alkwertatherium webbi*; **E**, *Diprotodon* sp.; **F**, *Euryzygoma dunense*; **G**, *Pyramios alcootense*; **H**, *Silvabestius johnnilandi*; **I**, *Ngapakaldia tedfordi*; scale bars=10 cm. **G**, after photograph in Archer and Bartholomai (1978); **F**, after a photograph (T. Rich); **H**, after photograph in Archer et al. (1991, p. 217).

Stirton et al. (1967) described the primary distinguishing feature of the Subfamily Zygomaturinae as a large, complex, bulbous-outlined P^3 with four or five cusps. A three-cusped zygomaturine genus, *Alkwertatherium webbi* Murray (1990a) is now known, as anticipated by the Stirton et al. (1967) reconstructed structural succession based on the initial development of a parastyle, then a hypocone (*Neohelos, Plaisiodon*), followed by the division of the parametacone into a distinct paracone and a metacone (*Kolopsis, Kolopsoides, Zygomaturus*) (fig. 5). The division or twinning of the parametacone arose independently in the Palorchestinae (*Palorchestes azeal*) and in the Diprotodontinae (some individuals of *Euryzygoma* and *Diprotodon* spp.).

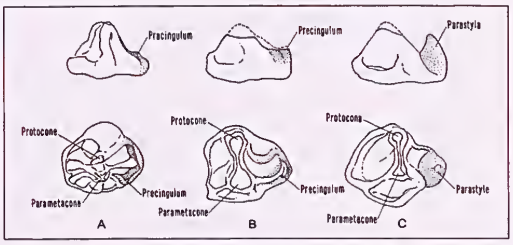

Figure 3. Structural series depicting stages of P^3 evolution leading to the Zygomaturinae; **A**, *Palorchestes azeal* (Palorchestinae); **B**, *Pyramios alcootense* (Diprotodontinae); **C**, *Alkwertatherium webbi* (Zygomaturinae).

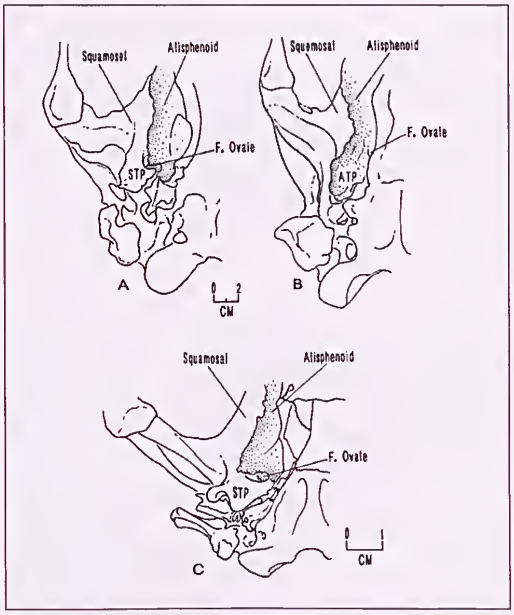

Figure 4. Comparison of tympanic wing structures in **A**, *Pyramios alcootense* (Diprotodontinae); **B**, *Alkwertatherium webbi* (Zygomaturinae); **C**, *Vombatus ursinus* (Vombatidae).

It is plainly evident from the morphology of the P^3 that *Neohelos* is structurally intermediate between the simpler, somewhat diprotodontine-like three-cusped condition in *Alkwertatherium* and the five-cusped condition of *Zygomaturus*. However, the actual phylogenetic position of *Neohelos* is not quite as transparent as its structure suggests. Two other genera with four-cusped P^3's are also present in the form of *Plaisiodon centralis* Woodburne 1967a and *Nimbadon* spp. (Hand et al. 1993). Moreover, it is probable that the division of the parametacone into two distinct cusps occurred more than once within the Zygomaturinae as indicated by *Kolopsoides cultridens* Plane 1967, which shows closer affinity to *Plaisiodon* than to either *Neohelos* or *Kolopsis* (Murray 1990a, 1992).

Neohelos Stirton, 1967a

Type species. Neohelos tirarensis, Stirton, 1967a

Referred species. Neohelos stirtoni n. sp.

Revised generic diagnosis. Diprotodontids possessing a four-cusped P^3 with a distinct, isolated parastyle and hypocone; canines vestigial to absent. Trapezoidal M^1 with large parastyle and metastyle, crown approximately the same length as P^3: upper molars with wide interproximal contacts. Lower incisor with distinct ventrolabial longitudinal groove; M^1, paralophid strong; lower molars with weak metalophids and low, wide transverse valleys. All other zygomaturine genera are distinguished from *Neohelos* by the following character differences; *Silvabestius* differs in having a feeble P^3 parastyle and in lacking a hypocone; *Alkwertatherium* differs in lacking a hypocone on P^3; *Nimbadon* differs in that the M^1 stylar corners are small and the interproximal contacts of molars are rounded and narrow; *Kolopsoides* differs in that the parastyle of P^3 is connected to the paracone by a high crest, the parametacone is divided and the hypocone is larger than the protocone; *Plaisiodon* differs in the absence of an anterolabial crest on the parastyle and absence of a mesostyle on P^3; *Kolopsis* differs in having fully differentiated paracone and metacone on P^3 and lacks a ventrolabial groove on I_1; the genera *Zygomaturus*, *Maokapia* (and possibly *Hulitherium*, in which only a fragment of its P^3 is known) differ in that the P^3 parametacone is fully divided, the P^3 is much smaller than M^1 and the parastyle and metastyle of M^1 are reduced (Murray 1992), (figs 6, 7; table 1).

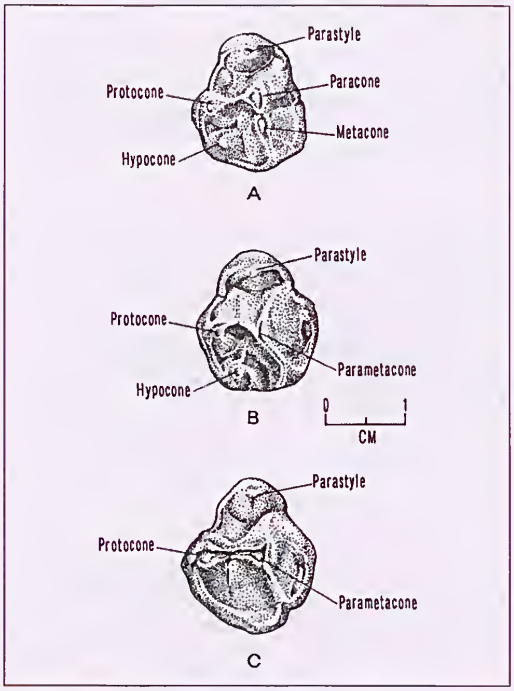

Figure 5. Elaboration of P^3 crown morphology in Zygomaturinae; **A**, *Kolopsis torus*; **B**, *Neohelos stirtoni* n. sp.; **C**, *Alkwertatherium webbi*. These examples show the structural succession for zygomaturines proposed by Stirton, Woodburne and Plane (1967) originating with a three-cusped form (*Alkwertatherium*) and culminating in a five-cusped form (*Kolopsis, Zygomaturus*).

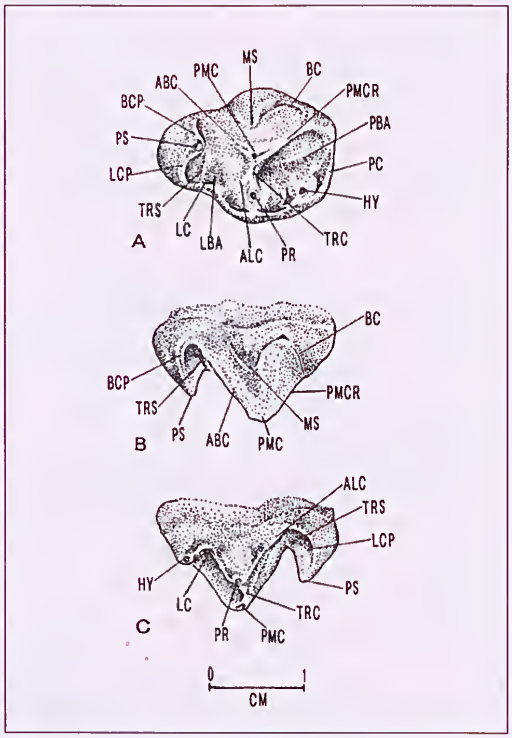

Figure 6. Left upper third premolar (P^3) of *Neohelos stirtoni* n. sp. (NTM P8695-141, Blast Site, Bullock Creek) showing typical crown morphology; **A**, occlusal aspect, **B**, labial aspect, **C**, lingual aspect.

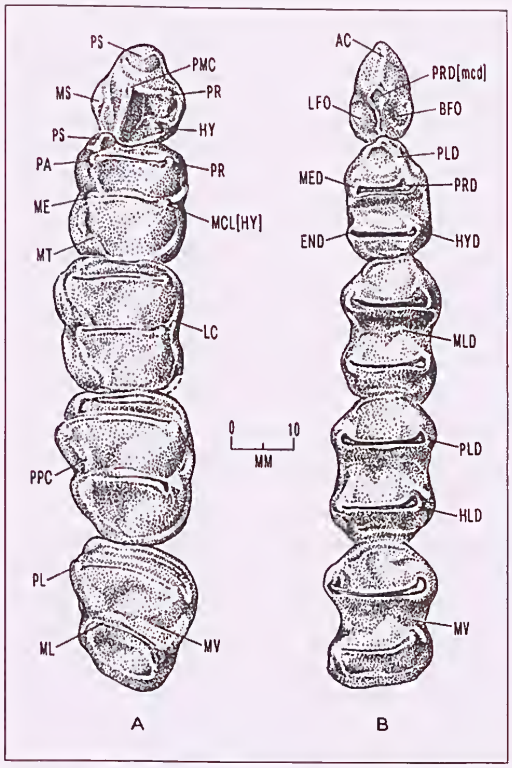

Figure 7. Upper, **A**, and lower, **B**, cheek-tooth rows of *Neohelos stirtoni* n. sp. (NTM P8551-13), Blast Site, Bullock Creek) exemplifying the basic structure of molar and premolar crowns in the genus. Note the simple, wide lophs, particularly the relatively wide protoloph on M^1; continuous, or nearly so, horizontal lingual cingulae, and wide interproximal contact in the uppers; strong, elongated paralophid on M_1, wide interlophid valleys and simple, nearly transverse lophids of the lowers.

***Neohelos stirtoni* n. sp.**

Holotype. CPC 22200 cranium with complete right and left cheek-tooth rows; parts of the right squamosal, parietal and zygomatic arch, and right and left I^{2-3} are missing (fig. 8).

Type locality and age. Small Hills Locality, 26 km east south-east of Camfield Station Homestead on Bullock Creek, Northern Territory (approximately Latitude 17° 07' S, Longitude 131° 31'E). Tertiary limestones of the Camfield Beds are considered to be mid Miocene on the basis of stage-of-evolution biochronology as discussed below.

Etymology. The late Professor Ruben A. Stirton of the University of California recognised the genus *Neohelos* on the basis of scanty material, at a time when the systematic significance of the dental morphology of diprotodontid marsupials was just beginning to be understood. His paper on *Neohelos tirarensis* was published a year after his death, and sadly he did not live to see the abundant, beautifully preserved material discovered at Bullock Creek in the Northern Territory during 1966 through 1968. This material, which amply justifies his new genus and demonstrates his intuitive skill and flair in suggesting the form that the anterior half of his holotype would have, is here described as a new species in his honour.

Referred specimens and localities. Neohelos stirtoni is known from several localities in the Bullock Creek area in the north-western Northern Territory.

Blast Site, Bullock Creek: CPC 34301, left dentary, P_3–M_{1-3}; CPC 34302, left maxilla, P^3–M^{1-2}; CPC 34300, left dentary, P_3–M_{1-3}; CPC 22189, right dentary, M_{1-2}; CPC 22190, right dentary, P_3–M_{1-4}; CPC 22191, cranium with right and left P^3–M^{1-4}; CPC 22192, crushed cranium with right and left P^3–M^{1-4}; CPC 22193, right half of cranium and maxilla, P^3–M^{1-4}; CPC 22194, right and left premaxilla and maxilla, I^1, P^3; CPC 22188, anterior half of cranium, left and right P^3–M^{1-4}; CPC 22196, edentulous premaxilla; CPC 22199, right dentary, M^{1-4}; CPC 22525, braincase and latex endocast; CPC 22526, cranium with top sheared-off, right and left P^3–M^{1-4}; CPC 22529, right maxilla, M^2; CPC 22530, left dentary, P_3–M_{1-3}; CPC 22537, left dentary, P_3–M_{1-2}; CPC 22539, palate and rostrum, right and left I^1, I^3, P^3–M^{1-4}; CPC 22540, left premaxilla, I^1; CPC 22541, left dentary, M_3; CPC 22542, right dentary, M_{3-4};CPC 22544, palate and posterior half of cranium, right M^{1-4}, left P^3–M^{1-4}; CPC 22545, right dentary, P_3–M_{1-4}; CPC 22546, left dentary, P_3–M_{1-4}; CPC 22549, left dentary, M_{3-4}; CPC 22551, left dentary, P_3–M_{1-4}; CPC 22552, right M^1; CPC 22555, left dentary, M_{2-3}; CPC 22556, right dentary, M_{3-4}; CPC 22557, left maxilla, P^3–M^1; CPC 22987, right maxilla, P^3-M^{1-2}; NMV P179368, right dentary, P_3–M_1; NMV P179862, left dentary, P_3–M_{1-4}; NMV P187283, cranium, left and right P^3–M^{1-4}; NMV P194537, left M^3; NMV P198541, left dentary, M_3; NMV P198542, left dentary, M_{1-4}; NMV P201031, left dentary, M_{3-4}; NTM P862-1, right I^3; NTM P862-6, right dentary, M_{1-4}; NTM P862-25, right I^2; NTM P868-1, right M_4; NTM P868-2, right maxilla, P^3–M^{1-4}; NTM P869-4, right P^3; NTM P8551-13, cranium, left and right P^3–M^{3-4}; NTM P859550, left premaxilla, I^{1-2}; NTM P8610-1, left dentary, P_3–M_{1-4}; NTM P8612-1, left premaxilla, I^1; NTM P8612-3, right P^3; NTM P8619-1, right dentary, M_{1-4}; NTM P8645-1, left I^3; NTM P8675-1, right I^2; NTM P8689, left maxilla, P^3–M^{1-2}; NTM P8690, maxillary palate, left P^3–M^{1-2}, right P^3–M^{1-4}; NTM P8691-1, left I^3; NTM P8691-23, left maxilla, M^{1-2}; NTM P8694-2, right maxilla, P^3–M^{1-4}; NTM P8694-3, left maxilla, orbit, jugal, P^3–M^{1-3}; NTM P8694-43, right I^1; NTM P8695-2, right I^1; NTM P8695-2, right I^3; NTM P8695-4, right dentary, P_3–M_1M_{3-4}; NTM P8695-38, cranium missing left zygomatic arch, left P^3M^{1-4}, right P^3–M^4; NTM P8695-39, left maxilla, P^3–M^{1-3}; NTM P8695-41, left maxilla, P^3-M^{1-2}; NTM P8695-42, left maxilla, M^{1-3}; NTM P8695-43, right maxilla, P^3–M^{1-3}; NTM P8695-44, right maxilla, P^3–M^1; NTM P8695-45, right M^2; NTM P8695-46, right maxilla, P^3–M^{1-2}; NTM

P8695-47, left premaxilla, I^1; NTM P8695-49, juvenile premaxilla, I^1; NTM P8695-51, left and right edentulous premaxillae; NTM P8695-52, left and right premaxillae, I^1; NTM P8695-53, left and right edentulous premaxillae; NTM P8695-61, right P^3; NTM P8695-63, left P^3; NTM P8695-64, right M^2; NTM P8695-67, right dentary, P_3–M_{1-4}; NTM P8695-69, right dentary, P_3–M_{1-2}; NTM P8695-70, right dentary, M_{3-4}; NTM P8695-71, left dentary, P_3–M_{1-3}; NTM P8695-72, left dentary, P_3–M_{1-4}; NTM P8695-73, left dentary, M_{3-4}; NTM P8695-74, left dentary, P_3–M_{1-4}; NTM P8695-76, right P_3; NTM P8695-78, maxilla, M^{3-4}; NTM P8695-141, left P^3; NTM P8695-211, left I_1; NTM P8695-218, right I^2; NTM P8695-221, right I^3; NTM P8695-222, left I^1; NTM P8695-223, left I^1; NTM P8695-224, left I^2; NTM P8695-225, left I^2; NTM P8695-226, left I^3; NTM P8695-269, left edentulous premaxilla; NTM P8695-286, right premaxilla, broken I^1; NTM P8695-, left scapula, left femur, left innominate, left tibia, left epipubic bone; NTM P8695a-e, three right and two left isolated petrosals; NTM P8711-9, left half of anterior part of cranium; NTM P8792-9, right I^3; NTM P8792-15, braincase and latex endocast; NTM P8792-16, edentulous left premaxilla; NTM P8792-17, left dentary, P_3–M_{1-4}; NTM P8792-18, left dentary, M_{2-4}; NTM P8792-19, cranium, left P^3-M^{1-4}, right P^3–M^{1-2}; NTM P8792-20, right M^2; NTM P9295, braincase and cranial base; NTM P87103-20, right M_2; NTM P87103- left ulna. NTM P87104-27, right premaxilla, I^1; NTM P87108-1, cranium missing rostrum, right M^{2-4}, left M^{3-4}; NTM P87108-6 left premaxilla, I^1; NTM P87108-38, left humerus NTM P87108-39, sacrum; NTM P87108-28, right premaxilla, I^1, I^3; NTM P87110, right dentary, P_3–M_{1-3}; NTM P87111-16, left and right premaxillae, I^3; NTM P87113-5, right I^3; NTM P87113-11, left dentary, P_3–M_{1-4}; NTM P87115, right dentary, P_3-M_{1-4}; NTM P87115-8, left maxilla, P^3–M^1; NTM P87115-16, left dentary, P_3–M_{1-4}.

Camp Quarry, Bullock Creek: NMV P187289, right dentary, P_3–M_{1-4}; NMV P187290, left dentary, M_{2-4}; NMV P194538, right maxilla, P^3–M^{1-3} and left P^3–M^1; NMV P194539, left dentary, M_{2-3}; NMV P194541, right M_2; NMV P197896, maxillae, left M^3 and right M^4; NMV P198543, left maxilla, P^3–M^3.

Horseshoe West, Bullock Creek: NMV P179244, right P_3; NMV P179369, left dentary, M_{1-2}; NMV P194364, right maxilla, P^3–M^1; NMV P194530, right maxilla, M^{2-3}; NMV P194532, left maxilla, P^3–M^{1-4}; NMV P194540, left M^3; NMV P194546, right dentary, M_{2-4}; NMV P194547, right M_4; NMV P194548, right maxilla, P^3–M^{1-2}; NMV P194549, right dentary, P_3–M_{1-3}; NMV P194551, right maxilla, P^3–M^1; NMV P194552, left maxilla, P^3–M^1; NMV P194553, left maxilla, P^3–M^1; NMV P194554, right M^1; NMV P194555, left M_3; NMV P194556, left maxilla, P^3–M^1; NMV P194557, right M_3; NMV P194558, left P^3; NMV P194565, right M^3.

Top Site, Bullock Creek: NMV P179106, left P^3; NMV P179159, right P^3; NMV P179857, left dentary, M_{2-4}; NMV P187284, right maxilla, M^{2-4}; NMV P187285, left maxilla, P^3–M^{1-4}; NMV P187286, left maxilla, M_{3-4}; NMV P187287, left maxilla, P^3–M^1; NMV P194533, right M_3; NMV P194534, left M^4; NMV P194535, right M_3; NMV P194536, right M^4; NMV P194544, right M^4; NMV P194545, right P^3; NMV P194559, left M_3; NMV P197892, cranium, left and right P^3–M^{1-4}; NMV P197893, left dentary, M_{1-4}; NMV P197894, left maxilla, M^{1-2}; NMV P197895, right maxilla, M^{2-4}; NMV P201027, right maxilla, M_{2-4}; NMV P201028, left dentary, P_3–M_1; NMV P201029, right dentary, M_4; NMV P201030, left maxilla, M^{2-4}; NMV P205129, left maxilla, M^{2-4}; NMV P205130, right maxilla, M^{2-4}; NMV P205131, right dentary, M_{2-4}; NTM P8662-9, left maxilla, M^{1-2}; NTM P8694-1, rostrum fragment; NTM P8697-1, cranium, left and right P^3–M^{1-2}.

Species diagnosis. Molars larger than *N. tirarensis*; P^3 parametacone cusp blade-like rather than conical or pyramidal; canine absent.

Remarks. Some specimens of *N. stirtoni* are among the best preserved Tertiary vertebrate fossils in Australia (figs 8, 9). Because of the completeness of the material, we have endeavoured to provide as detailed an anatomical study of the species as seems practical within the confines of a predominantly systematic paper. Unfortunately, we have not completed the study of the manus and pes, the addition of which would have considerably improved our restoration of the skeleton (fig. 27).

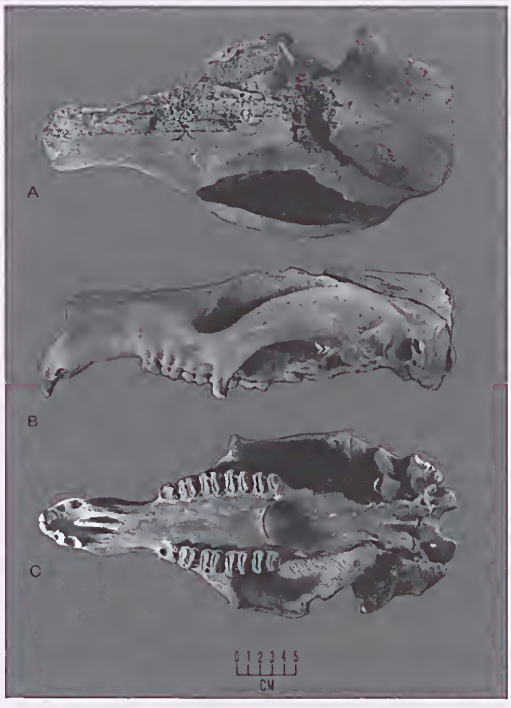

Figure 8. Cranium of *Neohelos stirtoni* n. sp. type (CPC F22200, Blast Site, Bullock Creek); **A**, dorsal aspect; **B**, lateral aspect; **C**, ventral aspect.

Description

Incisors. The labial outline of the upper incisor series is C-shaped or U-shaped with the I^3 alveolus situated posterolateral to the I^2 alveolus (fig. 10). The I^2 and I^3 have a horizontal wear surface while the I^1 is worn on its posterior surface; consequently its tip extends below the occlusal plane of the other two teeth.

I^1. The I^1 was an ever-growing tooth with roots that remained open throughout most, if not all of the animal's lifetime (fig. 11A–C). In a few highly worn examples, the apex of the root is partially closed, presumably indicative of extremely old individuals. The tip of I^1 bears a marked occlusal notch in all but the youngest specimens. Enamel is confined to the anterolateral surface of the tooth and to the distal one-fourth of the tooth in mature individuals. The mesial surface of the tooth is flat, the lateral surface concave and a section drawn midway between the tip and the root opening is D-shaped. A typical I^1 is 14.5 mm wide and 9.0 mm thick. When both first incisors are in place they converge at the tip, both emerging from the premaxilla in a ventromesial direction with a small gap between them.

I^2. I^2 is the least well represented of the incisors in the collection (fig. 11D). Only one specimen of premaxilla retains an I^2 in its socket. The 13.5–13.8 mm wide I^2 crown is about a quarter to a third wider transversely than the I^3. In lateral aspect the crown is an asymmetrical trapezoidal shape with the anterior angle being acute and the posterior angle being obtuse. The pointed anterior margin of the I^2 crown slightly overlaps the posterolateral side of I^1, leaving a triangular gap between the contact and the alveolus above. The lateral surface of the crown is inscribed by one or more longitudinal grooves. The occlusal surface is lozenge-shaped with a slight lingual thickening just behind the midpoint. The entire crown has an enamel perimeter.

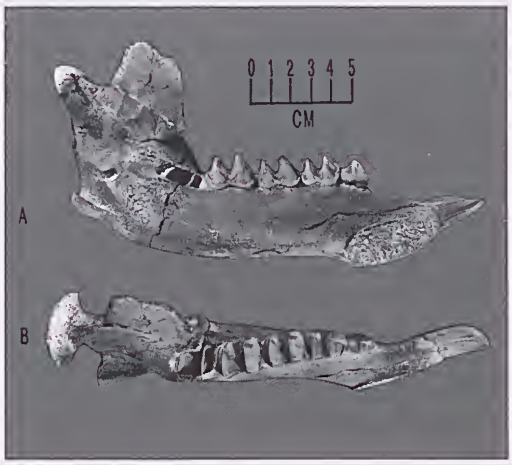

Figure 9. *Neohelos stirtoni* n. sp. juvenile left dentary (CPC F23025 Blast Site, Bullock Creek); **A**, internal aspect; **B**, occlusal (dorsal) aspect.

I^3. The 9.0-10.5 mm wide I^3 crowns have an elongated triangular occlusal surface with the apex directed posterolaterally (fig. 11E). A wide, shallow longitudinal groove divides the lateral surface of the crown into approximate halves. The crown is transversely narrow and tapers rapidly to the tip of the root. Enamel is developed on both labial and lingual surfaces and curves forward onto the anterior surface of the tooth.

I_1. The single paired lower incisors are broadly lanceolate (figs 9A–B, 11F–G). The appression facet indicates that these incisors converge and touch only at their tips. They curve gently upward and forward and bear enamel on the distal third of the tooth. The enamel is mainly confined to the ventrolabial surface but does curve around onto the lower third of the mesial surface near the tip. In little worn specimens, a ridge of dentine parallels the labial curve of the enamel. A deep, longitudinal groove is present on the internal dorsal surface. The ventral margin of the labial side of the crown also has a conspicuous longitudinal groove situated about 2.0 mm to 3.0 mm above a rounded enamel crest (fig. 11F). The lower incisors occlude with all of the upper incisors meeting the posterior surface of I^1 and the horizontal occlusal surfaces of the $I^{2\text{-}3}$. Older individuals developed a marked occlusal notch. The root is ovate to subrectangular in cross-section, with the dorsal surface broader than the ventral. The tooth root does taper, but appears to have remained open, even in old individuals.

Upper cheek teeth. *P^3*. The P^3 is a four-cusped tooth consisting of a protocone, parametacone, parastyle and hypocone (figs 7A, 12A–H; table 2). A mesostyle is developed at the base of the parametacone. The crown is widest across the protocone, parametacone and mesostyle and tapers both anteriorly and posteriorly from this plane. The parametacone is the highest cusp and is distinctly pyramidal in shape. One plane of the pyramid is approximately labial, the anterior plane is transverse, and the posterior plane runs obliquely from the posterolabial corner of the tooth to, or just labial of, the protocone.

The protocone is conical and in unworn specimens has a transverse labial link of variable strength to the base of the parametacone. The parastyle is also conical and is lower than the parametacone and protocone. In some specimens three ridges ascend from the apex: labially, lingually and posteriorly; while in other specimens the labial and lingual ridges become cingulae. In some examples, the posterior ridge links with a ridge which ascends anteriorly from the parametacone. The hypocone is the smallest and lowest cusp, situated approximately midway between the protocone and the back of the tooth. It is conical with well-developed lingual cingulae anterior and posterior to it. In some specimens it is located slightly posterolabial to the protocone.

The labial stylar cusp or mesostyle is variable in its development ranging from a small, sharp conical prominence to a larger, blunt swelling. A posterolabial

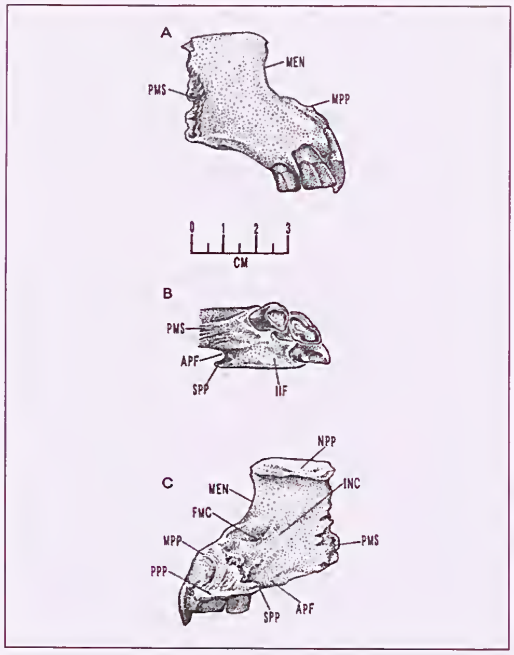

Figure 10. A–C, *Neohelos stirtoni* n. sp. Left premaxilla (NTM P87108-6 Blast Site, Bullock Creek); **A**, lateral aspect; **B**, ventral aspect; **C**, internal aspect.

cingulum is present in all specimens. The development of an anterolabial cingulum appears to be completely random. Lingual cingulae are always present between the bases of the protocone and hypocone. In most cases a posterior cingulum ascends from the posterior base of the hypocone across the back of the tooth and joins the post-parametacrista or posterior shearing ridge.

M¹. The M^1 is slightly longer than it is wide in all specimens (figs 12, 13D–E; table 2). The transverse lophs of both moieties are slightly curved or convex towards the front of the tooth. The convexity of the lophs increase with wear, and in some specimens the depression on the posterior surface of the protoloph form well-defined circular basins in the median valley. The protoloph is transversely narrower than the metaloph and the tooth tapers slightly towards the front. Anterior to the paracone is a strong parastyle, connected to the protoloph by a curved ridge. The parastyle also sends a ridge forward, ascending to the anterior cingulum. When viewed from the labial side of unworn specimens, the parastyle is separated from the protoloph by a deep, narrow commissure, and it is obvious that the parastyle forms a functional shear with the postparametacrista of P^1.

A small metastyle is found on the posterolabial corner of the metaloph. In most specimens it is a small cusp with an anterior and posterior ridge. The front ridge descends to the tip of the metacone while the back ridge rises in a posterolingual direction and continues across the base of the tooth to a lingual position above, and just lingual to

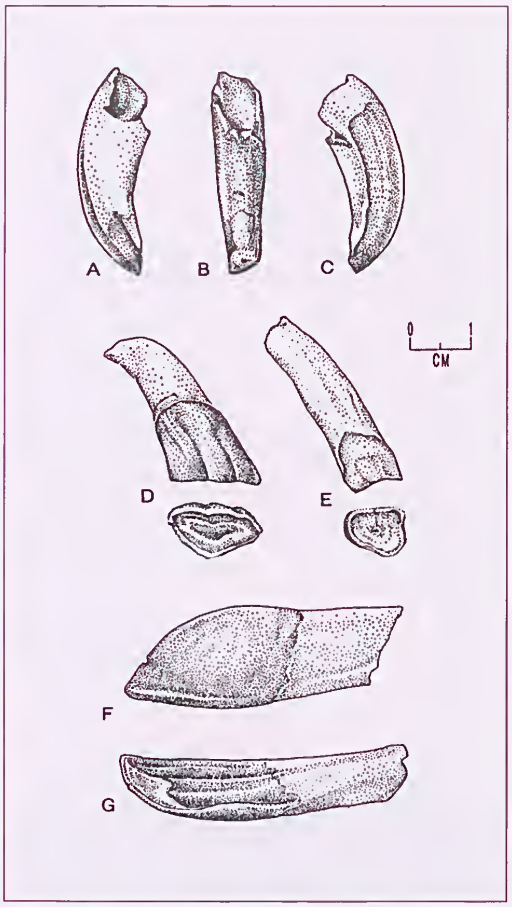

Figure 11. *Neohelos stirtoni* n. sp.; incisors; **A–C**, mesial, distal and labial views, respectively of I^1 (NTM P8695-2 Blast Site, Bullock Creek); **D**, labial and occlusal aspects of right I^2 (NTM P862-25 Blast Site, Bullock Creek); **E**, labial and occlusal aspects of right I^3 (NTM P87113-5 Blast Site, Bullock Creek); **F–G**, labial and dorsal (occlusal) aspects of I_1 (NTM P8695-211 Blast Site, Bullock Creek).

the metaconule. In some cases a secondary cusp is found on the anterior ridge, halfway between the metastyle and the metacone. A weak link ascends from behind the paracone into the median valley where it meets an even weaker ridge ascending forward from a point below and just lingual to the metacone on the anterior face of the metaloph. These weak crests merge just labial to the midline of the loph. A second, weak ridge ascends from the paracone to the labial edge of the median valley. At the lingual end of the transverse valley a cingulum connects the base of the protocone with the base of the metaconule. This is a variable feature, being predominantly developed in specimens with strong ridges up onto the lingual ends of the proto- and metalophs, whereas in others, these ridges are totally absent. If the ridges are present, they are always strongest on the two anteriormost molars.

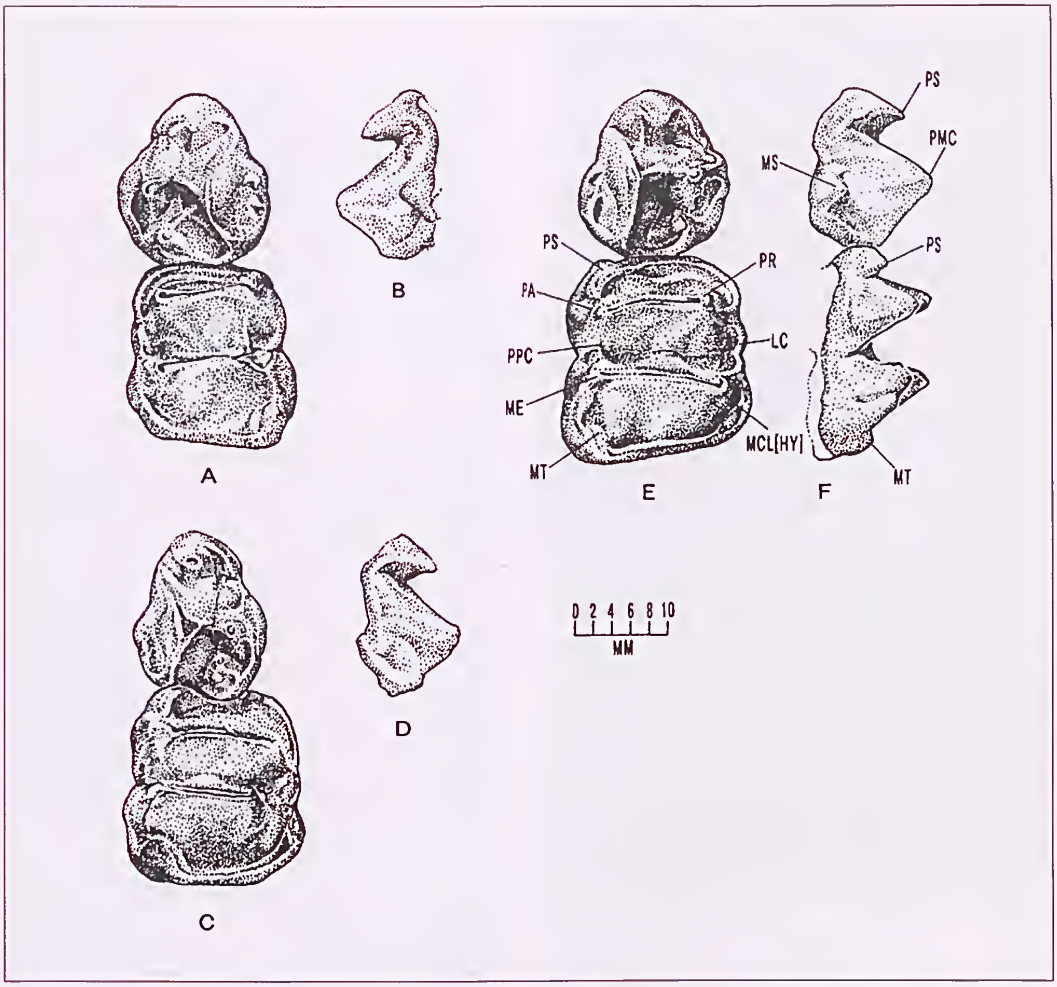

Figure 12. *Neohelos stirtoni* n. sp.; P^3 and M^1 specimens; **A–B**, occlusal and labial aspects of left P^3–M^1 (NTM P8695-41 Blast Site, Bullock Creek); **C–D**, occlusal and labial aspects of right P^3–M^1 (NTM P8695-44 Blast Site, Bullock Creek); **E–F**, occlusal and labial aspects of right P^3–M^1 (NTM P862-2 Blast Site, Bullock Creek).

M^{2-4}. The posterior molars are generally similar to M^1. In M^2, the protoloph is slightly wider than the metaloph, the parastyle is reduced in size and does not have such well developed anterior and posterior ridges, nor does it form a functional shear plane with the posterior ridge on M^1 (fig. 13D–E). The metastyle is considerably reduced as are the ridges in front of, and behind the metacone. In M^{3-4}, the protoloph is considerably wider than the metaloph, and in M^4 the metaloph is lingually offset, with the metaconule directly behind the protocone and the metacone considerably lingual to the paracone. In M^3 the metastyle is very small and lacks an anterior ridge, while in M^4 the metastyle is either completely missing or minute. The posterior cingulum is diminished in M^3 and often only faintly discernible in M^4.

Lower cheek teeth

P_3. The sectorial lower P_3 is oval in occlusal outline and is dominated by the large main cuspid or protoconid (figs 13A–C, 14A–D; table 3). The apex of the protoconid is situated in the center of the crown. In lateral aspect the anterior profile of the crown is convex and the posterior half, which forms a shearing blade, is concave. A sharp anterior blade extends to about three-quarters of the distance to the base of the crown. Anterolingually, a shallow, narrow longitudinal furrow that corresponds with a thegotic facet parallels the anterior crest, terminating inferiorly in a dimple emarginated by a short cingulid or cuspid. The posterior blade is formed by a steeply descending postprotocristid that unites with short labial and lingual basal cingulids to define a low posteromedial facet or ledge.

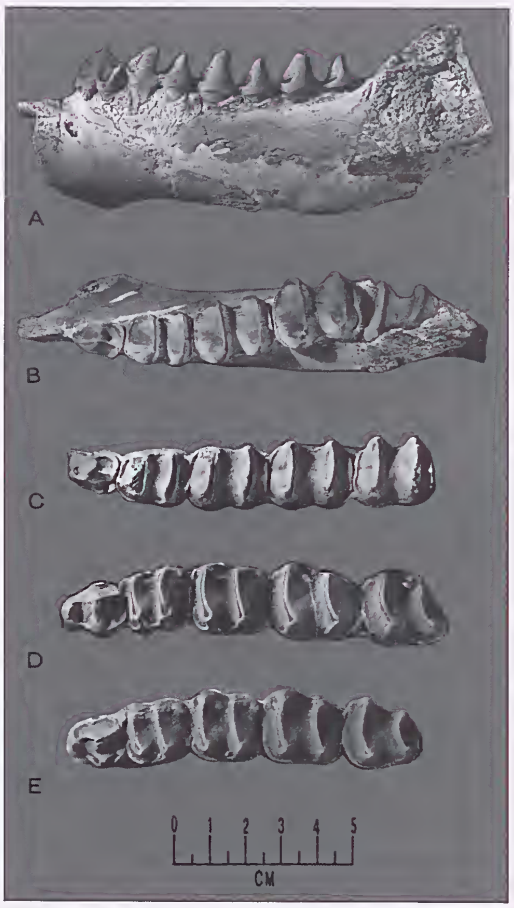

Figure 13. *Neohelos stirtoni* n. sp. Cheek-tooth rows from the Blast Site Bullock Creek; **A–B**, labial and occlusal aspects of left lower cheek teeth (CPC 22530); **C**, occlusal aspect of left lower cheek teeth (CPC 22551); **D**, occlusal aspect of left upper cheek teeth (CPC 22525); **E**, occlusal aspect of left upper cheek teeth (CPC 22195).

On worn specimens there is an illusion of a posteromedian cuspid, but unworn specimens demonstrate the apparent cuspid is an artefact or residual left when wear takes place on the crest that descends from the central cuspid. The posterolingual surface of the crown is a parabolic cavity extending from the apex of the protoconid down to a low, thick, obliquely-oriented lingual cingulid that emarginates a short, rounded posterolingual shelf. The labial posterior surface is also distinctly, though less concave. The posterolabial cingulid is divided by a vertical crease or furrow into posterior and anterior components. The posterior segment is longest and thickest. It ascends steeply towards the postprotocristid. The anterior segment is very short and usually less prominent. It is horizontal or may ascend towards the labial cristid of the protoconid. The posterolabial and posterolingual cingulids of P_3 terminate at the anterior margin of the posterior root in *N. stirtoni*. An anterolabial cingulid is present on some individuals.

M_1. M_1 is a rectangular-crowned tooth, a little longer than it is wide (figs 13A–C, 14A–D). The protolophid is narrower than the hypolophid. The tooth narrows to a blunt, steep interproximal face. A long, blade-like paralophid crest descends obliquely from the protoconid to a point between a third, to halfway from the labial edge of the tooth, to where it bends sharply onto the anterior cingulid. The anterior cingulid terminates at the anterolingual corner of the crown and is stronger on the lingual side of the tooth than on the labial. The paralophid crest extending from the protoconid to the anterior cingulid forms a functional shear in line with the postprotocristid of P_3. The metalophid is only weakly developed and descends anterolingually from the hypoconid.

A labial cingulid is present at the labial end of the transverse valley, and a very small cuspid on this cingulid is the origin of two slight ridges, which ascend towards the protoconid and the hypoconid. Similar ridges are present at the lingual end of the transverse valley. They meet at the base of the valley, the anterior ridge ascending towards the metaconid, but fading out approximately halfway up the lophid; while a similar ridge ascends posterodorsally towards the entoconid. A small postcrior cingulid crosses the bottom of the tooth from the base of the hypoconid to the base of the entoconid. There is a slight thickening of the cingulid at the midline, and it terminates at the lingual end in a very small cuspid, only visible in lightly worn specimens. From the lingual view, the floor of the median valley is V-shaped, while in labial view it is more U-shaped.

M_{2-4}. The M_2 is similar to M_1, as are M_{3-4}. However, the protolophid is wider than the hypolophid and the paralophid crest is short, descending only on-third the way down the crown (fig. 13C). The lingual crests which ascend the entoconid and metaconid are weaker and do not meet in a sharp V, but rather are U-shaped, and the median valley when viewed from the lingual side is also U-shaped. M_3 is very similar to M_2 except that the protolophid is markedly wider than the hypolophid and both the protoconid and metaconid are more inflated and bulbous. A slight metalophid is apparent on unworn teeth. M_4 is similar in that the hypolophid is less wide than the protolophid, but not greatly reduced as in the metaloph of the upper molars.

Cranium and dentary

General morphology of the cranium

Adult *N. stirtoni* crania range between 300 mm and 450 mm in condylobasal length, longer than any specimen of *Kolopsis torus* Woodburne (1967) and smaller than, but also similar in appearance to *Plaisiodon centralis* Woodburne (1967). The structural relations of the cranium of *N. stirtoni* are fundamentally wombat-like, though its elongated, narrow shape contrasts strongly with the dorsally flattened, rectangular crania of living wombats (figs 8, 15; tables 4, 5).

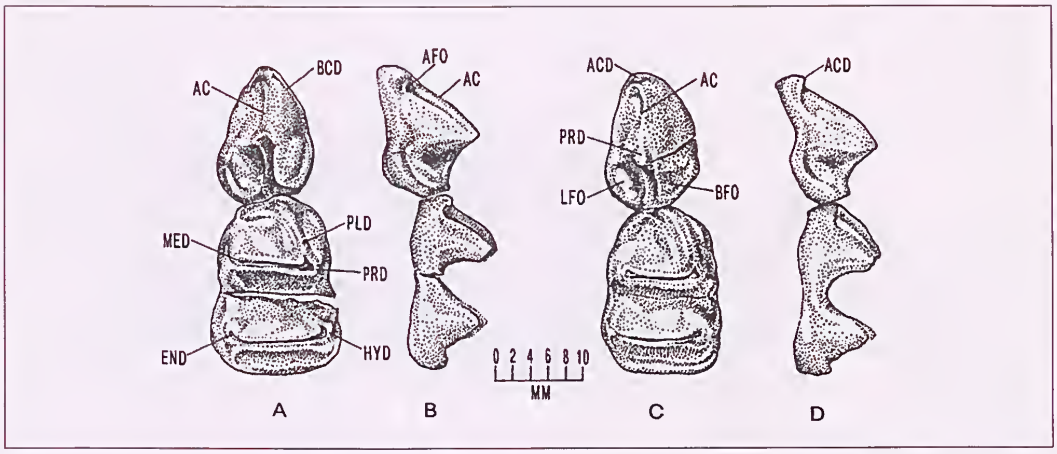

Figure 14. *Neohelos stirtoni* n. sp.; P_3 and M_1 specimens; **A–B**, occlusal and lingual aspects of right P_3–M_1 (NTM P87103-26 Blast Site, Bullock Creek); **B**, occlusal and lingual aspects of right P_3–M_1 (NTM P8695-69 Blast Site, Bullock Creek). Note small cuspid (ACD) and short, low cingulid developed at the base of the anterior median cristid of P_3 in this species.

The braincase of *N. stirtoni* is elongated, constituting over half of the total cranial length and overall, the cranium is relatively narrow transversely across the zygomatic arches (figs 8A, 15B–C; table 4). The cranial vault is convex in lateral profile and dome-like in the posterior aspect with prominent, inflated frontal bosses separated by a deep cleft that converge posteriorly into a low but stout sagittal crest. The broad occiput is outlined by smoothly arcing lambdoid crests. The zygomatic arches are elongated and fairly deep, flaring outward in smooth curves in dorsal aspect, whereas in ventral aspect they appear to be flat-sided and angular.

The masseteric processes are well-developed and elongated, though slender compared to *Plaisiodon* and *Zygomaturus*. The temporal fossae are large, egg-shaped vacuities, defined posteriorly by long squamosal sulci and anteriorly by the slight constrictions behind the posteriorly open orbits. The small orbits are situated about midway up the base of the rostrum. The snout is tubular, slightly flattened on the dorsal surface, gradually narrowing from anterior to the orbits to the infraorbital foramina, then gradually expanding anterior to the infraorbital foramina to flare out behind the narial opening. The floor of the narial aperture extends slightly anterior to the blunt termination of the nasal bones. The nasal bones are elongated, widest at their anterior and posterior extremities.

The cranial base is straight and only slightly elevated above the cheek-tooth row. The maxillary palate is flat, moderately expanded posteriorly and shallowly depressed in the midline. The median palatal sulcus becomes bounded on either side by sharp, parallel diastemal crests on the premaxillary palate, progressively deepening into a gutter-like interincisive fossa. In side view, the premaxillary alveolar process for the incisors is moderately to strongly decurved.

The interpterygoid fossa is a large, oval cavity that dominates the mid-region of the basicranium. Anteriorly, it is emarginated by rugose pharyngeal crests developed on the transverse palatal processes. Greater palatine fenestrae are absent. The glenoid fossae are rectangular, obliquely-oriented planoconcave surfaces bounded posteriorly by enormous, flap-like, sinus-inflated postglenoid processes and mesially by entoglenoid eminences and bulla-like, sinus-inflated structures (fig. 15B). The auditory arch is relatively small. The mastoid-paroccipital processes are massive and sinus-inflated. The occipital condyles are large and protrude directly backwards, parallel to the basicranial axis. The lateral profile of the occiput is abruptly vertical, ascending to a low lambdoid crest dorsally and wrapping around the sides of the cranium to expose the mastoid surfaces in lateral aspect.

Braincase, cranial sinuses, endocranial casts

Cranial walls. The dorsal profile of the elongated braincase is a gently inclined convex surface dominated anteriorly by the large frontals and posteriorly by the long, narrow parietals. The frontal is expanded by large sinuses into a pair of smooth crests or tori, each of which are about 27 mm wide and separated by an 8 mm deep, 33 mm long median sulcus surrounded by an oval nasofrontal fossa. In lateral view, the anterior process of the frontal projects above the orbit and makes contact with the lacrimal about 15 mm behind the anterointernal rim of the orbit. The 84 mm long orbitofrontal suture passes obliquely posteroinferiorly to contact the alisphenoid. The posterior process of the frontal is wedge-shaped, dividing the squamosal and the parietal over a distance of about 50 mm (fig. 16A). The descending posterior margin of the frontal is crescent-shaped, accommodating the low infratemporal process of the alisphenoid. The ventral border follows the dorsal margin of the infraorbital sulcus of the palatine to the orbital canal, to where it ascends up towards the lacrimal.

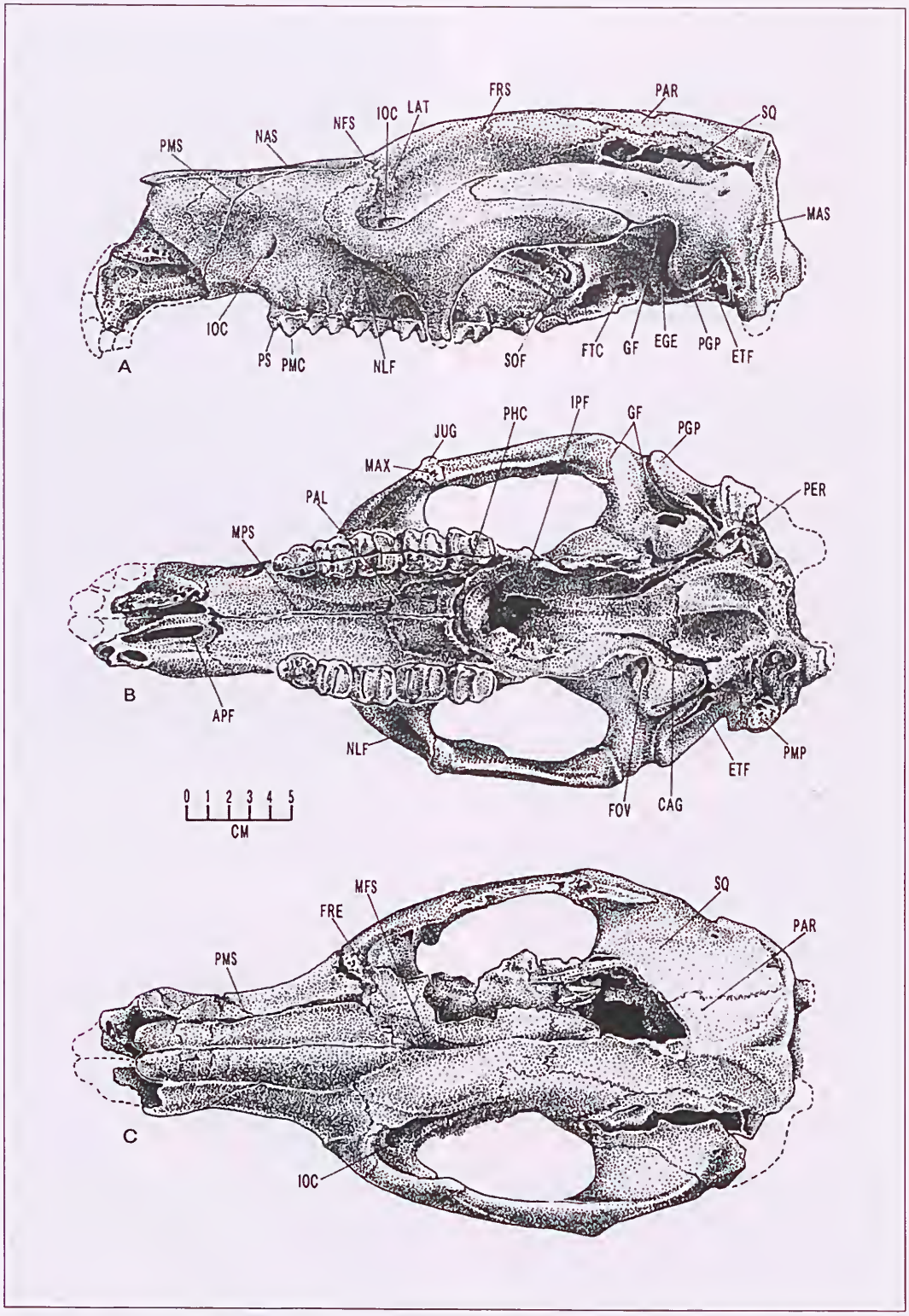

Figure 15. Cranial anatomy of *Neohelos stirtoni* n. sp. (NTM P8551-13 Blast Site, Bullock Creek); **A**, lateral aspect; **B**, ventral aspect; **C**, dorsal aspect.

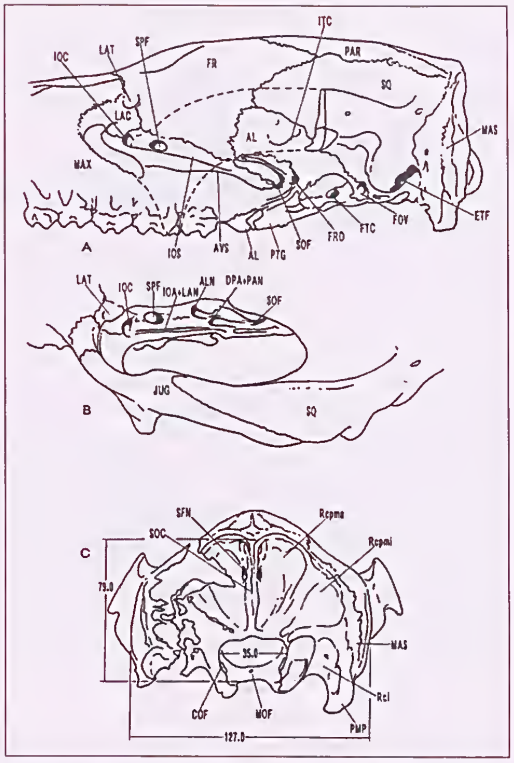

Figure 16. Orbital fossa, cranial side wall and occiput of *Neohelos stirtoni* n. sp. (NTM P8551-13 Blast Site, Bullock Creek); **A**, lateral aspect showing structures within the orbit and lateral cranial wall; **B**, dorsolateral aspect showing structures in and around the infraorbital sulcus; **C**, occipital aspect.

The 120 mm long, narrow parietals contact the squamosal along a straight, obliquely oriented suture over a distance of 75 mm. The anterior processes terminate bluntly at the midline in a short, sinuous transverse suture line about 10 mm long. The squamosal lamina extends high up the braincase, comprising about three-fourths of the vertical extent of the lateral surface. The anterior process extends anteriorly to about the same level as the anterior process of the parietal. The squamosoalisphenoid suture parallels the parietofrontal suture, resulting in a Z-shaped sutural inscription. The anterolateral surface of the squamosal is slightly convex, steepening near the zygomatic root and deflecting inwards anteriorly to form the posterior margin of the infratemporal fossa. Continuous with the squamosal infratemporal crest is the anterior edge of a deep, wide 45 mm long squamosal sulcus that shallows posteriorly and grades into the posterolateral surface, where in combination with the parietals and interparietals, the braincase becomes widely gabled and slab-sided.

Posteriorly, the squamosal develops a low crest, the continuation of the lambdoid crest, which runs downwards to form the posterolateral margin of the auditory arch. The squamosal-mastoid contact is exposed on the lateral side of a wide, crescentic, rugose surface that grades inferiorly into the mastoid-paroccipital process. The squamosomastoid suture is highly irregular over much of its extent. Above and at the base of the zygomatic root are a pair of small foramina that lead into the vascular network associated with venous sinuses of the braincase.

Infratemporal and orbital fossae. The ascending process of the alisphenoid is poorly developed in *N. stirtoni*, the anterior margin of which terminates abruptly in an oblique, complex frontoalisphenoid suture that parallels the anteroinferior trend of the frontoparietal suture (fig. 16A). The pillar-like descending process forms the anterior crest and dorsal half of the deep, oval pterygoid fossa posteriorly and the posterior crest of the foramen rotundum and sphenorbital fissure anteriorly. The posteroventral process of the alisphenoid extends a broad, posteriorly tapering lamina under a bulla-like structure that is situated immediately anterior to the middle ear cavity.

The squamosoalisphenoid suture follows the crest of the entoglenoid eminence (the lateral wall of the hypotympanic bulla) then ascends the wall of the infratemporal fossa at about a 45° angle, consequently bordering the inferior margin of the squamosal over a distance of about 80 mm. A 33 mm long by 17 mm wide and 11 mm deep pterygoid fossa is developed within the alisphenoid, encompassing the foramen of the transverse canal. The floor of the cavity is composed of the pterygoid. Opening posterolateral to the pterygoid fossa is the large 8.0 mm diameter foramen ovale.

The foramen rotundum is situated immediately posterolateral to the 30.5 mm long sphenorbital fissure (confluent lacerate and optic foramina). The orbitosphenoid suture is not discernible on any specimen of *N. stirtoni*. The orbital process of the palatine emerges along the anteroinferior margin of the sphenorbital fissure and continues anteriorly as a narrow strip in the base of the orbital wall, adjacent to the shelf-like extension of the maxilla, along which nerves and vessels emerging from foramen rotundum are conducted in a series of grooves. The anterior orbital process of the palatine appears to terminate at the sphenopalatine canal on the left side of NTM P8551-13 but forms part of the mesial wall of the infraorbital canal on the right side. In the type, CPC 22200, the infraorbital canal is entirely within the maxilla. The lacrimal is confined to the anteromesial corner of the orbit, extending dorsally to encompass the prominent lacrimal tuberosity, the lacrimal foramen situated immediately anteroinferior to the tuberosity and a thumbnail-sized corner of the anterodorsal orbital margin.

The suborbital shelf is about 13 mm wide and about 25 mm deep from its dorsal margin to the molar alveoli (fig. 16B). The dorsal surface of the shelf is inscribed with a series of narrow grooves, foramina and a wide sulcus for

the infraorbital artery and nerve that passes through the large, 11 mm wide infraorbital canal. A more posteriorly positioned foramen appears to represent the posterior palatine that transmits the descending branch of the palatine artery and alveolar nerve. Lateral to the infraorbital sulcus are a pair of deep, narrow grooves that terminate in foramina at various points along the shelf. These relate to the blood supply of the alveolar region. A more medial, attenuated groove which does not terminate in a foramen probably conveyed the lacrimal nerve. The sphenopalatine canal which transmits the posterior nasal nerve, an artery and a branch of V^2, opens about 25 mm behind the infraorbital canal within the infraorbital sulcus.

Endocranial sinuses. An interesting feature of the neurocrania of the larger diprotodontid marsupials is the development of large sinuses that surround a thin inner table that actually encases the brain (fig. 17). The extent to which these sinuses are developed appears to be partially size related, apparently as an allometric adjustment to provide additional external surface area for the attachment of the jaw muscles (Murray 1992). The neurocranial sinuses of *N. stirtoni* consist of two principle midline groups and three lateral groups. Anteriorly, the dorsolateral surfaces of the inner braincase are separated from the outer table by a series of frontal sinuses. Deep anterolateral sinuses encircle the lateral portion of the frontal lobes of the brain.

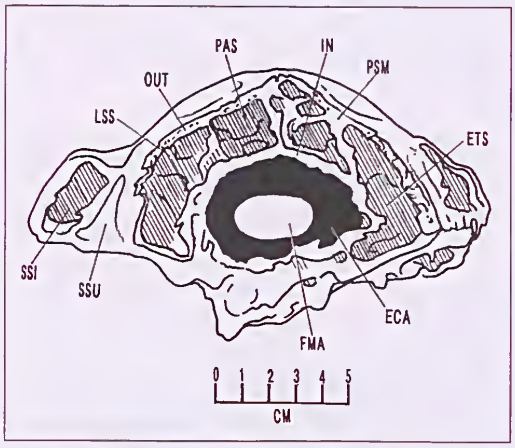

Figure 17. Drawing of natural section through the neurocranium of *N. stirtoni* n. sp. (CPC F23038 Blast Site, Bullock Creek) showing extent of endocranial sinus development (hachures) around the endocranial cavity (black).

The frontal sinus group is divided from the paired parietal sinus areas by a posteriorly curving transverse septum. The two parietal sinus groups, which are also subdivided, are separated by a short sagittal septum. The posterior parietal group is separated from the anterior parietals by a secondary transverse septum which curves in the opposite direction from the frontal septum, and in conjunction with the occipitomastoid septa, forms a large rhomboidal chamber in the posterior midline of the braincase. The squamosomastoid group form an interconnected network of chambers and passages surrounding the middle ear cavity and invading the zygomatic root. Particularly in the back of the cranium, these sinuses are closely associated with the endocranial venous circulation.

Endocranial casts. Two latex endocranial casts (fig. 18A–B) were prepared from broken specimens (NTM P8792-15 and CPC F23038). Latex endocast CPC F23038 extends just anterior to the temporal lobes. NTM P8792-15 terminates immediately behind the frontal lobes. In dorsal aspect, the cerebellar outline is rectangular, with low, but broad oval protuberances of the paraflocculus. The cerebral cortex is broad transversely with little relief. The poles of the temporal lobes project laterally, suggesting a relatively thin neocortex. The brain is compressed dorsoventrally and roundly rectangular in transverse section immediately anterior to the temporal lobes. The endocranial surface representing the neocortex shows faint convolutions trending predominantly anteroposteriorly. In contrast to the strongly convoluted, gyrencephalic cortex of living vombatids, it is more similar to the lissencephalic Koala (*Phascolarctos cinereus*) in this respect. The frontal lobes and olfactory stalks and bulbs are not preserved on these endocasts.

The descriptive terminology below follows Haight and Murray (1981). The faintly visible rhinal fissure transects the lower third of the temporal lobe. Commencing dorsally from the sagittal sinus, a clearly defined interbrachial sulcus (IB) curves forward to isolate an elongated central gyrus on either side of the midline. A pair of dimples immediately anterior to the central gyri are interpreted to represent sulci a. The posterior part of the Jugular sulcus (J) is indistinctly present on both endocasts. Sulcus b for the middle cerebral artery is well defined. A short, straight sulcus L is present on CPC F23038. Sulcus d is a shallow, rounded depression in the posterior portion of the temporal lobe and sulcus m is represented by a smaller depression above and posterior to the former.

The morphology of these endocasts resembles that of living vombatids and phascolarctids. In basic outline shape, the resemblance is closer to that of *Vombatus* than *Phascolarctos*, while in terms of the sulcal morphology of the cerebral cortex, they are more like *Phascolarctos*. In terms of basic shape, proportions and sulcal development, the endocasts of *N. stirtoni* show a closer resemblance to *Vombatus* and to endocasts of the palorchestid *Propalorchestes novaculacephalus* than to the superficially phalangerid-like endocast of *Wynyardia bassiana* (Haight & Murray 1981).

Occipital region. The occiput of *N. stirtoni* is low and broad in posterior aspect and nearly vertical in lateral view (fig. 16A, C). Its posterior surface is dominated by a large fossae for the attachment of the rectus capitus muscles. A median crest separates the two main surfaces

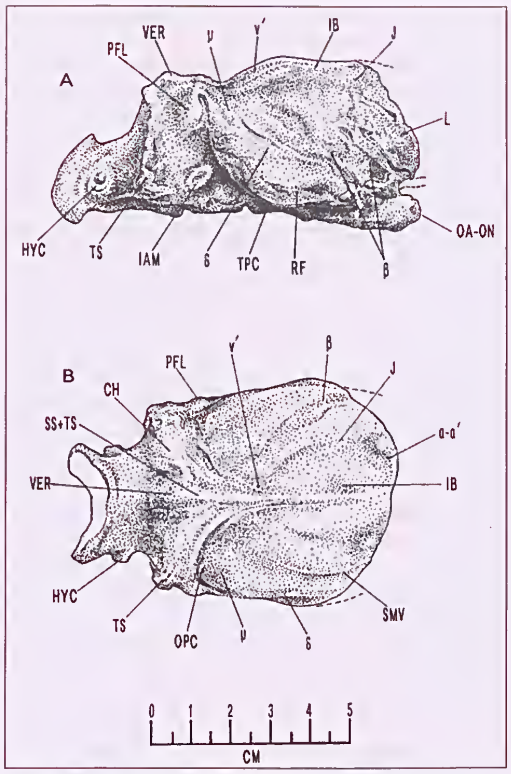

Figure 18. Drawings of endocranial casts of *Neohelos stirtoni* n. sp.; **A**, lateral aspect (CPC F23038); **B**, dorsal aspect (NTM P8792-15).

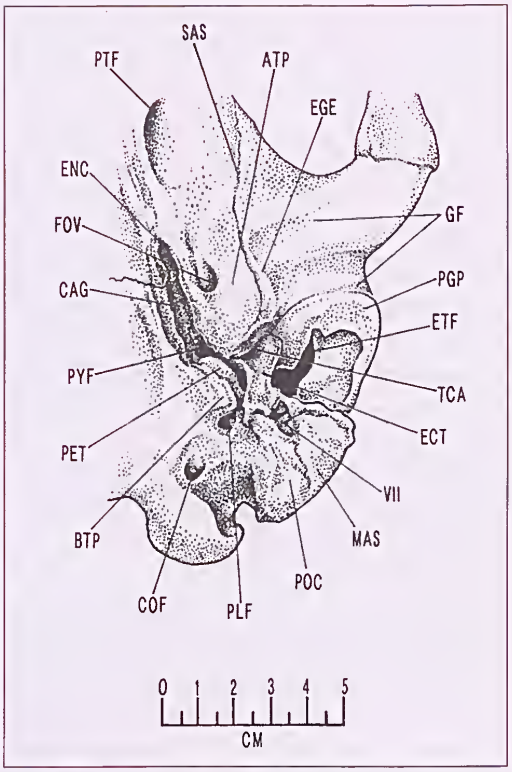

Figure 19. Ventral aspect of left basicranial quadrant of cranium of *Neohelos stirtoni* n. sp. (CPC F23038 Blast Site, Bullock Creek).

both of which are perforated by the supraoccipital emissary foramina. A small, shallow supracondylar fossa is present, in contrast with palorchestids, for example, in which the structure is large. The condylar sulcus is wide and deep, grading into a distinct lunate depression on the medial surface of the paroccipital process. This fossa may correspond to the insertion of the rectus capitus lateralis muscle. The occipital condyles are large and prominent but narrow transversely relative to their length. The foramen magnum is rectangular in shape and wider (35.0 mm) than high (23.5 mm). Large hypoglossal foramina are just visible in posterior aspect within the lateral walls of the foramen magnum.

A small median foramen opens posteriorly in the floor of the basioccipital. The paroccipital processes are stout, rectangular structures which have a mastoid contribution on the lateral side. The paroccipital-supraoccipital suture appears to course obliquely across the occiput from the median dorsal margin of the foramen magnum to converge dorsolaterally with the superior termination of the interposed mastoid bone. The external squamosomastoid suture is difficult to trace, but the anterior suture does not appear to contact the lambdoid-squamosal crest, and although it is fairly broad inferiorly, it remains confined to the lateral side of the occiput.

Basicranium and middle ear region

Tympanic cavity. The ear region of *N. stirtoni* is basically similar to that of *Ngapakaldia* Stirton, 1967b, and to that of the mid Miocene palorchestid *Propalorchestes* Murray, 1986. The relations of the auditory region of the basicranium include the glenoid fossa laterally, the roof of the middle ear cavity dorsally, the mastoid region posteriorly and the basioccipital and basisphenoid mesially (fig. 19). Anteriorly the pterygoid and alisphenoid bones predominate. The floor of the middle ear cavity in *N. stirtoni* is open except for a small lobate process of the basioccipital.

The anterior wall of the tympanic cavity is represented by a shallow fossa in the posterior wall of the large hypotympanic swelling or bulla developed in the squamosal. The bulla is floored by a posteroventral process of the alisphenoid, which extends a few millimetres under the tympanic cavity as a short tympanic wing. A slightly concave or flattened lateral surface of the petrosal contributes the posteromesial wall of the cavity and a small, isosceles triangle-shaped process, the tegmen tympani, forms part of its roof (fig. 20C). The tegmen is recessed with a 3.0 mm diameter fossa or attic accommodating the auditory ossicles; behind which a smaller, lower fossa accommodates the posterior ligament

of the incus. A short (~5.0 mm) low tympanic crest defines the mesial end of a long, funnel-like acoustic arch which is breached dorsally by a slit-like (20 mm x 5 mm) epitympanic fenestra.

The epitympanic recess is very confined mesially. The incisura tympanica is a narrow groove between the tegmen of the petrosal and the crista tympanica of the squamosal. Anterolaterally the incisura meets a perpendicular groove for the attachment of the anterior crus of the ectotympanic. The lightly attached ectotympanics (fig. 19), which are usually missing, have remained in place in one specimen (CPC F22525). The ectotympanics are transversely narrow, 6.0 mm wide and 15.5 mm long anteroposteriorly, under the acoustic arch. The ventral surface of the ectotympanics are slightly arched, resembling small bridges. The internal contour of the bony meatus is an elliptical orifice about 8 mm high by 5 mm across. The posterior crus of the ectotympanic sends out a blunt dorsolateral process that surrounds the otherwise open groove for the facial nerve, to form a stylomastoid foramen.

Petrosal. In specimens lacking the ectotympanics, the ventrolateral aspect of the petrosal is fully visible (fig. 20). The pars petrosus is a short, oval or even slightly cube-shaped structure approximately ~12 mm wide by ~15 mm long (fig. 20A–C). The ventral surface is rugose, the pars cochlearis being nearly flat, bulging posteroventrally at the promontory. The superior periotic process is blunt, often terminating in an irregular pit. The cochlear fenestra opens posteroventrally towards the stapedial fossa of the posterior tympanic recess. The fenestra is elliptical, ~2.6 mm by ~1.6 mm, and is set in a smooth-walled fossula. The cochlear fenestra is separated from the smaller ~1.5 mm by ~1.8 mm vestibular fenestra by a 2.0 mm rounded crest. In anatomical position, the vestibular fenestra, which opens posterolaterally towards the acoustic arch, is situated anterodorsal to the cochlear fenestra.

Dorsolateral to the vestibular fenestra, a shallow groove descends posteriorly to merge with a deep perpendicular groove in the anterior surface of the mastoid, which is the previously mentioned facial nerve sulcus. Immediately below this sulcus is a shallower, more irregular groove for the posterior crus of the ectotympanic. The facial groove continues anteriorly from above the vestibular fenestra for about 5 mm where it opens into the facial nerve foramen, which is up to about 2.0 mm by 1.5 mm in some specimens of *Neohelos stirtoni*. In some specimens the groove continues anteriorly from the foramen parallel to the anterior periotic process, whereas in others a small canal leads anteriorly from the foramen to transmit the chorda tympani branch of the facial nerve.

The internal side of the periotic is divided by a low crest (prominence of the anterior and posterior semicircular canals) into two fossae: dorsally, a shallow floccular fossa and ventrally an approximately 6 mm diameter internal acoustic meatus with a slot-like fundus about 4 mm deep. A crista transversa between the facial and vestibulocochlear nerves is not visible on any of the specimens, but two channels can be visualised in the figure-eight-like recess, dorsally for the facial nerve and ventrally for the cochlear nerve.

Epitympanic fenestrae and glenoid processes. In *N. stirtoni*, the epitympanic fenestra is usually an oblique slit-like opening that extends from the tympanic crest, through the roof of the auditory arch to invade the base of the postglenoid process (figs 8C, 15B, 19, 20C). Its shape and size is variable in the species. Located under the posterior margin of the fenestra is the postglenoid canal which is usually a large circular opening. Superolateral to the epitympanic fenestrae are variable fossae composed of merged circular depressions that occupy the dorsal surface of the superficies meatus and the posterior margins of the postglenoid processes. In some *N. stirtoni* specimens the posterior end of the fossa opens into the mastoid region to form a posterior epitympanic fossa. The postglenoid process is developed from an extensive swelling (a lateral or postglenoid hypotympanic sinus) about 50 mm long and 16 mm wide that extends from the tympanic crest to the lateral margin of the squamosal.

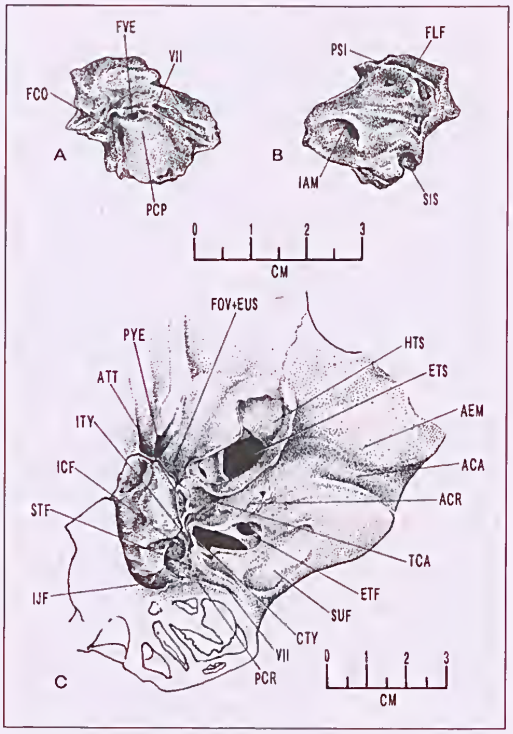

Figure 20. **A–B**, right petrosal of *Neohelos stirtoni* n. sp. (NTM P8695-78 Blast Site, Bullock Creek); **C**, ventral aspect of left basicranial aspect of cranium of *Neohelos stirtoni* showing structures surrounding the middle ear region revealed by missing ectotympanic and basioccipital tympanic process (NTM P8792-15 Blast Site, Bullock Creek).

Mesially, the internal side of the base of the postglenoid process is separated from the posterior wall of the entoglenoid surface of the bulla by a 12 mm deep, 3 mm–6 mm wide, 32 mm long glenoid incisura. The glenoid incisura leads directly into the tympanic cavity and along its ventral margin are the roughenings for the attachment of the anterior crus of the ectotympanic. Anteriorly, the cleft opens into the mesial side of the 10 mm wide, 32 mm long transverse articular groove of the glenoid fossa, anterior to which is a flat, 40 mm wide by 20 long (anteroposteriorly) articular eminence that extends onto the ventral surface of the jugal.

Entoglenoid eminences and bullae. The base of the 26 mm by 32 mm bulla-like hypotympanic swelling which is continuous with a 20 mm wide, 16 mm deep entoglenoid eminence laterally and the anterior wall of the tympanic cavity posteriorly, is composed of the squamosal. Its ventral surface is sealed off by a V-shaped process of the alisphenoid which has the appearance of having folded itself around the structure (figs 8C, 15B, 19). On the ventral anterolateral corner of the bulla, the alisphenoid-squamosal suture remains open, possibly for the transmission of the chorda tympani nerve. The course of the alisphenoid-squamosal suture can be traced around the tympanic process where, on the anteromesial corner of the bulla, it forms an arch under the large 7.0 mm by 8.0 mm diameter foramen ovale, in combination with the posterior process of the pterygoid crest.

Basicranial structures. Anterolateral to the blunt, hollowed out superior periotic process of the petrosal, a deep irregular cavity, the pyriform fenestra, is composed of the middle lacerate foramen, the posterior end of the internal carotid groove, the mesial wall of the hypotympanic bulla and bounded laterally by a thin process of the squamosal. The 4 mm deep entocarotid groove extends some 25 mm along the lateral margins of the basioccipital and basisphenoid. The foramen for the internal branch of the internal carotid artery opens about 15 mm anterior to the basisphenoid-basioccipital suture in the lateral edge of the basisphenoid.

The basisphenoid-basioccipital suture lies 48 mm anterior to the foramen magnum. The basioccipital is broad, particularly where it is extended laterally to send a small process under the petrosal and tympanic cavity. The basisphenoid narrows within the interpterygoid fossa, extending anteriorly about 45 mm to meet the presphenoid along a clearly defined chevron-shaped suture. The pterygoid crests in *N. stirtoni* are low, thick laminae that form the floors of the deep, oval pterygoid fossae, perforated centrally by large transverse canal foramina. The crests deepen ventrally and widen laterally to form the walls of the pharyngeal cavity. The internal nares is a 34 mm deep, oval opening with smooth, steep walls laterally, bounded by a prominent, curving transverse palatine crest ventrally. Dorsally within the 60 mm long, 45 mm wide 35 mm deep interpterygoid fossa, the ventral surfaces of the basisphenoid and presphenoid are widely exposed.

Facial cranium

Palate. The posterior margin of the palatine bones are formed by high, posteriorly swept transverse palatine crests which blend into the pterygoids (fig. 15B). Anterolaterally, the crests are deep, V-shaped clefts on either side, dorsomedial to the M^4 alveolus, into which open the orifices of the postcrolateral palatine foramina. The palatine processes are devoid of greater palatal fenestrae. The maxillopalatine suture courses parallel to the molar alveoli for about 40 mm then turns mesially to meet in the palatal midline, level with interproximal M^{2-3}. The palatal surface is flat with a shallow median sulcus commencing at about the level of the posterior end of M^1. This furrow deepens as it continues onto the 60–65 mm long by 20–25 mm wide diastemal palate where its edges become more crisply delineated by low diastemal crests.

The straight, parallel diastemal crests become sharper and higher lateral to the anterior palatal fenestrae, the latter being encompassed by a deep, gutter-like interincisive fossa. The 23 mm long by 7 mm wide anterior palatal fenestrae are separated by a high, rounded premaxillary septal process. The overall proportion of the cheek-tooth bearing palate is a 2:1 rectangle. The diastemal palate narrows to about two-thirds of the width of the cheektooth palate, and constitutes slightly less than half of the total palatal length. The incisive arcade is U-shaped and expands laterally behind the I^3 alveoli to about twice the width of the diastema. The premaxillomaxillary suture commences in the midline immediately behind the premaxillary septal process. The suture courses anteriorly on the lateral palatal surface to about 20 mm behind the I^3, then runs posteriorly at an acute angle to the mesial suture line to form a narrow V. The suture then makes a nearly vertical ascent of the lateral side of the rostrum about midway between the I^3 and the P^3.

Rostrum. The tubular rostrum comprises about one-third of the total length of the cranium of *N. stirtoni*. The nasals are elongated. The proximal surface is gently arched and widest immediately above the orbits, where the tapering frontal processes terminate at the anterior edge of the median frontal fossa. The nasals contract to their minimum width (10–15 mm) at the level of the infraorbital foramen, then expand laterally again to their maximum anterior width just behind the margin of the narial aperture (15–18 mm) and maximum posterior width of 20 to 24 mm. The nasals terminate in blunt, slightly rounded margins above the level of I^3.

The narial aperture is a large, transversely oval opening, 45 mm to 65 mm wide, with smooth, thick premaxillary lateral margins that thin dorsally to agree with the lateral margins of the nasal bones (fig. 21A–B). The floor of the narial aperture is divided by a deep, wide trough through which the anterior palatine fenestrae open directly into the nasal cavity. The inferolateral margins of the nares are produced into wide, shelf-like processes, the inferior nasal crests, each of which bears a large oval sulcus that accommodated the anterior portion of the middle concha

of the turbinate bones (fig. 10C). Bending forces on the anterior premaxillary processes, which support the incisor roots, appear to have been distributed through the floor of the narial aperture via the robust inferior nasal crests. The superior crest or process of the premaxilla is a variable triangular to rhomboidal protuberance representing the anterior-most prominence of the cranium. This low protuberance is sometimes perforated by small foramina and appears to have supported a dense connective tissue mass possibly serving as the median attachment for a large mobile upper lip and / or the lower portion of a large rhinarium.

Small nasopremaxillary notches are present on the dorsolateral margin of the nares. This area is vascularized via a foramen that emerges from within the internal nasal crests. The lateral aspect of the rostrum is dominated by the broad maxilla. The maxilla is divided from the premaxilla by an initially nearly vertical suture that commences in lateral aspect behind the mid point of the diastema. About two-thirds of the way to the nasals, the suture sharply bends posteriorly in a shallow arc to terminate dorsally about midway along the span of the nasals. A large infraorbital foramen opens in the lower half of the maxilla about 26 mm posterior to the premaxillomaxillary suture.

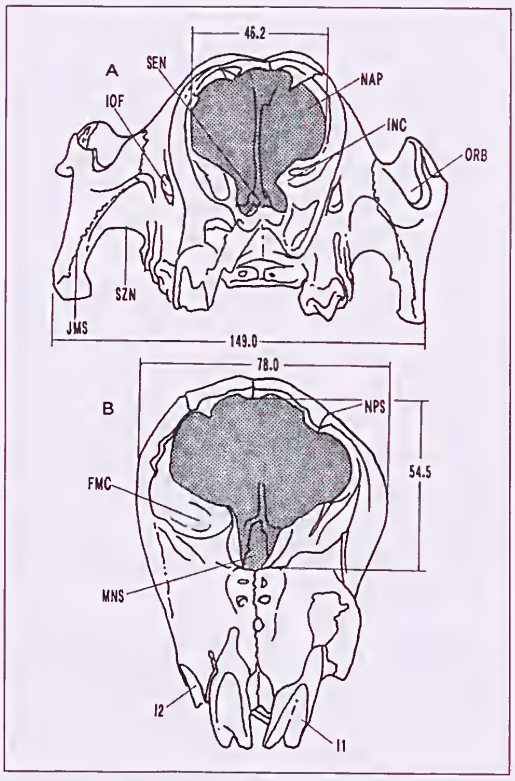

Figure 21. Anterior views of the rostra of two specimens of *Neohelos stirtoni* n. sp. from the Blast Site, Bullock Creek; **A**, NTM P8551-13; **B**, NTM P8695-38. Note differences in the size and shape of the narial apertures.

Orbit and zygomatic arch. Anterior to the infraorbital foramen is a shallow, approximately 20 mm by 30 mm fossa, above Which there is a distinct, rounded facial crest that flows posteriorly into the orbital margin. Anterodorsal to the orbital margins, the maxilla becomes slightly inflated and attains its greatest breadth at the root of the jugal. The maxillojugal suture follows the anterior contour of the rounded anterolaterally protruding orbital margin down to the masseteric process which is neatly formed by approximately equal contributions of both the maxilla and the jugal. The subzygomatic notch between the cheek-tooth alveolus and the masseteric process is 32 mm deep and 17 mm wide. Immediately below the orbital margin is a 35 mm by 20 mm maxillolabial fossa.

The orbit is small, about 27 mm to 30 mm wide, set off posteriorly by a low, thin, postorbital process of the jugal. A prominent lacrimal tubercle is located on the dorsomedial orbital wall. There are no distinct postorbital processes of the frontal. A deep masseteric sulcus and crest is confined to the lower half of the entire length of the jugal. The zygomatic process of the jugal is long and relatively deep posteriorly, tapering anteriorly to a rounded process that fits into the corresponding notch in the postorbital process of the jugal. The jugal-squamosal suture is nearly straight and relatively long, about half the total length of either zygomatic process. The maximum width of the cranium of *Neohelos* is across the lateral glenoid eminences of the jugals. In lateral profile, the glenoid fossa forms a right angle notch in the lower squamosal root, bounded posteriorly by a massive postglenoid process. The auditory arch is an inverted U or V-shaped notch.

Dentary

The dentary is long with a slender horizontal ramus (figs 9A, B, 22A–C; table 5). The body of the dentary usually tapers anteriorly from the inferior coronoid crest to the level of P_3. The longitudinal axis of the horizontal ramus is fairly straight. In lateral aspect, the inferior border of the dentary is sinuous and the alveolar border is nearly straight to slightly concave. A weak digastric eminence is invariably present. The horizontal ramus is strongly convex in section just anterior to the ascending ramus, after which it becomes much flatter in section. The diastemal crest is short and sharp on its superior margin. The mental foramen is situated immediately anteroinferior to the anterior root P_3. The lower incisor is procumbent. The long, shallow symphysis is oval to trapezoidal in outline and remains unankylosed throughout the animal's lifetime. Deep round or oval genial pits are present. A small posterior mental foramen is present in the middle of the horizontal ramus at about the level of interproximal M_{2-3}. A distinct mid-ramal torus extends a short distance forward from the base of the coronoid crest.

The ascending ramus comprises one-third to one-quarter of the total length of the dentary. The coronoid process is high and blade-like with a blunt, transversely wide tip. The coronoid notch is short and shallow. The condyle is situated high above the occlusal line of the cheek teeth. The posterior edge of the ascending ramus is constricted at the neck of the condyle to about 20 mm, then expands

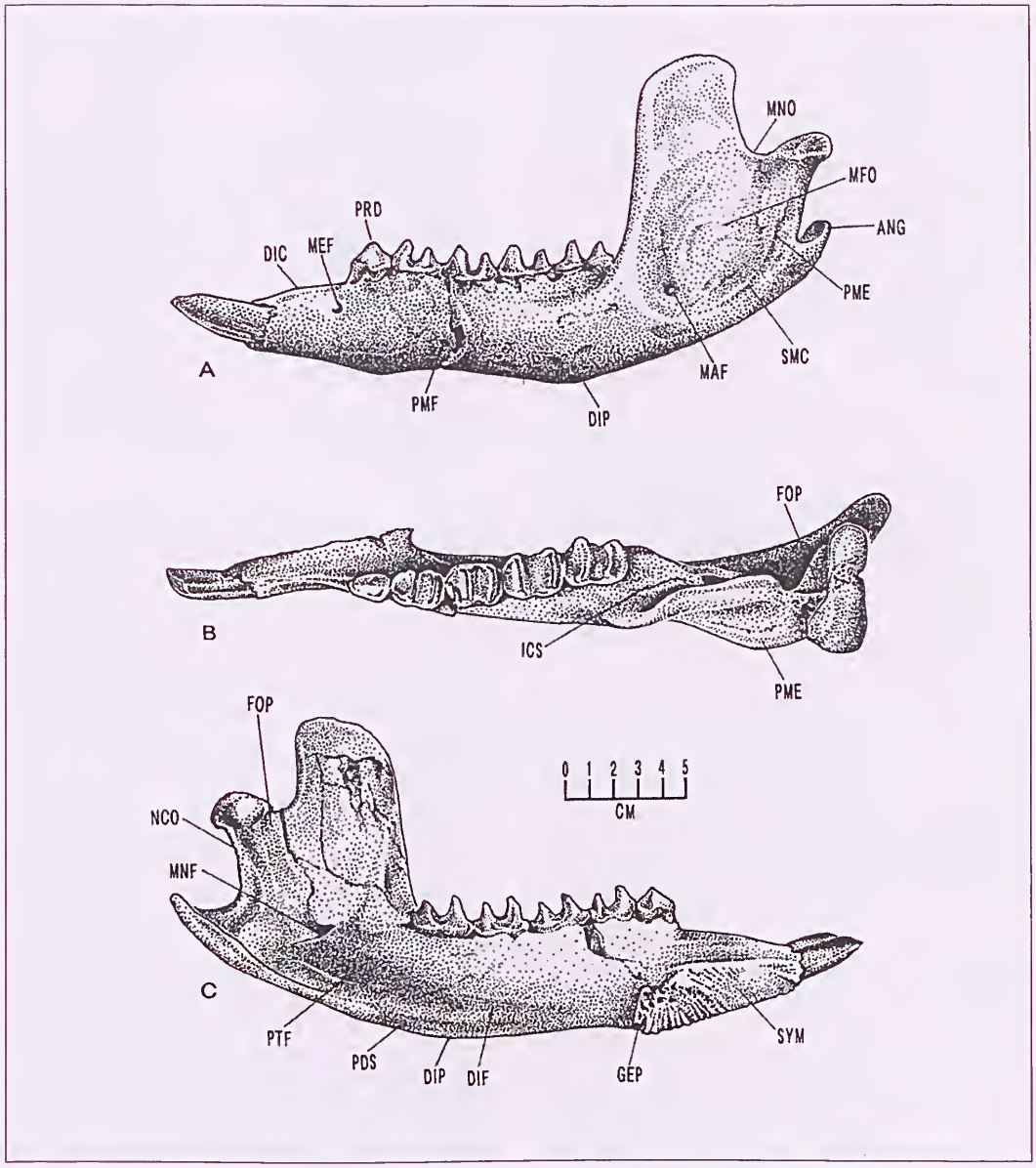

Figure 22. *Neohelos stirtoni* n. sp. left dentary (NTM P8695-74 Blast Site, Bullock Creek) broken incisor tip and coronoid process tip restored; **A**, lateral aspect; **B**, occlusal (dorsal) aspect; **C**, internal aspect.

to a condylar width of about 50 mm. The condyle is transversely wide, convex posteriorly and presents an anteriorly inclined, flat articular surface laterally, narrowing medially to a more conical process. The masseteric fossa is a crisply defined concavity bounded inferiorly by a distinct submasseteric crest. The posterior masseteric crest is prominent and flange-like. A small, oval 3.5 mm to 4.5 mm diameter masseteric foramen is present.

The digastric fossa is elongated, extending anteriorly to below the level of interproximal M_{1-2}, and is usually posteriorly confluent with the pterygoid fossa, but rarely, a faint crest partially divides the two cavities. The medial edge of the pterygoid fossa is marked by a strong flat border about 10 mm wide that terminates dorsally at the angular process. The angular process projects slightly above the level of the tooth row and the posterior masseteric eminence on the lateral side. The pterygoid fossa is deep and rugose. The mandibular foramen opens posterodorsally in line with the base of the tooth row. It is ovoid with its largest dimension varying from 8 mm to 15 mm. A postalveolar process is present 20 mm to 23 mm behind M_5.

Postcranial skeleton

Some elements of the postcranial skeleton of *Neohelos stirtoni* are described and compared with the few zygomaturine genera for which a substantial portion of the skeleton is known (figs 23–27; table 6). Manus and pes elements of *Neohelos* are represented in the Bullock Creek collection, but have not been studied sufficiently to include them in the description. The material described and illustrated here is primarily intended to provide an impression of the overall structure of *Neohelos stirtoni*. Comparisons of the material with other zygomaturines gives some indications of structural changes in subsequent zygomaturine lineages.

Vertebral column

The cervical vertebral bodies are slightly compressed, but with low neural spines compared to those of *Zygomaturus*. The thoracic and lumbar vertebral bodies are fairly long with circular to slightly oval articular facets. The pedicals are stout and broad. The transverse processes of both the thoracic and lumbar vertebrae are relatively short. The neural spines of the anterior-most thoracic vertebrae are slender, elongated and tapered distally. They are not bifurcated as in *Diprotodon*. The neural spines of the hind-most thoracic and all of the lumbar vertebrae are low and longitudinally broad. The distal ends of the lower thoracic and lumbar neural spines are expanded to form large, oval tuberosities related to the insertion of the transversospinalis group of back muscles. Judging from the series of small caudal vertebrae assigned to the species, the tail was weak, rapidly tapering and short. Ribs are poorly represented and fragmentary, though the curvature and length of some of the fragments indicate that the rib cage was deep and relatively wide (fig. 27).

Scapula

The blade of the scapula is ovo-rectangular, measuring 300 mm long by 153 mm wide (fig. 23A–C). The vertebral, caudal and cranial borders are strongly emarginated. The cranial border is convex above a wide, is nearly straight The vertebral border is convey, about 125 mm wide. The distinctly concave suprascapular fossa is about one-third the width (58 mm) of the infrascapular fossa (87 mm). The robust, slightly sinuous scapular spine traverses the entire length of the blade. It is greatly elevated proximally (51.5 mm), terminating in a 42 mm wide, strap-shaped acromion process. The coracoid process is short and blunt; divided from the glenoid fossa by a transverse groove. The glenoid cavity is oval, measuring 45 mm by 60 mm. An infraglenoid tuberosity is absent.

In *Kolopsis torus* the scapular blade is narrower overall and more acuminate at the vertebral border. A well developed infraglenoid tuberosity is present and the coracoid process is elevated into a low crest. In *Plaisiodon centralis* the infraglenoid region is expanded, but does not develop a distinct process or tuberosity. Its scapula otherwise resembles an enlarged version of that

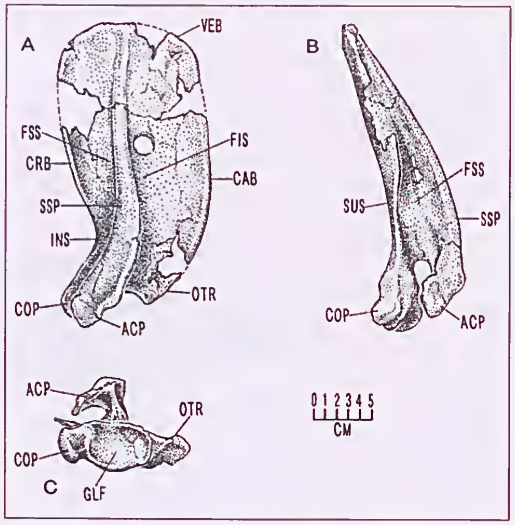

Figure 23. *Neohelos stirtoni* n. sp.; left scapula A, lateral aspect; B, anterior aspect; C, glenoid aspect (NTM P8695-273) Blast Site, Bullock Creek).

of *Neohelos*. In *Zygomaturus trilobus* the infraglenoid tuberosity is greatly elongated, extending below and behind the glenoid fossa in the form of a flange-like process. The vertebral border is distinctly pointed and rugose.

Humerus

The humeral diaphysis is robust, straight and triangular in section for most of its length. Its estimated length is 310–315 mm and its transverse dimensions are 40 mm by 45 mm above the deltopectoral tubercle (fig. 24A–B). The head is a broad, partial hemisphere about 55 mm by 55 mm, bounded laterally by a massive, rectangular major tuberosity and anteromedially by a thick transverse crest forming a minor tuberosity. A deep intertubercular sulcus is present between the two tuberosities, accentuated inferiorly by a sharp, very prominent pectoral crest that descends from the anterior side of the major tuberosity to the middle of the shaft. The pectoral crest merges with a flange-like deltopectoral eminence, which is buttressed distally by a pair of low crests originating from the entepicondylar bridge medially and from the lateral margin of the coronoid fossa laterally. The deltopectoral eminence is probably homologous to the deltoid tuberosity in vombatids, but it is not separated from the pectoral crest as in the latter.

Though damaged in the illustrated specimen, the supinator crest of the ectepicondyle is a wide, thin flange extending proximally for about one-third the length of the entire bone. The coronoid fossa is a large (39 mm x 30 mm x 3 mm), shallow, oval depression situated directly above the trochlea. The radial fossa immediately above the capitulum is smaller (20 mm x 20 mm x 3 mm). The distal articular surfaces are transversely wide, about 110 mm across. The arc of the articular surface of the trochle

is slightly flattened. It is relatively broad (>27 mm) and elongated (40 mm). The capitular articular surface is also slightly flattened, measuring approximately 35 mm by 35 mm.

The posterior surface of the humerus is nearly flat, being bordered by two crests; medially, a short low crest for the teres major muscle and laterally, by a longer crest for the brachioradialis muscle. The olecranon fossa is a sharply defined, oval depression measuring 35 mm x 20 mm x 5 mm. The humerus of *N. stirtoni* closely resembles that of *K. torus* in its basic morphology, but is relatively more robust. In both genera the pectoral component of the deltoid tuberosity is only weakly developed, whereas in *Zygomaturus trilobus*, a distinct pectoral tuberosity is developed adjacent to the deltoid tuberosity, similar to the condition in vombatids. Separate deltoid and pectoral tuberosities are also present in *Plaisiodon centralis*.

Ulna

The estimated length of the illustrated specimen is approximately 270 mm. The entire bone is compressed mediolaterally and tapers strongly toward the distal end. The olecranon process is short, terminating in a rugose, elliptical, superomedially-directed tuberosity (fig. 24C–D). The entire bone is gently bowed laterally and posteriorly. The medial surface of the ulna is predominantly concave and the lateral surface is flat to convex. A strong crest for the interosseous membrane overlaps the anterolateral margin of the shaft. The interosseous crest is continuous proximally with the supinator crest, which terminates at the ventral margin of the greatly expanded radial incisure of the semilunar cavity.

The coronoid process is a massive flange surmounted by a large, concave, circular articular surface for the trochlea. The radial incisure is shaped like a human ear, about 52 mm long; below which there is a large circular scar, the ulnar tuberosity, for the attachment of the brachialis muscle. Distally, the styloid process is a large hemispherical process situated in the centre of the ulnar capitulum. As with the other bones of the forelimb, the ulna of *Neohelos* is most similar to that of *Kolopsis torus*. The ulna of *Kolopsis* differs from that of *Neohelos* in being more lightly constructed and in having a short, transversely broader olecranon process. It is structurally intermediate between *Neohelos* and *Zygomaturus* in the state of this particular attribute.

Innominate

The estimated length of the innominate is approximately 400 mm from the base of the pubic ramus to the restored iliac crest. The iliac blade is relatively long and narrow, flaring distally into a crescentic iliac crest (fig. 25A–B). The iliac body is stout and triangular in section. The acetabulum is large, 67 mm x 73 mm. The dorsal acetabular crest is laterally expanded, greatly overhanging the acetabular fossa. A large, oval acetabular notch is present in the lower half of the acetabular fossa.

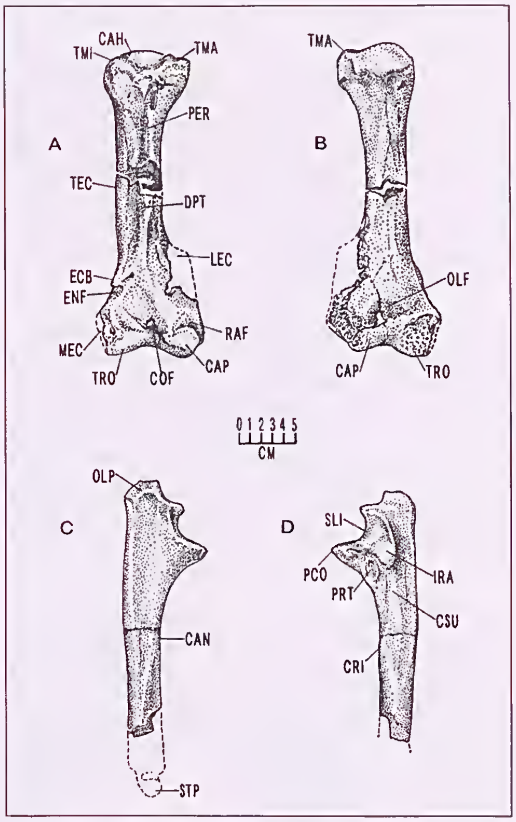

Figure 24. *Neohelos stirtoni* n. sp. from Blast Site, Bullock Creek; **A–B**, anterior and posterior aspect of left humerus (NTM P87108-30); **C–D**, lateral and internal aspect of left ulna (NTM P87103-45, P8695-278).

The ischial ramus is relatively elongated, terminating in a short ischial tuberosity. The obturator foramen is a large ovo-triangular-shaped vacuity 94 mm long. A low iliopectineal eminence is present. The innominates of both *Neohelos stirtoni* and *Kolopsis torus* are much narrower than that of *Zygomaturus trilobus* in which the iliac alae are greatly expanded laterally and the body of the ilium is short. The ischial ramus in *K. torus* is considerably shorter than that of *N. stirtoni*.

Femur

The proximal and distal ends of the femur are greatly expanded transversely relative to its shaft. The greater trochanter terminates in a rugose, conical tuberosity, expanding laterally into a thick, convex crest that extends down about one-third the length of the bone (fig. 26A–C). The large 65 mm x 65 mm, hemispherical femoral head projects dorsomedially about 65 mm beyond the midline axis of the diaphysis and overhangs the anteromedial surface of the diaphysis by approximately 35 mm. The lesser trochanter is a thin, convex flange extending from immediately below the medial side of the head to about the same level as the termination of the lateral crest of the greater trochanter.

On the posterior surface, the lesser and greater trochanters are united by a strong intertrochanteric crest for the iliofemoral ligament. The diaphysis is planoconvex to oval in section, about 47 mm minimum width. The posterior surface of the diaphysis is marked by a faint linea aspera with irregular, oval scars for the attachment of the adductor magnus muscle. A low ridge continues distally onto the popliteal surface, extending to the base of the medial condyle. Proximally, a deep, thickly emarginated trochanteric fossa extends about 40 mm into the trochanteric crest.

The condylar surfaces are complex and asymmetrical. Distally, the medial condyle is transversely narrower but anteroposteriorly longer than the lateral condyle. The condyles are separated posterodistally by a 30 mm deep, 20 mm wide intercondylar sulcus. The distal articular surface is greatly expanded anteriorly by an extensive rotular surface. The medial side of the rotular sulcus is elevated into a prominent, rounded crest. The lateral margin of the rotular sulcus is defined by a lower, sharper crest arising anteromedial to the ectepicondyle.

The estimated maximum length of the illustrated specimen is 320–325 mm. The femora of *Kolopsis torus* are more slender relative to their length than in *Neohelos* or *Zygomaturus trilobus*. The diaphysis in *K. torus* is more compressed anteroposteriorly than in *N. stirtoni*, but not to the extent seen in *Zygomaturus trilobus*, which has a more flattened oval section to its wider relative to length, femoral shaft.

Tibia

The proximal surface of the tibia is transversely wide. The medial condylar surface is concave and the lateral condylar surface is convex. The intercondylar eminence is a very prominent, 20 mm high triangular structure composed of a medial and a lateral tubercle separated by an oval pit. The tibial tuberosity is low and wide (fig. 26D–F). The tibial facet is 35 mm by 18 mm, overhanging the lateral surface of the diaphysis approximately 25 mm. The anterior (tibial) crest is smoothly rounded proximally, narrowing and merging distally with the interosseus crest. A strong popliteal crest runs down the proximal third of the posterolateral border of the diaphysis. Medially, about midway down the shaft, a sharp crest and rugose scar denotes the probable attachments of the tibialis anterior musculature.

The distal articular surface is elongated anteroposteriorly. The medial malleolus is a short, broad conical process situated directly in line with the tibial crest. The astragalar facet is an oval convex surface 40 mm by 30 mm. The total length of the illustrated specimen is 260 mm. The tibia *of N. stirtoni* is essentially identical to that of *Kolopsis torus* except for its greater robusticity. In *Zygomaturus trilobus* the tibial shaft is relatively more slender mediolaterally relative to its proximal and distal ends, than in *Neohelos* and *Kolopsis*. *Zygomaturus* has a more prominent tibial tuberosity and the entire bone is much shorter in relation to its anteroposterior width than in *Neohelos* and *Kolopsis*.

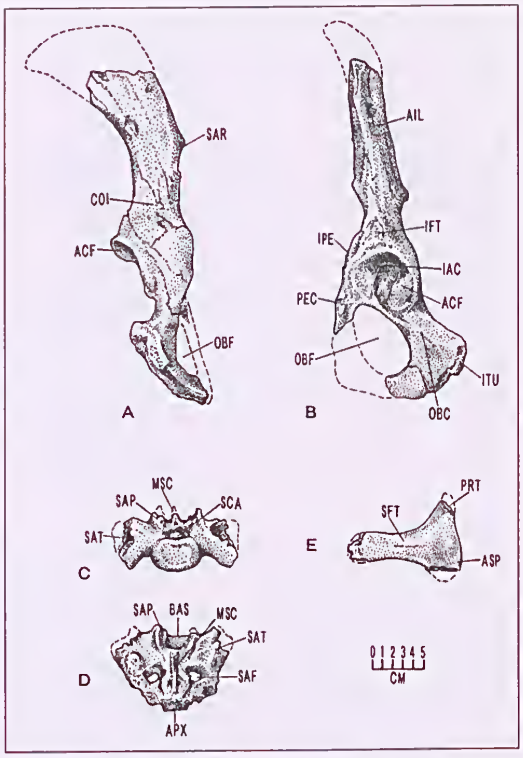

Figure 25. *Neohelos stirtoni* n. sp. from Blast Site, Bullock Creek. **A–B**, posterior and lateral aspects of left innominate (NTM P8695-274); **C–D**, anterior and dorsal aspects of sacrum (NTM P87108-31); **E**, left epipubic bone (NTM P8695-277).

Intermembral proportions between *Neohelos stirtoni* and *Kolopsis torus* are similar: the ulna is 0.86 of the length of the humerus in both species. The tibia is 0.80 of the length of the femur in *N. stirtoni* and 0.70 in *K torus*. In *Zygomaturus trilobus* the ulna is 0.70 of the length of the humerus and the tibia is 0.60 of the length of the femur. In *Plaisiodon centralis* the ulna is 0.75 of the length of the humerus and the tibia is 0.79 the length of the femur, its intermembral proportions being more like those of *Neohelos stirtoni* than the other zygomaturine species noted.

Weight estimations of *Neohelos stirtoni* calculated from Anderson et al.'s (1985) formula, which is based on upper limb bone diameters for quadrupedal mammals, suggest a mass of 250 kg for a large (male?) individual. For comparison, the same formula yields a mass of 673 kg for *Zygomaturus trilobus*. A small (female?) *Kolopsis torus* specimen may have weighed about 112 kg and a larger specimen (male?) may have weighed about 200 kg. Upper limb shaft diameters *of Plaisiodon centralis* indicate that this animal weighed about 550 kg. The postcranial elements have not been examined from a functional perspective, thus the characteristic standing posture of the

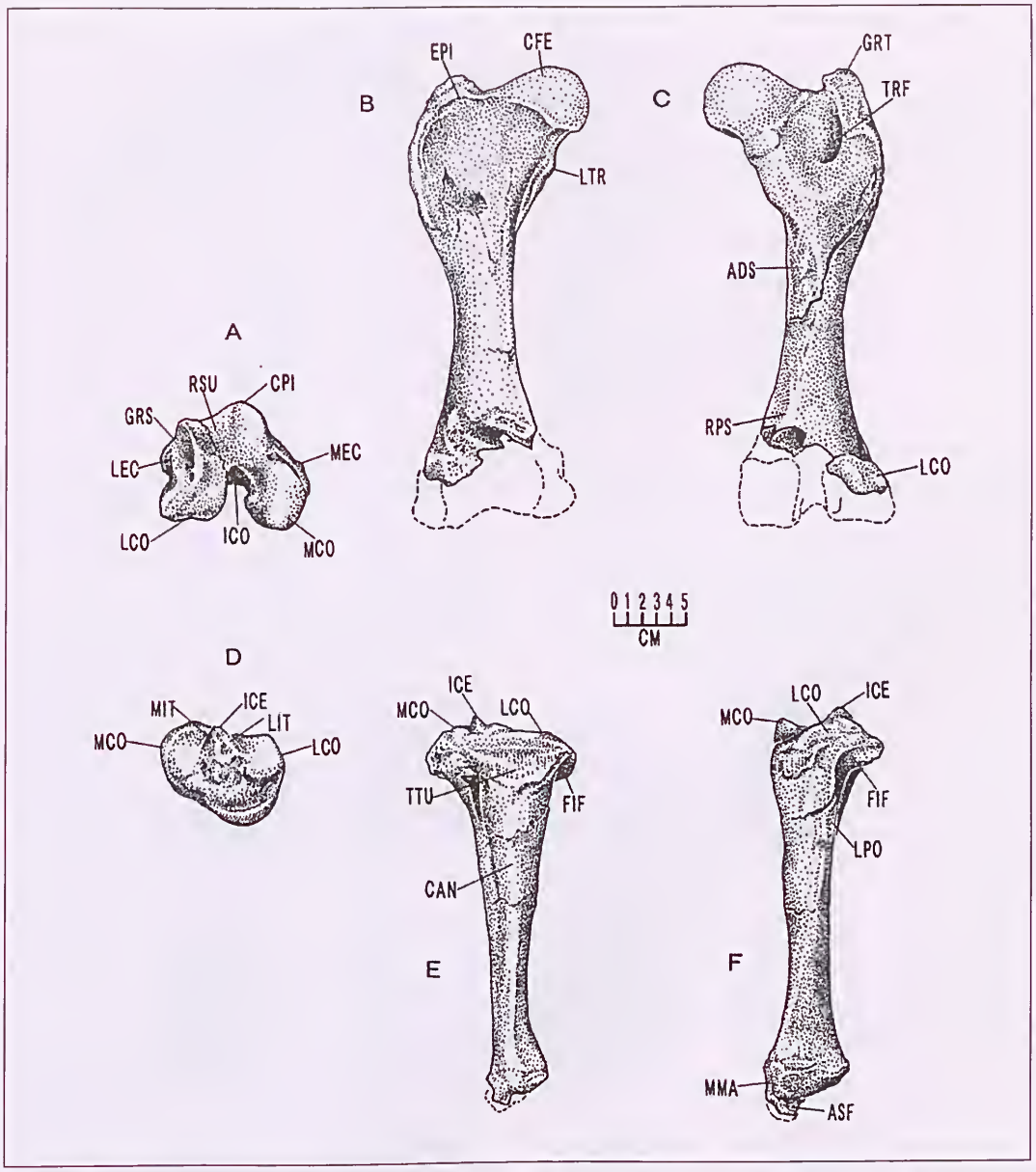

Figure 26. *Neohelos stirtoni* n. sp. from Blast Site, Bullock Creek. **A–C**, anterior and posterior aspects of right femur (NTM P8695-275, P87103-44); **C–D**, distal articular surfaces of femur; **E**, proximal articular surface of left tibia; **F–G**, anterior and fibular (lateral) aspects of tibia (P8695-276 / P87103-45).

animal is not known. *N. stirtoni* was about the size of a large ram, though more heavily built and shorter-limbed (fig. 27).

Variability in *Neohelos stirtoni*

By variation, we are referring to predominantly minor differences in traits or characters that have no apparent phylogenetic utility, though some labile characters in *Neohelos stirtoni* and other zygomaturines are applicable to systematic problems. Three types of variability occur in *Neohelos stirtoni*: 1) random and variable (including continuously varying) expression; 2) sexual dimorphism and age-related character expression and 3) on-off distribution of character states within groupings at various taxonomic levels.

By far the largest sample of *Neohelos stirtoni* comes from the Blast Site (Small Hills locality, Camfield). We have found no indication from the biological content or lithology of that quarry to suggest that more than one

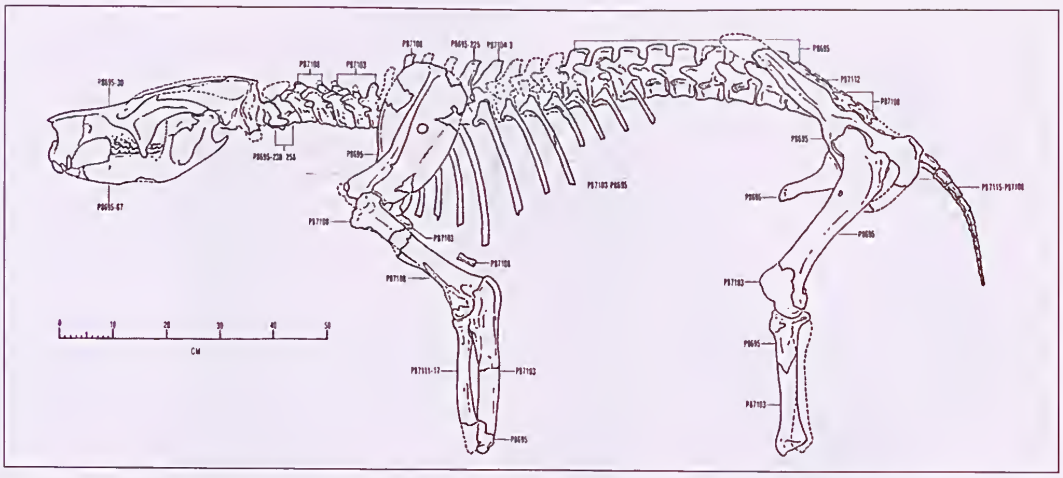

Figure 27. *Neohelos stirtoni* n. sp.; partial restoration of skeleton of Bullock Creek Local Fauna *Neohelos stirtoni* n. sp. NTM catalogue numbers of referred specimens are given on the illustrations. No attempt has been made to restore the posture of the animal.

stratigraphic horizon is locally present, and can find no basis for the discrimination of more than one morphospecies from this source. Therefore, the Blast Site sample is regarded as representing a population, and its features are treated as analogous to the variations recorded within a large living population.

Random and variable expression

Character lability is frequently seen in the morphology of the paroccipital-mastoid processes, which range from massive, inflated knobs in about one-third of individuals to slender, tapering projections in the majority. The expression of a supratympanic fossa ranges from absent in 28.6% of specimens, to well-developed, even multiple expressions in the rest. The posterior epitympanic fossa is absent in 43% of specimens. The tympanic bullae vary from relatively narrow and oval (50% of individuals), to broad and triangular in shape. Cranial nerve foramina vary considerably in size and expression, with accessory foramina being common.

Variability in palatal width and contour are not closely correlated with the overall size of the cranium or the cheek teeth, though there may be a tendency for small individuals to have broad palates. The palatal surfaces vary from nearly flat, to distinctly though shallowly, concave. Also apparently unrelated to the size of the individual, the frontal region varies considerably in its appearance ranging from smooth, roundly inflated frontal bosses in 40% of specimens to narrow, sharper crests in 60%.

The cheek teeth of *Neohelos stirtoni* are quite variable in appearance, particularly in the degree of development of cingulae, styles and minor proportions of the crowns. However, the dimensional range of variation of the molars does not attract specific comments here, other than to point out that there is not a close correlation between the size of the teeth (either expressed as tooth row length or individual crown dimensions) and the overall size of the cranium.

Because of its systematic importance, variability of the P^3 of *Neohelos stirtoni* is considered in more detail. The crowns vary in their expression of ancillary cusps, cingulae, overall shape, and form of their primary cusps (fig. 28; table 6). There is also considerable variation in absolute size and size of P^3 relative to M^2. Because the general impression of high variability is a somewhat subjective observation, we have compared the dimensions of the P^3 crown of *Neohelos stirtoni* with those of the closely-related zygomaturine species *Kolopsis torus* from the late Miocene Alcoota Local Fauna. In terms of dimensions length by width, the *N. stirtoni* P^3 examples yield a low correlation coefficient of r=0.55. The Pearson's coefficient of variation for crown lengths is 7.9 and for crown widths it is 6.7.

Comparing these figures with *Kolopsis torus*, the scatter is less diffuse and the correlation coefficient is higher at r=0.74. The Pearson's coefficient of variation in *Kolopsis* is 5.1 for crown lengths and 5.0 for crown widths. These examples indicate that the P^3 of *Neohelos stirtoni* is absolutely more variable than in *Kolopsis torus*, which is also very similar in size (*Neohelos* mean P^3 length=18.2 mm; width=15.8 mm; *Kolopsis* mean length=18.9 mm; width 15.3 mm). The differences in variability between the Alcoota sample and the Bullock Creek sample could be a reflection of a greater temporal range at Bullock Creek, or it could represent a condition inherent to the entire genus.

The most interesting aspect of the P^3 variability in *Neohelos stirtoni* is that certain occasionally expressed features are similar to characteristically fixed, often apomorphous characters of other genera. The more obvious variations include expression of a 'hooked' parastyle characteristic of *Nimbadon* and *Plaisiodon* in

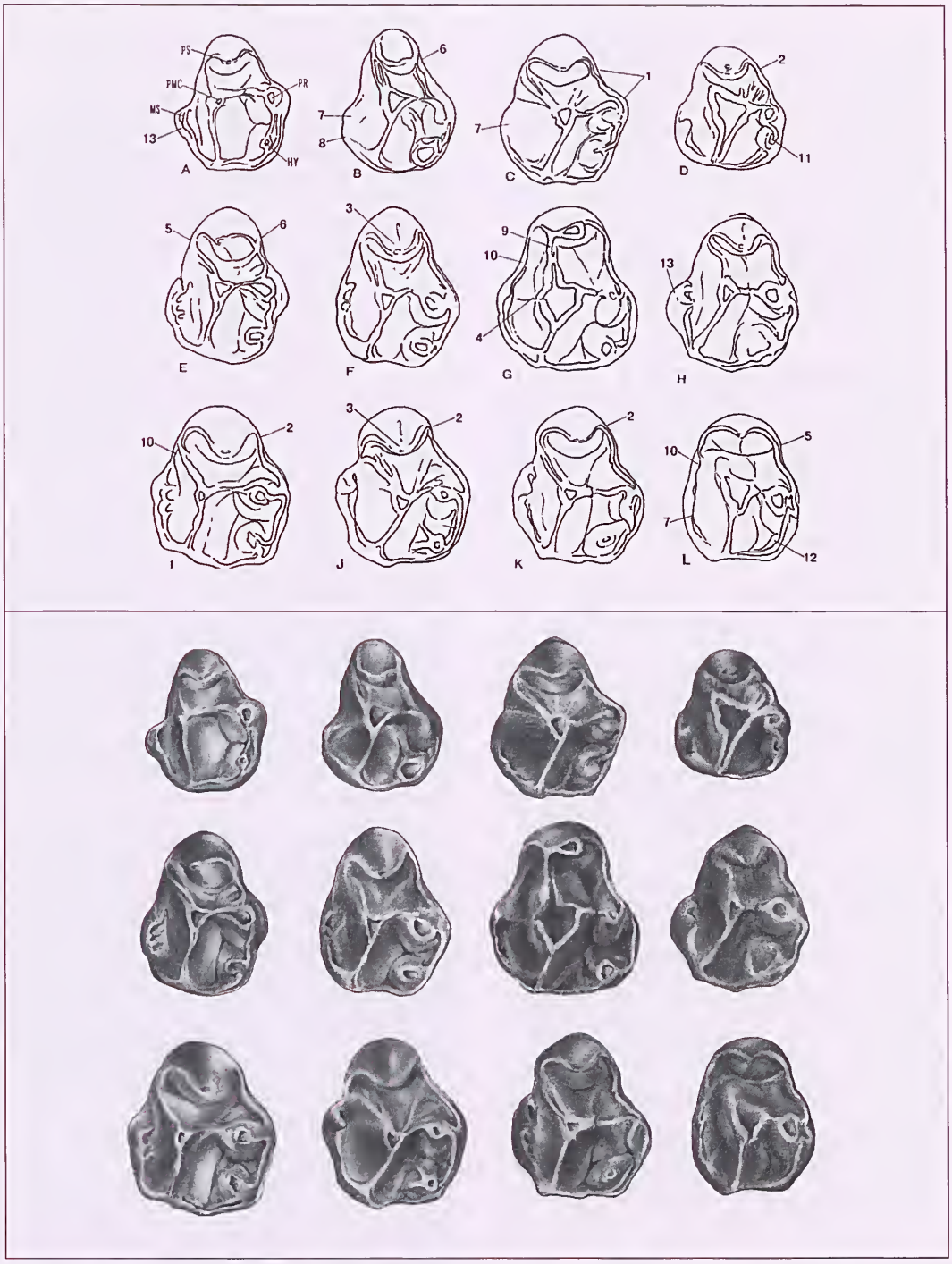

Figure 28. Line and shaded drawings of some morphological variations of the right P^3 of *N. stirtoni*. Numerals on line diagrams denote specific character variations: **1**, strong compared to **2**, weak emargination between protocone and parastyle; **3**, posteriorly inclined or 'hooked' parastyle; **4**, incipient division of paraeone and metaeone (note division of pair of enamel bulges by a faint sulcus on labial side of parametaeone); **5**, strong labial crest on parastyle; **6**, strong lingual crest on parastyle; **7**, absence of mesostyle; **8**, weak-absent posterolabial cingulum; **9**, elevated crest connecting parastyle with parametaeone; **10**, well-developed anterolabial cingulum; **11**, small hypocone closely pressed to (twinned from?) the protocone; **12**, hypocone absent; **13**, large labially projecting mesostyle is absent or poorly developed in this species.

about 6% of the *Neohelos stirtoni* population, and the presence of a high preparaconal crest like that of *Kolopsoides* in 13% of *Neohelos stirtoni* specimens. Twenty-three per cent of *Neohelos stirtoni* have a strong anterolabial cingulum as in *Kolopsis torus* P^3s; 3% have incipiently divided paramctacones anticipating the more derived genera *Kolopsis* and *Zygomaturus*. As a key character, the hypocone is absent in a small number of individuals of *Neohelos stirtoni.*

There are very few isolated otherwise 'apomorphous' P^3 traits of other zygomaturine species that are not expressed to some degree by individual *Neohelos stirtoni* specimens.

Sexually dimorphic and age-related traits

The *Neohelos stirtoni* assemblage presents a striking range of sizes and shapes, some crania being nearly twice the size of others; some broad and low with deep maxillae; others being narrow, elongated or 'stretched' variants. Some individuals have strong sagittal crests, whereas others have none; some individuals have broad, distally flared snouts while others are narrow or even somewhat pointed (figs 29–31). The zygomatic arches of some individuals are deep and strongly convex, whereas in others they are shallow and relatively straight.

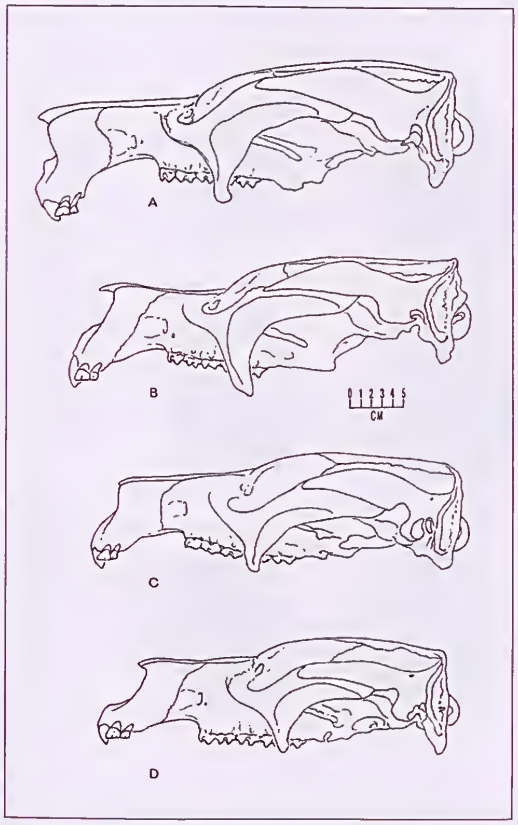

Figure 29. Restored crania of *Neohelos stirtoni* n. sp. from Bullock Creek showing variation probably as an expression of sexual dimorphism; **A**, ? male (NTM P8695-38); **B**, ? male (NTM P8697-1); **C**, ? female CPC 22200 (type); **D**, ? female (NTM P8551-13).

The masseteric processes range from elongated and transversely flattened to short, slender and conical. In 50% of the specimens with the snout preserved, the anterior end of the rostrum is elevated and dorsoventrally expanded overall, from the incisor alveoli to the top of the nasals (fig. 30E–F). This configuration would result in a distinctive snout profile in a living animal. It is, therefore, possible that exaggeration of the anterior end of the rostrum in *Neohelos stirtoni* anticipates the development of conspicuous nasal bosses in *Zygomaturus*. Some dentary horizontal rami are nearly twice as deep, though about the same length as others. The gonial angle of the ascending rami ranges from perpendicular to the longitudinal axis of the horizontal ramus to a distinctly obtuse angle of 120° or more (fig. 31I–J). Variations also occur in the angle of the dentary symphysis and implantation angle of the lower incisors.

It is often difficult to substantiate sexual dimorphism in fossil populations due to small sample sizes and the difficulty of distinguishing sexually dimorphic characters from merely size-related allometric relationships. That a component of the variability of *Neohelos stirtoni* may be due to sexual dimorphism can be drawn from analogy with other sexually dimorphic mammalian species. In the case of *N. stirtoni*, though the usable sample size of complete crania is small, the dimensions of the sagittal crest and the narial aperture show an indication of bimodality in their distribution, which is probably more indicative of sexual dimorphism than it is of simple growth allometry.

Estimates of sexual dimorphism in cranial dimensions of Bullock Creek *Neohelos stirtoni* range from about 25% to 50%. Other variations in cranial and dentary shape seem to be related to stage of growth and a considerable range in individual body sizes and shapes in both sexes. The horizontal ramus tends to deepen as the animals mature, although the deepest and most robust jaws probably belong to males. It seems reasonable to assume that the deep dentaries would be associated with crania having deep maxillae. The variation in the angle of the horizontal ramus may be correlated with extremes in cranial length, but there are no associations of dentaries and crania to substantiate these remarks.

On / off distribution of character states

Certain characters appear to oscillate between genera, species or higher taxa with no apparent phylogenetic significance, though such characters may be consistently present or absent within a particular species and thus be useful in distinguishing a taxon. The presence or absence of the posterior mental foramen and the masseteric foramen are typical on / off traits in many diprotodontian groups. In *Neohelos stirtoni* the masseteric foramen is present, whereas it is usually absent in closely related *Kolopsis torus*. *Alkwertatherium webbi* lacks the foramen whereas it is present in *Plaisiodon centralis*.

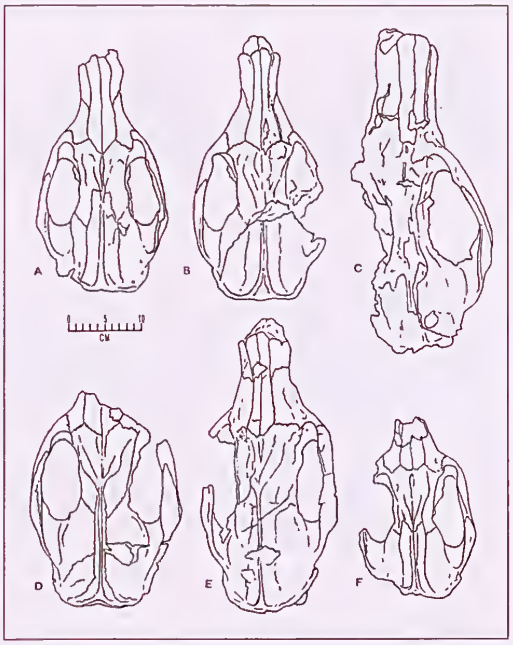

Figure 30. **A–F**, dorsal aspect of crania showing variability in shape and size of adult crania of *Neohelos stirtoni* n. sp. from Bullock Creek suggestive of sexual dimorphism; **A**, NTM P8551-13; **B**, CPC 22200 (type); **C**, NTM P8695-38; **D**, NTM P87018-1; **E**, NTM P8697-1; **F**, NMV P187283.

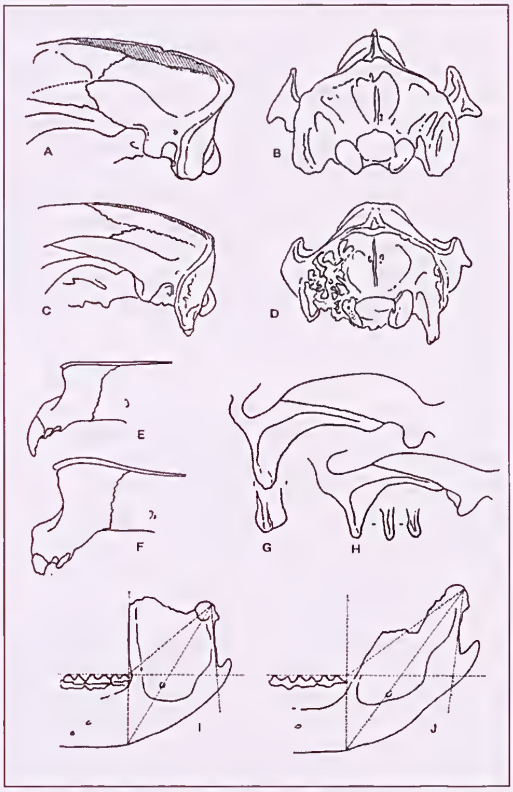

Figure 31. Examples of variable attributes in the skull of *Neohelos stirtoni*; **A–D**, sexually dimorphic variation in the sagittal crest; **E–F**, sexually dimorphic variation in shape of rostrum; **G–H**, variations in zygomatic arch depth and relative development of masseteric processes; **I–J**, variation in shape and inclination of posterior part of dentary.

Marshall et al. (1994, p. 12283) observe that in populations undergoing adaptive radiation '... features may "flicker" on and off, resulting in a distribution of character states that does not reflect the phylogeny of the group.' They state that unexpressed genes and dormant developmental pathways for such traits may be successfully reactivated as long as six million years after their disappearance, but after ten million years, the possibility of reactivation of the character becomes remote. Marshall et al.'s (1994) conclusions have important consequences for cladistic methodology in that on-off character expression in rapidly speciating groups is likely to result in considerable homoplasy. Because cladistics favours the most parsimonious cladogram, a more complex, though perhaps more accurate phylogenetic reconstruction, is likely to be rejected.

The maintenance of a high degree of individual variability within the *Neohelos stirtoni* population may have some significance in subsequent zygomaturine radiations. General heteromorphy could be linked to sexual selection for large body size in males resulting in extending overall morphological range of the species. A bull and harem type of mating pattern, often associated with sexual dimorphism, might result in smaller population isolates that would encourage a higher degree of individual variability within the general population.

However, it is likely that selection for sexual dimorphism and maintenance of individual variability within the *Neohelos* populations are subsets of predominantly environmental selective factors As indicated by recent palaeoenvironmental evidence (Murray & Megirian 1992), northern and central Australia was already undergoing vegetational changes in the early-mid Miocene. *Neohelos* spp. appear to have been the most widespread early zygomaturine, having taken advantage of more open, possibly more varied and correspondingly less predictable, though sporadically more productive habitat. As a pioneer species, its niche confines were relatively broad with perhaps correspondingly wide morphological constraints. Regardless of the particular selective agencies, it is often the case that groups undergoing rapid speciation show high individual variability.

NEOHELOS PHYLOGENY

Zygomaturines originated from the Diprotodontinae as originally suggested by Stirton et al. (1967). Stirton et al. constructed an intercalary lineage of diprotodontids, the Nototheriinae, to denote the closer relationships of the more primitive diprotodontines *Pyramios* and

Nototherium to the zygomaturines. They were unable to further refine their hypothesis, because no structurally intermediate forms were known at the time. Two recently discovered zygomaturine genera provide evidence for the structural transition from primitive diprotodontine-like diprotodontids to primitive zygomaturines and from primitive zygomaturines to the typical zygomaturines represented by *Neohelos*. The structural succession from *Neohelos* to derived zygomaturine states found in Plio-Pleistocene genera, as proposed by Stirton and his colleagues, are supported by new evidence from anatomy and recently discovered structurally intermediate species (fig. 32; tables 7, 8).

Stirton et al. recognised the two-cusped P^3 of *Pyramios alcootense* as a structural predecessor to the zygomaturines because of its enlarged anterior lobe of the crown or presumptive parastylar base, and by the zygomaturine-like proportions of its protocone and parametacone (fig. 3). The structure of the P^3 in other diprotodontines is derived or autapomorphous (e.g. lophodont in *Diprotodon*) or plesiomorphic (palorchestid-like, as in *Ngapakaldia* and *Pitikantia*).

The recent discoveries of two primitive zygomaturines, *Silvabestius* Black (1997) and *Alkwertatherium* Murray (1990a) (fig. 32G, H) provide the previously lacking structural evidence for the origin of the Zygomaturinae from the Diprotodontinae. *Silvabestius johnnilandi* shows two primary zygomaturine apomorphies in its possession of a small, but distinct parastyle, with strongly developed associated crests and a large, lobate parastylar extension of the crown on the P^3, and in the expression of an alisphenoid ventral tympanic process. The species otherwise shows many close structural similarities with the diprotodontines, particularly *Pyramios alcootense*.

Alkwertatherium webbi possesses a large parastyle, though its P^3 remains primitive in lacking a hypocone. The cranium and dentary of *Alkwertatherium* also expresses strong phenetic resemblances with both *Pyramios* (spatulate lower incisors, fused dentary symphysis, palatal shape, slight obliquity of molars) and *Plaisiodon* (cranial shape, similarity of cheek teeth, palatal form and cranial base), suggesting that *Alkwertatherium* originated from a species closely related to the antecedent of four-cusped P^3 zygomaturines (Murray 1990a).

Three genera of zygomaturines possessing a P^3 with four primary cusps are currently recognised: *Neohelos*, *Plaisiodon* and *Nimbadon*, each being distinguished from the previously discussed genera by possessing a hypocone on the posterolingual corner of the crown (fig. 32C, D, F). As of 1994, following the publication of *Nimbadon* (Hand et al. 1993) our assessment of *Neohelos* did not differ significantly from their conclusions.

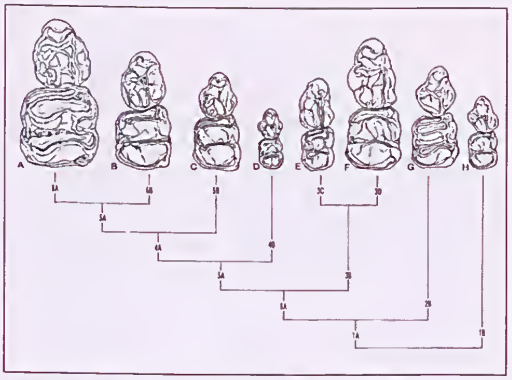

Figure 32. Diagram depicting primary nodes (genera) in zygomaturine phylogeny based on P^3–M^1 morphology. Illustrated representative genera and species: **A**, *Zygomaturus trilobus*; **B**, *Kolopsis yperus*; **C**, *Neohelos stirtoni*; **D**, *Nimbadon whitelawi*; **E**, *Kolopsoides cultridens*; **F**, *Plaisiodon centralis*; **G**, *Alkwertatherium webbi*; **H**, *Silvabestius johnnilandi*. Character states as follows:

1: Anterior part of crown elongated, incipient parastyle evident
- 1A: P^3 parastyle large
- 1B: P^3 parastyle small, base from precingulum, hypocone absent

2: P^3 parastyle large
- 2A: P^3 hypocone present
- 2B: P^3 hypocone absent

3: Hypocone present
- 3A: P^3 with posterolabial cingulum and mesostyle
- 3B: Posterolabial cingulum and mesostyle absent on P^3
- 3C: P^3 parastyle conjoined to PMC by crest, hypocone>protocone
- 3D: P^3 parastyle hook-like, crown elongated

4: P^3 with posterolabial cingulum and mesostyle
- 4A: M^1 broad with large parastyle and metastyle
- 4B: M^1 narrow with reduced parastyle and metastyle

5: M^1 broad with large parastyle and metastyle
- 5A: P^3 parametacone divided into paracone and metacone
- 5B: P^3 parametacone undivided and M^{1-3} postcingulum continuous horizontally aroundmetaconule

6: Parametacone of P^3 divided
- 6A: M^1 parastyle and metastyle reduced, square outline
- 6B: M^1 parastyle and metastyle large, trapezoidal outline.

The relationships among these very similar genera are not completely resolved by phylogenetic analysis due to the obfuscation of characters by the derived states of *Plaisiodon* and the fineness of the character distinctions in question, which are at the level of species discriminations. *Plaisiodon* is so far known from only one late Miocene species. Although considered among the four-cusped P^3 forms, *Plaisiodon centralis* shows an elongation of the parametacone and an incipient lobate division of the parametaconal crest (fig. 33C–D).

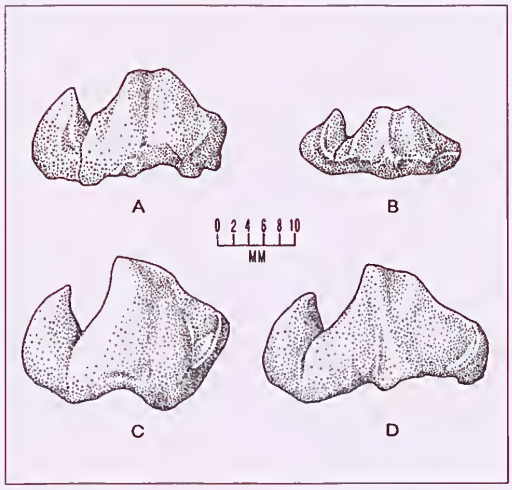

Figure 33. Comparison of P^3s of zygomaturine species in which the parametacone is divided into two cusps. **A**, *Kolopsis yperus*; **B**, *Kolopsis torus*; **C–D**, *Plaisiodon centralis*.

The possibility of a close relationship between *Kolopsoides* and *Plaisiodon*, as first suggested by Archer (1984) is supported by a number of shared derived features of the P^3 including incipient division of the parametacone, reduction or loss of a posterolabial cingulum, elongation of the crown and posterior inclination of the parastyle. Other strong similarities include asymmetrically curved, pointed upper incisors and a rounded anterior cristid of the P_3 protoconid. It is, therefore, likely that the presence of a transversely divided parametacone in *Kolopsoides*, which was originally interpreted by Plane (1967) as apomorphous with *Kolopsis*, represents a homoplasious synapomorphy with *Plaisiodon* (table 7).

The fifth primary cusp of the zygomaturine P^3 is represented by a transverse division of the parametacone into two distinct cusps (fig. 32A-B). Five zygomaturine genera are known to share this apomorphic state: *Kolopsis* spp., *Zygomaturus* spp., *Maokapia*, possibly *Hulitherium* and the previously mentioned genus *Kolopsoides*. We have situated *Neohelos* as the morphological basis of a complex crown group represented by a cluster of species in the genera *Zygomaturus* Owen, *Maokapia* Flannery, *'Kolopsis' rotundus* Plane, *Hulitherium* Flannery and Plane and *Kolopsis* Woodburne.

A few specimens of *Neohelos stirtoni* show twinning of the P^3 to a lesser degree (e.g. NTM P87115-8 and P8695-61). These variants also possesses a strong anterolabial cingulum and an elevated crest between the parastyle and the anterolabial crest of the parametacone, which is frequently present in *Kolopsis torus*. Consequently there is an indication that *Neohelos stirtoni* is potentially close to the ancestry of, if not directly ancestral to, *Kolopsis torus*.

Fossil evidence from Alcoota (Ongeva Local Fauna) indicates that *K. yperus* Murray, Megirian and Wells, 1993, is structurally antecedent to, or perhaps synonymous with *Zygomaturus gilli*. *Zygomaturus gilli* is known only from an isolated premolar, which we do not consider to be sufficient evidence for the assignment of the specimen to the genus *Zygomaturus* because the character states of its M^2 are not known. *K. yperus* has been retained in the genus *Kolopsis* because of certain symplesiomorphic similarities, which contrast with derived states of *Zygomaturus*; primarily in its retention of large styles on the M^2 and its retention of a large P^3 relative to M^2, the former being reduced in all Plio-Pleistocene members of the *Zygomaturus* clade (Murray 1992).

The Beaumaris '*Kolopsis*' specimens (MVP15911, P16279) variously assigned to *Z. gilli* (Woodburne 1969) or K sp. (Rich 1976) remain taxonomically ambiguous, primarily due to the lack of an associated P^3. This species has relatively high-crowned, transversely narrow lower molars with strong metalophids and conspicuous apical crests on the anterolabial and anterolingual cuspids of each lophid. The P_3 is similar to that of *Kolopis torus* in possessing a strong anterolabial cingulid. Unlike *Kolopsis* spp., the Beaumaris species possesses a masseteric foramen. However, the lower molars of *Neohelos stirtoni* and *Kolopsis torus* appear to be proportionally and structurally more alike than either species is to the Beaumaris form. Because a masseteric foramen is present in one specimen (the region is obscured by matrix in the other), and because the molar crowns are more narrow

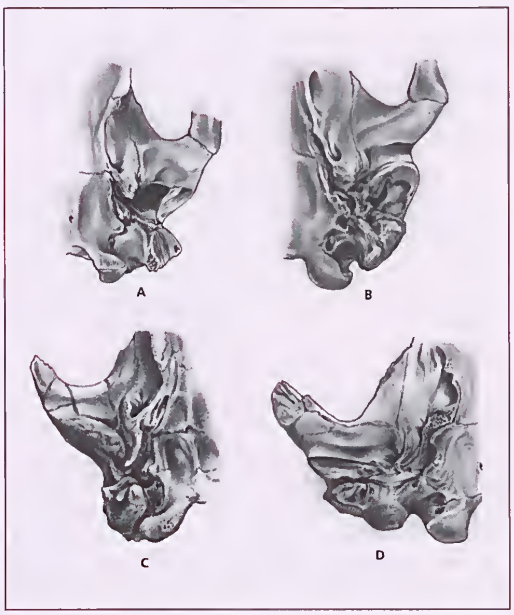

Figure 34. Comparison of the stuctures surrounding the middle ear in the cranial bases of **A**, *Silvabestius johnnilandi*; **B**, *Neohelos stirtoni*; **C**, *Kolopsis torus*; **D**, *Zyogmaturus trilobus*.

relative to their length in comparison to *Kolopsis torus* than compared to known *Neolhelos* species, it is possible that it represents another, more derived species of *Neolhelos*. However, it does not seem possible to resolve the position of this form without the evidence of the upper premolar.

An account of the morphological evidence for the proposed phylogeny of the later Zygomaturines is given by Murray (1992). In general, the available fossil evidence points to a radiation of heavy-bodied zygomaturine browsers with short, deep snouts, broad crania, with upward flexion of the basicranial axis, tusk-like, divergent upper central incisors and frontated orbits. Species of the *Zygomaturus* clade became gigantic on mainland Australia and Tasmania (*Z. trilobus*) and became dwarf-like in New Guinea (*'Kolopsis' rotundus*, *Hulitherium*, *Maokapia*). The immediate antecedent(s) of this group of genera (*Zygomaturus*, *Maokapia*, *Hulitherium*) have not been identified, although *Zygomaturus gilli* and *Z. keanei* remain in essentially the same basal relationship to the radiation that was postulated by Stirton et al. (1967).

The comparative anatomy of the cranial base in zygomaturines reinforces the broad outlines of gradual structural changes leading from primitive zygomaturines to the genus *Zygomaturus* as proposed by Stirton et al. (1967). Evidence from *Silvabestius johnnilandi* shows the plesiomorphous state of structures surrounding the middle ear (figs 34–35). Its structural relations are fundamentally similar to that of *Ngapakaldia*: the epitympanic fenestra is large, the postglenoid process is poorly developed, low and thin, and the entoglenoid eminence and tympanic process is low and relatively small. Unlike *Ngapakaldia* and diprotodontines, the ventral surface of the tympanic process is composed of the alisphenoid instead of the squamosal, as in all members of the Zygomaturinae.

In *Neolhelos* the basic structural relationships are similar to *Silvabestius johnnilandi* but the hypotympanic sinus within the tympanic wing is enlarged and the postglenoid process has become elevated and expanded mesially and posteriorly (figs 34B–35B). The ventral crest of the postglenoid process has overgrown its posterior margin to partially seal off the epitympanic fenestra.

In *Kolopsis torus* the posterior wall of the postglenoid process is complete, entirely sealing off the epitympanic fenestra (figs 34C–35C). The inner corner of the postglenoid process has encroached medially to contact the posteriorly elongated alisphenoid tympanic process, which is compressed into a narrow crest. The wide contact between the postglenoid process and the alisphenoid crest eliminates the ventrally open glenoid notch that connects the tympanic cavity with the glenoid fossa in *Neolhelos stirtoni*, but which, in *Kolopsis torus*, has become a partially enclosed glenoid canal.

In *Zygomaturus trilobus* the crest-like alisphenoid tympanic process has become fused with the base of the mastoid forming a complete tympanic wing over the tympanic cavity and has become situated parallel with, and posterior to the postglenoid process (figs 34D–35D). The postglenoid process has become oriented nearly at a right angle to the basicranial axis and all elements surrounding the middle ear are strongly fused.

The progressive fusion of the elements over the middle ear cavity in zygomaturines is chronologically successive and non-disjunctive anatomically, providing clear evidence of gradual evolution over a period of 15 to 20 million years. An analogous process appears to have occurred in the Diprotodontinae, in which the Plio-Pleistocene genera *Euryzygoma* and *Diprotodon* have also undergone a process of fusion of the structures surrounding the middle ear (fig. 36G–H).

Although much less is known of the evolution of the posteranial skeleton of the Zygomaturinae, especially the earlier forms, we have some evidence of a structural succession leading from *Neolhelos* to *Kolopsis* and *Zygomaturus*. The posteranial skeletons of *Neolhelos* and *Kolopsis* are very similar except for certain features of the forelimb, in which *Kolopsis* shows some similarities with *Zygomaturus*. In *Neolhelos* the vertebral border of the scapula is broad, whereas it is narrower and more pointed in *Kolopsis* (fig. 37A, C). A rudimentary infraglenoid tuberosity is present in *Kolopsis* which is not present in *Neolhelos*. In *Kolopsis* the olecranon process of the ulna is

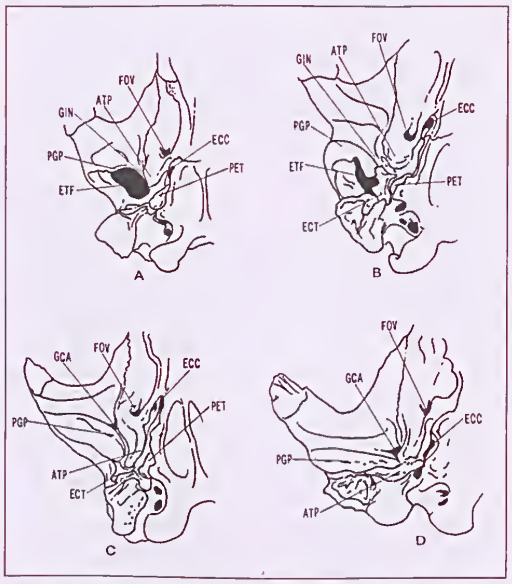

Figure 35. Diagrams showing evolutionary trends in the middle ear structural relations in a chronological sequence from **A**, early Miocene *Silvabestius johnnilandi* (reversed for comparison with C–D); **B**, middle Miocene *Neolhelos stirtoni*; **C**, late Miocene *Kolopsis torus*; **D**, late Pleistocene *Zygomaturus trilobus*.

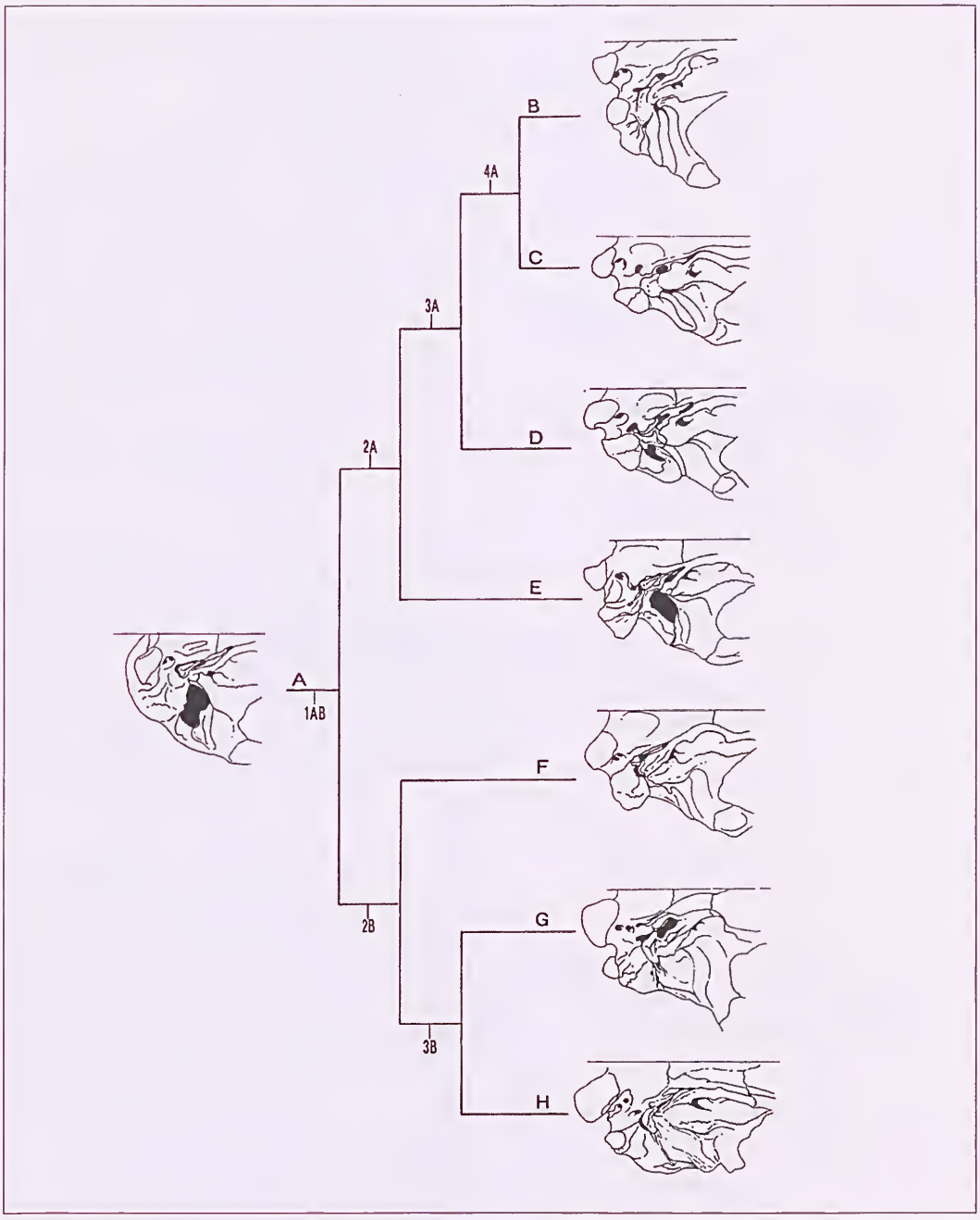

Figure 36. Phylogeny of the Diprodontidae determined by the morphology of the basicranium of representative genera: **A**, *Ngapakaldia tedfordi* is depicted as representing the plesiomorphic state for the family Diprotodontidae. **B–E** are members of subfamily Zygomaturinae; F–H, are members of subfamily Diprotodontinae. B, *Zygomaturus trilobus*; C, *Kolopsis torus*; D, *Neohelos stirtoni* n. sp.; E, *Silvabestius johnnilandi*; F, *Pyramios alcootense*; G, *Euryzygoma dunense*; H, *Diprotodon* sp.; Apomorphies at designated notes: 1AB=large epitympanic fenestra, weak postglenoid process and squamosal tympanic process; 2B=wider, deeper, but thin postglenoid process, not fused to posterior or mesial elements; reduced or absent epitympanic fenestra, squamosal tympanic process enlarged; 3B=posterior elongation and fusion of the postglenoid process mesially with the tympanic process and with the mastoid-squamosal posteriorly forming complete auditory meatus; 2A=alisphenoid tympanic process; 3A=reduced epitympanic fenestra, inflated entoglenoid eminence or bulla; 4A=loss of epitympanic fenestra, elongation and fusion of alisphenoid tympanic process and postglenoid process.

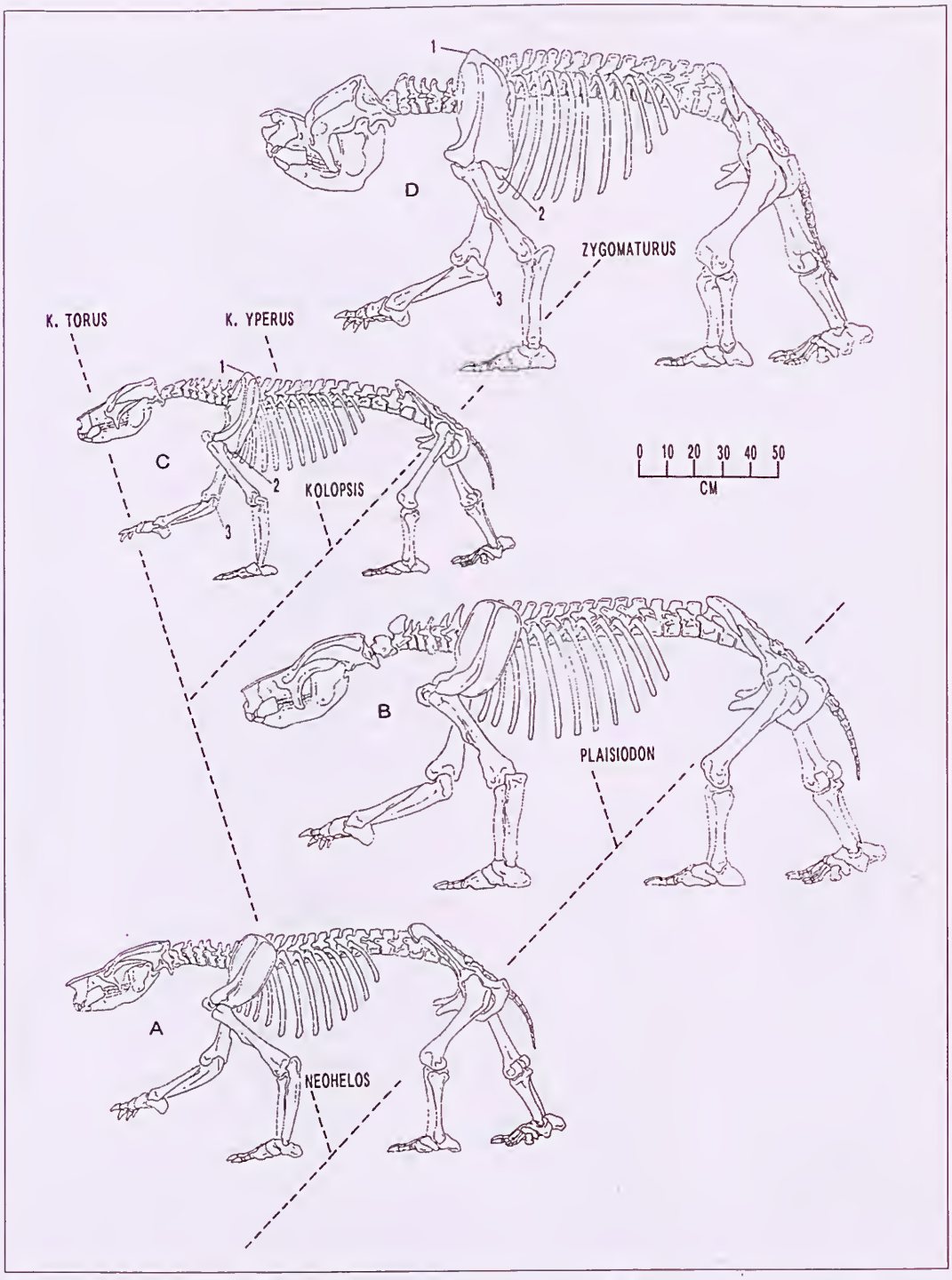

Figure 37. Restored skeletons of **A**, *Neohelos stirtoni*; **B**, *Plaisiodon centralis*; **C**, *Zygomaturus trilobus*; broken lines indicate relationships based on postcranial morphology: *Neohelos–Plaisiodon*=symplesiomorphous; *Kolopsis–Zygomaturus*=synapomorphous: 1, similarity in olecranon process shape; 2, pointed, thickened vertebral border of scapula; 3, elongated infraglenoid process. The form of the manus and pes are inferred from incomplete material, some of which is known for each genus depicted. All of these genera have laterally flanged 5th metatarsals and metacarpals, large calcanei and pisiforms, large ungual phalanges on both manus and pes, short, broad phalanges and reduced metatarsals II–III.

transversely expanded in comparison to that of *Neohelos*. Each of these characters appear to be transitional states between *Neohelos stirtoni* and *Zygomaturus trilobus* (fig. 37A, C, D).

The postcranial morphology of *Plaisiodon centralis* is proportionally more similar to that of *Neohelos* than the other zygomaturine genera for which the posteranial skeleton is reasonably well-known (fig. 37B). *Plaisiodon centralis* is derived relative to *Neohelos* and homoplasious relative to *Kolopsis* and Zygomaturus in possessing a broadened infraglenoid table of the seapula, which however, is not developed into a distinct process. As in *Neohelos*, the vertebral border is broad and relatively thin, rather than narrow and thickened, as characteristic of *Kolopsis* and *Zygomaturus*. The oleeranon process of the ulna of *Plaisiodon* is broad compared to that of *Neohelos* but takes the form of a very short, flattened tuberosity, quite distinct from that of *Kolopsis* and *Zygomaturus*.

As in *Zygomaturus*, but not *Neohelos* or *Kolopsis*, a distinct pectoral tuberosity appears to have been present adjacent to a well-developed deltoid tuberosity. Because this region is damaged in all of the available specimens of *Plaisiodon*, a more detailed comparison with the humerus of *Zygomaturus* must await a more perfect specimen. Comparisons of the available posteranial material indicates that *Neohelos* is the more suitable structural precursor to the lineage leading to *Zygomaturus*. *Plaisiodon centralis* is too derived in certain features, while otherwise retaining a majority of states closely resembling those of *Neohelos*.

CONCLUSIONS

A vast collection of *Neohelos stirtoni* n. sp. material has been recovered from the Bullock Creek area, Northern Territory. The specimens are preserved as rich concentrations of isolated or loosely associated bones in a freshwater limestone. While skulls and jaws predominate, posteranial elements are quite common. Despite occurring at four sites in the Camfield Beds scattered over a distance of 5 km, there is no evidence forthcoming to suggest that this material accumulated during a significant period of geologic time.

The skeleton of *Neohelos stirtoni* n. sp. is intermediate in size between the oldest known zygomaturines and the late Miocene–Pleistocene *Zygomaturus*. The Bullock Creek material of this species provides a firm basis for estimating the amount of intraspecific variation to be expected within intermediate-sized zygomaturines.

ACKNOWLEDGEMENTS

We thank the Managers of Camfield Station, past and present, for their hospitality and continued interest and support. Financial support from the National Estate Grants Program (Northern Territory) and the Australian Research Council is gratefully acknowledged. We thank our various excavation teams, composed of students, volunteers and colleagues, for their great efforts. Leslie Kool and Michael Whitelaw (Monash University) and Richard Brown (Bureau of Mineral Resources) are thanked for preparation of specimens. We are indebted to Drs William Clemens, Richard Tedford, Michael Woodburne and Tim Flannery for their valuable comments on the original manuscript.

NEOHELOS		ZYG	MAO	KOL	NIM	KOD	PLA	ALK	SIL
I_1	lanceolate with ventrolabial groove and lingual longitudinal crest	tusk-like	tusk-like	V–L groove absent	unknown	spatulate	V–L groove	spatulate and lingual crest absent	unknown
I^1	mesially flattened, pointed crown	tusk-like	tusk-like	=*Neohelos*	unknown	=*Neohelos*	=*Neohelos*	unknown	=*Neohelos*
I^2	mesiodistally elongated , triangular occlusal surface with 1–2 vertical grooves labially	=*Neohelos*	=*Neohelos*	=*Neohelos*	unknown	unknown	elliptical occlusal surface	unknown	unknown
I^3	short triangular occlusal surface shallow labial groove or sulcus	=*Neohelos*	=*Neohelos*	=*Neohelos*	unknown	unknown	=*Neohelos*	unknown	unknown
Canine	present or entirely absent	absent	absent	absent	present	absent	absent	absent	present
P^3	4 primary cusps, variable mesostyle, medium-large parastyle with labial crest separated from paracone by transverse sulcus; cuspate PMC with loph connected to protocone, small hypocone connected to protocone by short lingual crest	5 cusps	5 cusps	5 cusps	loph to cingulum	5 cusps, hypocone >protocone, parastyle connected to paracone by crest	mesostyle, labial crest absent	hypocone absent	parastyle incipient, hypocone absent
M^1	length=P^3, narrow, curved protoloph, large parastyle and metastyle, wide IP contact	L>P^3 styles reduced	L>P^3 styles reduced	=*Neohelos*	styles small narrow	L<P^3 styles small IP contact	L<P^3	styles small	styles small
P_3	conical main cuspid with anterior and posterior median crests and anterobasal cuspid or pit; crown shorter than M_1	=*Neohelos*	=*Neohelos*	=*Neohelos*	=*Neohelos*	anterior crest absent L>M_1	anterior crest absent	anterior crest absent	unknown
M_1	narrow elongated trigonid, protolophid narrower than hypolophid; prominent paralophid crest, weak metalophid	=*Neohelos*	=*Neohelos*	=*Neohelos*	distinct protostylid	strong metalophid	strong metalophid	short trigonid, weak paralophid	unknown

Table 1. Summary of diagnostic features of the genus *Neohelos* Stirton; Abbreviations: ZYG =*Zygomaturus*; MAO = *Maokapia*; KOL = *Kolopsis*; NIM =*Nimbadon*; KOD =*Kolopsoides*; PLA =*Plaisiodon*; ALK =*Alkwertatherium*; SIL =*Silvabestius*.

UPPER CHEEK TEETH OF *NEOHELOS STIRTONI* N. SP. (MM)

			P3		M1			M2			M3			M4		
SPECIMEN	SITE	SIDE	L	W	L	AW	PW	L	AW	PW	L	AW	PW	L	AW	PW
CPC 22188	Blast Site	L	19.2	15.3	19.6	16.6	17.5	20.9	19.4	18.6	22.3	20.7	18.4			
CPC 22188	Blast Site	R	19.4	15.8	18.8	16.7	17.5	21.0	19.0	19.1	22.0	20.2	18.3			
CPC 22191	Blast Site	L	18.5	16.8	20.6	19.8	17.7	22.1	20.0	18.5	23.6	21.7	18.7	23.1	20.2	15.4
CPC 22191	Blast Site	R	17.8	17.6	19.6	18.0	17.9	21.8	20.6	19.0	24.2	21.7	19.6	23.5	20.0	15.1
CPC 22192	Blast Site	L	19.1	17.8				21.7	20.0	19.7	22.4	21.0				
CPC 22192	Blast Site	R			20.0			21.5			22.4			22.1		
CPC 22193	Blast Site	R	20.2	16.6	20.0	18.5	18.7	21.3		19.7	23.6	22.1		21.8		
CPC 22200	Blast Site	L	19.4	16.3	20.4	19.4	20.2	22.1	21.9	21.5	24.4	22.3	20.5	24.2	20.0	16.9
CPC 22200	Blast Site	R	18.8		20.4	19.1		22.1	20.8	21.4	24.0	22.4	20.4	25.0	20.2	16.8
CPC 22525	Blast Site	L									23.0			23.9		15.9
CPC 22525	Blast Site	R								19.2	23.4			22.9		
CPC 22526	Blast Site	L	17.9	15.5	20.5	16.3	17.6	23.0	19.6	18.7	24.6	21.0	18.6	23.8	20.1	15.0
CPC 22526	Blast Site	R	19.6	15.1	20.2	16.1	17.5					22.2	18.8	25.0	20.0	14.9
CPC 22529	Blast Site	R			19.8	18.0	17.9									
CPC 22539	Blast Site	L	16.2	14.2	19.6	17.2	17.6	19.4	20.0	18.9	22.4	21.0	17.8	22.2	19.5	14.4
CPC 22539	Blast Site	R	18.3	15.5	19.6	17.5	17.9	21.0	19.4							
CPC 22539	Blast Site	R			19.1	17.1	17.4	20.6	20.0	18.9	23.4	21.1	17.9	21.8	19.2	14.6
CPC 22552	Blast Site	R						22.7		20.6						
CPC 22557	Blast Site	L	18.1	15.6		17.3										
CPC 22987	Blast Site	R	18.0	16.8	20.5	18.6	19.6	22.1	20.7	19.9		21.1				
CPC 34302	Blast Site	L	16.8	14.9	19.0	18.4	19.5		21.0	19.7						
NMV P179106	Top Quarry	L	16.2	14.4												
NMV P179159	Top Quarry	R	18.3	16.6												
NMV P179159	Top Quarry	R	19.2	17.2												
NMV P187283	Blast Site	L	16.2	15.4	17.4	16.4	17.0									
NMV P187283	Blast Site	R	17.6	15.2	17.2	16.1	16.4	19.6	18.0	18.5	21.0	19.3	18.0	21.9	18.2	
NMV P187284	Top Quarry	R						20.1	19.7	19.3	22.5	21.3	18.0	22.1	19.1	14.1
NMV P187285	Top Quarry	L	16.6	14.8	17.8	15.9	18.0	21.2	19.0	19.4	23.1	20.9	18.5	21.5		14.9
NMV P187286	Top Quarry	L									21.9	20.3	17.8	21.5	18.8	15.5
NMV P187287	Top Quarry	L	16.8	15.0	17.9	16.4	16.8									
NMV P194364	Horseshoe W	R	18.1	16.1	18.9	18.1	19.0									
NMV P194530	Horseshoe W	L						22.7	21.6	20.3	25.1	22.3				
NMV P194530	Horseshoe W	R						22.9	21.7	19.9		20.7				
NMV P194532	Horseshoe W	L	17.0	16.4	18.1	17.0	18.0	21.7	19.7	19.1	22.4	21.0	18.2	22.4	18.2	14.0
NMV P194534	Top Quarry	L												21.6	18.9	14.7
NMV P194536	Top Quarry	R												23.0	19.6	17.1
NMV P194537	Top Quarry	L									21.3	19.0	17.7			
NMV P194538	Camp Quarry	L	16.4	14.7	19.0	17.1	18.5									
NMV P194538	Camp Quarry	R	16.5	14.3	18.9	17.0	18.5	20.5	19.7	19.1	21.4	20.0				
NMV P194540	Horseshoe W	L									25.2	20.6	22.4			
NMV P194544	Top Quarry	R												27.5	19.4	15.4
NMV P194545	Top Quarry	R	16.7	14.6												
NMV P194548	Horseshoe W	R			19.0	17.5	17.6	20.1	18.0	18.4						
NMV P194551	Horseshoe W	R			21.3	18.4	19.9									
NMV P194552	Horseshoe W	L			19.5	16.8	17.7									
NMV P194553	Horseshoe W	L			19.2	16.9	17.5									
NMV P194554	Horseshoe W	R			19.1	16.5	16.5									
NMV P194556	Horseshoe W	L			19.3	16.0	17.0									
NMV P194558	Horseshoe W	L	17.8	15.5												
NMV P194565	Horseshoe W	R									18.8	21.5				
NMV P197892	Top Quarry	L	16.4	14.4	19.9	17.7	18.6	20.6	20.7	19.5	22.6	22.3	19.2	23.5	20.3	15.1
NMV P197892	Top Quarry	R	16.7	14.6	20.1	17.9	18.7	21.3	20.8	19.5	22.7	22.1	18.6	22.8	20.1	15.0
NMV P197894	Top Quarry	L			20.6	18.1	20.1	22.2	20.8	21.0						
NMV P197895	Top Quarry	R						23.4	22.4	20.5	23.2	22.3	19.1	22.4	20.3	15.1
NMV P197896	Camp Quarry	L									23.0	20.1	17.4			
NMV P197896	Camp Quarry	R												18.6		
NMV P198543	Camp Quarry	L	16.7	14.8	18.6	17.9	18.8	20.9	20.2	18.2						
NMV P201027	Top Quarry	R						20.4	21.3	19.7	22.4	22.1	18.8	22.4	20.5	15.8
NMV P201030	Top Quarry	L						19.4	18.4	18.0	21.1	19.4	17.5	21.1	18.7	14.8
NMV P205129	Top Quarry	L						18.9	19.0	17.9	21.5	20.8		21.2	18.9	13.8
NMV P205130	Top Quarry	R			19.2	17.9	18.2	21.0	20.3	18.4	22.5	21.0	18.1	21.2	19.6	14.8
NTM P8551-13	Blast Site	L	17.5	16.2	19.9	18.7	19.8	22.0	22.1	21.0	25.5	23.0	21.4	24.2	22.2	17.9
NTM P8551-13	Blast Site	R	17.6	16.3	19.4	18.0	18.9	21.9	20.9	19.2	24.2	20.1	19.0	24.1	20.6	15.6
NTM P8612-3	Blast Site	R	20.2	16.0												
NTM P8662-9	Blast Site	L						20.1		18.0	22.3					

UPPER CHEEK TEETH OF *NEOHELOS STIRTONI* N. SP. (MM) (cont.)

			P3		M1			M2			M3			M4	
SPECIMEN	SITE	SIDE	L	W	L	AW	PW	L	AW	PW	L	AW	PW	L	AW	PW
NTM P868-2	Blast Site	R	18.7	16.7	21.7	19.1	20.2	21.9	20.6	21.0	22.0	20.8	20.3		20.5	
NTM P8689	Blast Site	L	15.8	14.5	18.6	16.9	17.8	20.5	19.3	18.4						
NTM P869-4	Blast Site	R	16.0		18.5											
NTM P8690	Blast Site	L			19.0	16.1	16.9	20.5	18.9	18.4						
NTM P8690	Blast Site	R	16.0	15.4	18.2	16.2	17.1	20.3	19.0	18.4	21.9	20.1	17.9		18.7	
NTM P8691-23	Blast Site	L						20.7			22.8					
NTM P8694-2	Blast Site	R	18.2	15.7	19.4	17.5	17.9	21.2	20.0	18.8	23.4	21.1	18.0	23.5	18.8	14.4
NTM P8694-3	Blast Site	L	18.7		18.4			20.2			21.6	19.3				
NTM P8695-38	Blast Site	L	20.4	17.6	19.7	17.8	18.1	22.7	20.6	19.3	24.5	22.0	19.7	24.6	21.9	15.9
NTM P8695-38	Blast Site	R	19.6	16.2												16.2
NTM P8695-39	Blast Site	L			19.7		17.9	21.0	19.3		23.5		18.6	22.5		
NTM P8695-40	Blast Site	L									24.0	7.0	19.0	7.0	21.0	1.0
NTM P8695-41	Blast Site	L	20.2	17.0	19.2	17.5	18.9	21.4	20.0	19.8						
NTM P8695-42	Blast Site	L						21.6			24.0	22.0				
NTM P8695-43	Blast Site	R	18.3	16.0	19.4	17.3	17.9	22.0	20.0	19.0	23.6	21.2	18.4			
NTM P8695-44	Blast Site	R	18.7	15.3	19.8	17.0	17.9	22.1								
NTM P8695-45	Blast Site	R						21.2								
NTM P8695-46	Blast Site	R	19.2	17.0	20.9	18.5	18.6	22.2	21.3	19.8						
NTM P8695-61	Blast Site	R	17.6	15.7												
NTM P8695-63	Blast Site	L	18.6	15.7												
NTM P8695-64	Blast Site	R						22.9	20.6	18.3						
NTM P8695-65	Blast Site	L												21.3	19.3	15.6
NTM P8695-78	Blast Site	L											19.0	23.7	20.3	16.4
NTM P8697-1	Blast Site	L	17.5	15.3	20.0		18.3	21.8	20.3	20.1						
NTM P8697-1	Blast Site	R	17.6	15.0	19.5	17.8	19.4	21.2	20.4	20.1						
NTM P87108-1	Blast Site	L									23.8	23.0	21.0	22.8	21.8	17.5
NTM P87108-1	Blast Site	R											21.0	22.6	22.0	16.9
NTM P8792-19	Blast Site	L	15.1		19.0	19.0	19.1	21.4	19.9	19.1	23.0	21.6	19.0	22.3		
NTM P8792-19	Blast Site	R	18.8	15.3	19.2	18.3	18.6	21.6	20.1	19.3						
NTM P8792-20	Blast Site	R						20.7	18.9	18.1						

Table 2. Measurements (millimetres) of the upper cheek teeth of *Neohelos stirtoni* n. sp.

LOWER CHEEK TEETH OF *NEOHELOS STIRTONI* N. SP. (MM)

SPECIMEN	SITE	SIDE	P3 L	P3 W	M1 L	M1 AW	M1 PW	M2 L	M2 AW	M2 PW	M3 L	M3 AW	M3 PW	M4 L	M4 AW	M4 PW
CPC 22189	Blast Site	R			20.8	13.6	14.8	23.2								
CPC 22190	Blast Site	R	14.8	10.6	19.8	15.1	15.6	22.5	17.9		24.4		23.1	18.5	16.0	
CPC 22199	Blast Site	R						22.1		18.9	24.3	19.3	18.2	22.9	19.6	
CPC 22530	Blast Site	L	14.6	11.6	19.1	14.3	15.8	21.9	18.3	17.0	23.9	20.1	18.0			
CPC 22537	Blast Site	L	16.3	11.7	21.0	13.8	16.0	23.3	18.0	19.5						
CPC 22541	Blast Site	L										17.4				
CPC 22542	Blast Site	R									26.2	20.0	26.0	20.8		
CPC 22545	Blast Site	R	13.1		8.9			20.1			22.3		22.9			
CPC 22546	Blast Site	L			20.2			23.9			24.6			20.0		
CPC 22549	Blast Site	L									25.1	18.9	17.4	24.9	18.5	
CPC 22551	Blast Site	L	15.0	11.9	20.1	14.5	15.7	22.6	17.7	17.3	23.9	18.5	18.3	22.2	18.5	18.3
CPC 22555	Blast Site	L						22.4		18.0	23.8					
CPC 22556	Blast Site	R									22.0	16.7	16.1	22.0	17.1	15.9
CPC 34301	Blast Site	L	13.8		19.7	13.3	15.6	22.1	18.1	17.3	24.4	18.8	17.8			
CPC F34300	Blast Site	L	14.2	9.7	18.7	13.2	13.7	21.5	16.8	16.3	23.0	17.7	17.3			
NMV P179244	Horseshoe W	R	17.9	13.0												
NMV P179368	Blast Site	R	13.5	9.0	19.1	13.0	14.9									
NMV P179369	Horseshoe W	L			19.8	12.9	14.9	21.9	16.9							
NMV P179857	Top Quarry	L						21.8		17.8	24.4	19.9	18.6	25.0	20.3	
NMV P179862	Blast Site	L	11.5	10.7	17.3	13.3	14.6	19.1	17.2	16.3			25.0	18.3	17.1	
NMV P187289	Camp Quarry	R	13.0	9.3	17.4	12.5	14.0	19.6	16.0	15.9	22.4	18.1	17.6	22.7		
NMV P187290	Camp Quarry	L						17.9	20.0	18.1	26.6	21.7	20.7	28.0	21.3	19.8
NMV P194533	Top Quarry	R									24.5	17.0	17.0			
NMV P194535	Top Quarry	R			18.5	14.0	15.7									
NMV P194539	Camp Quarry	L								16.5	23.9	18.8	18.7			
NMV P194541	Blast Site	R						21.2	16.9	15.7						
NMV P194546	Horseshoe W	R									20.8	16.5	23.5		15.5	
NMV P194547	Horseshoe W	R											23.5	18.4		
NMV P194549	Horseshoe W	R			19.7	14.6	16.1	22.7	18.6	12.8	24.8	19.7	18.7			
NMV P194555	Horseshoe W	L									25.5	19.1	18.7			
NMV P194557	Horseshoe W	R									22.3	16.7	15.9			
NMV P194559	Top Quarry	L									23.9	18.2	16.6			
NMV P197893	Top Quarry	L			19.9	13.7	16.4	24.2	17.7	18.2						
NMV P198541	Camp Quarry	L											27.0	19.2	19.1	
NMV P198542	Blast Site	L			21.2	13.9	15.6	23.2	17.3	17.3	25.9	19.1	19.3			
NMV P201028	Top Quarry	L			19.8											
NMV P201029	Top Quarry	R											22.5	16.3	14.8	
NMV P201031	Top Quarry	L											23.3	17.8	14.9	
NMV P205131	Top Quarry	R						21.7	17.3	16.9	23.5	17.8	17.2	23.5	17.7	
NTM 8695-71	Blast Site	L			22.7	16.7	18.7			19.4	25.5	21.4	19.7			
NTM P8610-1	Blast Site	L			17.8	12.5	13.5	19.4	15.6	15.0	22.7	17.0	16.1	22.0		
NTM P8612-2	Blast Site	L	14.1	10.3												
NTM P8619-1	Blast Site	R						22.0		17.3	24.2	18.6	24.6		17.9	
NTM P862-5	Blast Site	R									23.0	17.9	22.3	17.2	16.5	
NTM P862-6	Blast Site	R						21.2	17.1	16.8	22.5	17.5	16.9	22.0	16.5	15.0
NTM P868-1	Blast Site	R											25.6	18.7	18.6	
NTM P8695-4	Blast Site	R	14.2	10.4	18.8	13.6	14.8				23.3	17.6	16.4	24.2	17.7	16.3
NTM P8695-67	Blast Site	R	14.6	10.5	19.5	13.4	14.7	22.4	17.6	16.5	24.6	18.8	17.9	22.0	18.4	17.4
NTM P8695-69	Blast Site	R	16.8	11.3	20.6	13.8	15.1	21.4	17.1	16.5						
NTM P8596-70	Blast Site	R										15.1	21.1	17.1		
NTM P8695-72	Blast Site	L			18.1	12.4	13.2	21.3	16.4	15.1	24.0	17.6	16.4	23.5	17.8	15.9
NTM P8695-73	Blast Site	L									24.3	19.1	18.2	25.1	18.9	18.2
NTM P8695-74	Blast Site	L	14.7	10.7	19.7	13.7	15.0									
NTM P8695-75	Blast Site	L	13.9													
NTM P8695-76	Blast Site	R	15.2	10.3												
NTM P87103-20	Blast Site	R						21.4	16.4	16.1	23.2	18.0	17.0	24.3		16.0
NTM P87110	Blast Site	R	14.9	10.4	20.3	14.5	15.9	22.0	18.0	17.0	23.7	19.0	17.3			
NTM P87113-11	Blast Site	L	15.0	10.3	18.2	13.3	14.7	20.2	16.5	16.0	22.7	17.9	16.8	22.0	17.5	16.0
NTM P87115-116	Blast Site	L	15.0	10.1	20.4	14.5	16.0	23.0	18.0	17.6	24.3	19.0	17.9	24.5	18.5	16.6
NTM P87115-7	Blast Site	R	14.5	10.4	20.0	14.0	16.4	23.3	18.0	17.8	25.6	20.1	19.7	25.4		17.1
NTM P8792-17	Blast Site	L			19.2		15.6	21.7			23.6	18.0	16.9	22.7	17.2	16.5
NTM P8792-18	Blast Site	L								15.7	24.3	17.8	17.4	25.2	17.5	17.4

Table 3. Measurements (millimetres) of lower cheek teeth of *Neohelos stirtoni* n. sp.

MEASUREMENTS IN MILLIMETRES	CPC 22200	NTM P8697-1	CPC 2252	CPC 22526	CPC 22192	CPC 22188	NTM P8551-13	NTM P8695-78	NTM P87108-1	NTM P8695-38
Width across masseteric processes	148	172	—	165	152	148	149	—	184	—
Width (minimum) between diastemal crests	17	20	—	26	21	—	25	—	—	24
Width of diastema between I^1 alveoli	23	27	—	30	22	—	24	—	—	29
Length diastema (ant. P^1 alveolus-post. I^1 alveolus)	66	65	—	72	60	67	61	—	—	84
Width of palate across posterolateral pal. for.	44	44	47	41	42	—	32	42	42	40
Length of basioccipital at midline	51	58	51	55	45	—	49	50	60	56
Length basicranium (pharyng. crest to for. magnum)	153	180	169	175	147	—	149	—	165	186
Width of glenoid fossa (entogl. pr. to lateral edge)	42	38	50	37	—	—	41	55	47	58
Length of glenoid fossa	28	22	—	27	22	—	21	22	23	23
Width between entoglenoid eminences	83	84	93	—	—	—	86	94	88	76
Length anterior palatal foramen	22	28	—	—	—	31	24	—	—	—
Width interpterygoid fossa	53	58	—	58	56	—	46	—	51	—
Length of palate (pharyngeal crest to P^1 alveolus)	176	181	—	—	170	—	166	—	—	207
Width (minimum) of rostrum at infraorbital foramen	49	62	—	46	—	47	53	—	—	—
Length of nasals	131	129	—	—	—	118	122	—	—	152
Width across postorbital constriction	76	68	61	53	—	—	58	62	54	48
Width cranium (maximum) across zygomatic arches	182	182	—	178	—	—	175	—	207	224
Width cranium across occiput (at lambdoid crests)	128	129	156	—	136	—	127	152	143	—
Dorsal length of temporal fossa	169	184	176	137	157	—	162	183	182	207
Ventral length of temporal fossa	101	108	122	—	114	—	91	120	106	122
Width of temporal fossa	45	—	—	54	—	—	42	—	41	—
Width posterior cranium across glenoid fossa	65	72	76	—	—	—	62	80	67	83
Width rostrum at narial aperture	55	65	—	—	—	61	59	—	—	76
Width narial aperture	47	51	—	—	—	53	48	—	—	66
Height narial aperture	36	42	—	—	—	—	41	—	—	55
Height rostrum (dorsal surface nasals to I^1 alveolus)	70	86	—	—	—	—	72	—	—	100
Cranial length (maximum) condyles to I^1 alveolus	358	394	—	—	—	—	338	—	—	436
Height (maximum) of zygomatic arch	41	—	—	—	—	—	39	60	56	—
Cranial height (basioccipital suture to sagittal crest)	85	—	88	—	—	—	90	—	113	—
Length of masseteric processes (orbital margin-tip)	51	73	—	63	59	62	61	76	65	81
Projection of masseteric processes below tooth row	09	15	—	06	11	19	12	—	16	—
Occipital height (dorsal edge for. mag.-lambdoid cr.)	78	—	—	—	—	—	56	—	93	—
Diameter of orbit	30	31	—	—	—	26	31	—	35	—
Cranial length (dorsal) tip nasals-lambdoid crest	325	355	—	373	—	300	—	—	—	386
Height foramen magnum	19	—	22	—	21	—	22	25	26	—
Width foramen magnum	32	44	36	—	31	—	34	40	35	52
Height occipital condyle	34	41	40	—	34	—	34	39	35	47
Width occipital condyle	10	18	21	—	17	—	15	19	19	20
Length of cheektooth row (P^3 to M^4)	108	107	—	108	102	—	103	—	—	110
Width of palate at hypoloph of M^2	47	46	58	50	45	47	44	—	54	48

Table 4. Cranial measurements of *Neohelos stirtoni* n. sp.

MEASUREMENTS IN MILLIMETRES	NTM P8695-74/P87103-1	NTM P8695-67	NTM P8695-72	NTM P8695-168	NTM P862-4	NTM P8695-71	NTM P8695-4	NTM P8619-1	NTM P87112-2
Length of diastema	37	48	—	43	—	38	46	—	59
Width of jaw behind M_3	26	28	24	27	28	33	26	27	28
Transverse width of condyle	42	44	—	—	—	40	—	—	—
Anteroposterior width of condyle	13	17	—	—	—	16	15	—	—
Length from mandibular canal-postalveolar pr.	25	33	29	31	35	16	29	43	33
Length from behind condyle to edge asc. ram.	70	—	—	—	—	75	85	—	88
Depth of horizontal ramus below M_3	43	61	46	50	47	51	48	56	56
Depth horizontal ramus below M_4	45	63	45	45	47	55	48	55	54
Depth horizontal ramus at P_3	17	28	—	20	—	26	18	—	25
Distance ant. root P_3 to mental foramen	01	04	—	05	—	03	04	—	00
Length rear of symphysis to digastric process	76	114	96	91	93	111	80	100	87
Distance behind P_3 to behind condyle	186	229	—	—	—	206	201	—	220
Distance P_3 to mandibular canal	135	161	136	142	136	153	137	161	155
Distance P_3 to postalveolar process	114	134	112	117	109	138	117	125	125
Length tooth row P_3-M_4	105	107	101	102	98	111	102	103	106
Length from dorsal I_1 alveolus-behind condyle	225	280	—	—	—	246	248	—	278
Length from dorsal I_1 alveolus-postalveolar proc.	155	186	—	157	—	180	162	—	186
Length from dorsal I_1 alveolus to behind M_4	147	159	—	144	—	153	151	—	167
Length of symphysis	70	—	—	—	—	—	73	—	95

Table 5. Measurements of dentaries of *Neohelos stirtoni* n. sp.

ELEMENT	MEASUREMENT	MILLIMETRES
Scapula (NTM P8695-273)	Length	300.0
	Width	153.0
	Length vertebral border	125.0
	Width supraseapular fossa	58.0
	Width infrascapular fossa	87.0
	Depth (maximum) seapular spine	51.5
	Width (maximum) acromion	42.0
	Dimensions glenoid cavity	45.0 x 60.0
Humerus (NTM P87108-38)	Estimated length	310.0-315.0
	Diameter above D-P tuberosity	40.0 x 45.0
	Dimensions head	55.0 x 55.0
	Dimensions coronoid fossa	30.0 x 39.0
	Dimensions radial fossa	20.0 x 20.0
	Width distal articulation	110.0
	Dimensions trochlea	27.0 x 40.0
	Dimensions capitulum	35.0 x 35.0
	Dimensions olecranon fossa	20.0 x 35.0
Ulna (NTM P87103-60)	Estimated length	270.0
	Length radial incisure	52.0
	Width coronoid incisure	39.2
	Length coronoid incisure	51.0
	Length olecranon process	47.0
	A-P width at coronoid process	82.5
	Distal A-P width of shaft	31.0
Innominate (NTM P8695-274)	Estimated length	400.0
	Dimensions acetabulum	67.0 x 73.0
	Diameter (maximum) obturator for.	94.0
	Width body of ilium	41.0
	Dimensions saeral articulation	50.0 x 115.0
	Length ischial tuberosity	88.0
Femur (NTM P8695-275)	Estimated length	320.0-325.0
	Dimensions head	65.0 x 65.0
	Width (middle) diaphysis	47.0
	Width medial condyle	37.0
	Depth medial condyle	47.2
	Width lateral condyle	47.0
	Depth lateral condyle	40.0
Tibia (NTM P8695-276)	Estimated length	260.0
	Dimensions tibial facet	18.0 x 35.0
	Dimensions astragalar facet	30.0 x 40.0
	A-P diameter shaft	32.6
	M-L width proximal end	89.0
	M-L width distal end	37.0
Epipubic bone (NTM P8695-277)	Length	125.0
	Proximal height	82.0
Sacrum (NTM P87108-39)	Length	82.5
	Width	120.0

Table 6. Measurements of postcranial elements of *Neohelos stirtoni* n. sp.

		CHARACTER	APOMORPHIC	PLESIOMORPHIC	PRIMITIVE
Incisors	1	UPPER I^1	divergent tips	convergent tips	convergent tips
	2	UPPER I^{2-3}	small, buttress I^1	large, independant of I^1	large
	3	INCISOR ARCADE	narrow, U-shape	broad, C-shape	broad
C	4	UPPER CANINE	absent	present-vestigial	present
P^3	5	P^3 PARASTYLE	broad, low, close to PMC	large, separated from PMC	rudimentary
	6	HYPOCONE	large (variable)	small (variable) to absent	absent
	7	PARAMETACONE	differentiated PAC, MEC	undifferentiated-incipient	undifferentiated
	8	PARAMETACRISTAE	buccal side of crown	nearer mid-line of crown	poorly developed
	9	BUCCAL CINGULUM	weak	strong	present
	10	LINK PRC-PMC	strong	weak-absent	absent
M^1	11	OCCLUSAL SHAPE	square	trapezoidal	rectangular
	12	LOPH SHAPE	straight	slight curve, oblique	curved
	13	STYLES	reduced	large	small
Molars	14	OCCLUSAL PLANE	convex	straight	straight
	15	TOOTH ROW SHAPE	convex	straight to slight curvature	straight
	16	ROW COVERGENCE	anterior	parallel	posterior
Cranium	17	ORBIT	frontated	lateral	lateral
	18	MASSETERIC PROCESS	long, wide	short, narrow	short, small
	19	ORBITAL PROCESS	narrow	wide	wide
	20	NASAL PROCESS	large	small-moderate	small
	21	UPPER DIASTEMA	short, constricted	long, wide to constricted	long, wide
	22	PALATE	deep, arched	shallow, flat	shallow, flat
	23	FRONTAL CRESTS	enlarged, vertical	moderately inflated	small
	24	POSTORBITAL PROCESS	absent	weak-absent	weak
	25	PMX-MX SUTURE	concave	straight, short	straight, long
	26	BASICRANIAL AXIS	marked flexion	slight flexion	straight
	27	ALISPH. TYMP. PROC.	complete, fused to mastoid	incomplete, elongated	incomplete, short
	28	POSTGLENOID PROC.	high, wide, thick, straight	high, wide, thick, oblique	low, narrow, thin
	29	EPITYMPANIC FENES.	absent	reduced, oval	large, circular
Dentary	30	ASCENDING RAMUS	elevated, upright	inclined, elevated	inclined, low
	31	DIGASTRIC EMINENCE	strong, posterior	low, mid-ramus position	weak
	32	MEDIAL FOSSAE	separated	confluent	confluent
	33	LOWER INCISOR	recumbent, pointed	procumbent, spatulate	procumbent
	34	SYMPHYSIS	long deep, fused	short, shallow, unfused	short, shallow
	35	MASSETERIC FOR.	absent	present	present
Other	36	VERT. BORD. SCAPULA	pointed, rugose	broad, thin	——
	37	INFRAGL. PR. SCAPULA	large	weak-absent	——
	38	OLECRANON PR. ULNA	wide, flange-like	narrow	——
	39	ALAE ILIUM	broad, short	narrow, long	——
	40	DELTOPECTORAL TUB.	differentiated	undifferentiated	——

Table 7. Character state polarities in the Zygomaturinae as determined by a diprotodontine outgroup (*Ngapakaldia tedfordi*) and ingroup comparisons based on primitive zygomaturines from Riversleigh and Alcoota.

CHARACTER		*Maokapia*	*Hulitherium*	*'Kolopsis' rotundus*	*Zygomaturus spp.*	*Kolopsis spp.*	*Beaumaris 'Kolopsis'*	*Neohelos spp.*	*Nimbadon spp.*	*Kolopsoides*	*Plaisoidon*	*Alkwertatherium*	*Riversleigh zygomaturine*	*Raemeotherium*
INCISORS	1	A	—	—	A	P	—	P	—	P	P	P	P	—
	2	A	—	—	A	P	—	P	—	—	P	P	P	—
	3	A	A	—	A	P	—	P	—	—	P	P	P	—
CANINE	4	A	A	A	A	A	—	AP	?	—	A	A	P	—
P^3	5	A	?	A	A	AP	—	P	P	A	P	P	P	—
	6	A	?	A	A	A	—	AP	P	A	P	PV	PV	—
	7	A	A	A	A	A	—	P	P	A	P	P	PV	—
	8	A	A	A	A	A	—	P	P	P	P	P	P	—
	9	A	A	A	A	A	—	P	P	A(H)	A	P	P	—
	10	A	?	A	A	A	—	AP	P	P	A	PV	PV	—
M^1	11	A	A	—	A	P	—	P	P	P	P	P	P	—
	12	A	A	—	A	P	—	P	P	P	P	P	P	—
	13	A	A	—	A	P	—	P	P	PV	PV	PV	PV	—
MOLAR ROW	14	A	A	A	A	P	—	P	P	P	P	P	P	—
	15	A	?	?	A	AP	—	AP	P	P	P	P	P	—
	16	A	A	?	A	P	—	P	P	P	P	P	PV	—
CRANIUM	17	A	A	?	A	P	—	P	—	—	P	P	P	—
	18	A	A	?	A	P	—	P	—	—	A(H)	P	P	—
	19	A	A	?	A	P	—	P	—	—	P	P	P	—
	20	A	A	?	A	P	—	P	—	—	P	P	P	—
	21	A	A	?	A	P	—	P	—	—	P	P	P	—
	22	A	A	?	A	P	—	P	P	—	P	P	P	—
	23	A	A	—	A	P	—	P	—	—	P	P	P	—
	24	A	—	—	A	P	—	AP	—	—	P	—	P	—
	25	A	—	—	A	P	—	P	—	—	P	P	PV	—
	26	A	—	—	A	P	—	P	—	—	A(H)	—	P	—
	27	—	—	—	A	AP	P	P	—	—	P	P	P	—
	28	—	—	—	A	A	P	P	—	—	P	P	PV	—
	29	—	—	—	A	A	P	P	—	—	P	P	PV	—
DENTARY	30	A	—	A	A	P	—	P	—	P	P	P	—	P
	31	A	—	A	A	P	P	P	—	P	P	P	—	P
	32	A	—	A	A	P	P	P	—	P	P	P	—	P
	33	A	—	A	A	P	—	P	—	P	P	P	—	P
	34	A	—	A	A	AP	P	P	—	A(H)	A(H)	A(H)	—	P
	35	A	—	—	A	A	P	P	—	A(H)	P	A	—	P
POSTCRANIAL	36	—	—	—	A	A	—	P	—	—	P	—	—	—
	37	—	—	—	A	A	—	P	—	—	A(H)	—	—	—
	38	—	—	—	A	A	—	P	—	—	A(H)	—	—	—
	39	A	—	—	A	A	—	P	—	—	P	—	—	—
	40	—	?	—	A	P	—	P	—	—	A(H)	—	—	—

Table 8. Distribution of character states in representative zygomaturine taxa; key: A=apomorphic; P=plesiomorphic; PV=primitive; AP=morphocline within genus ranges from plesiomorphic to apomorphic; (H)=homoplaisious characters, possible synapomorphies of *Plaisiodon* and *Kolopsoides*.

APPENDIX

Key to abbreviations

AC	Anterior cingulum
AG	Anterior groove I^2
ALC	Anterolingual cingulum
BC	Buccal cingulum
BCP	Buccal crest of parastyle of P^3
DEN	Dentine exposure
DEJ	Dentine-enamel junction
dP3	Deciduous third premolar
ENA	Enamel surface
FOS	Fossa and basin on posterior loph surfaces and median valley
HY	Hypocone, posterolingual cusp on upper cheekteeth
[HY]	Hypocone damaged or missing due to breakage or wear
[hy]	Approximate position of congenitally missing hypocone
I	Incisor
IGR, VG	Longitudinal groove on ventrolateral edge of lower incisor
LBA	Lingual basin on P^3
LC	Lingual cingulum
LCP	Lingual crest on parastyle of P^3
LS	Longitudinal sulcus in posterior basin of P^3
M	Molar
ME	Metacone, posterolabial cusp on upper cheek teeth
ML	Metaloph, posterior transverse crest on upper molar
MS	Mesostyle, labial cuspule on P^3
MT	Metastyle, posterolabial cuspule on upper molars
MV	Median valley or transverse sulcus between molar lophs
OR	Open-rooted termination of upper central incisors (I^1)
P3	Permanent upper premolar
PA	Paracone, anterolabial cusp on upper cheek teeth
PBA	Posterior basin of P^3
PC	Postcingulum or posterior cingulum of upper cheek teeth
PES	Posterior enamel salient on I^2
PG	Posterior groove on I^2
PMC	Parametaconc, large pyramidal labial cusp of P^3
PMCR	Post(Para-)metacrista, posteriorcrest of parametacone
PR	Protocone, anterolingual cusp of upper cheek teeth
PRD	Protoconid, large cusp on P3; anterolabial cusp of lower molar
PPC	Postparacrista, a crest behind the paracone
PPF	Postprotoconal fossa or basin, a basin behind the protocone
PS	Parastyle, anterolabial cuspule on upper cheek teeth
TCR	Transverse crest or link, crest between PMC and PR
TRS	Transverse sulcus, groove between parastyle and parametacone
VG, IGR	Ventral longitudinal groove on I^1

Cranial structures:

AIF, IOF2	Auxiliary infraorbital foramen
AL	Alisphenoid bone
ALN	Alveolar nerve foramen
ALS	Alveolar shelf or suborbital shelf
APF	Anterior palatal fenestra or incisive foramen
CAL	Canine tooth alveolus
COF	Condylar foramen, hypoglossal canal
DPA+PAN	Foramen for descending palatal artery and palatine nerves
ECC	Entocarotid canal, foramen for internal carotid artery
EGE	Entoglenoid eminence, swelling or bulla medial to glenoid fossa
ETF	Epitympanic fenestra, opening into epitympanic sinuses
FCO	Fenestra cochlearis, ventral cochlear opening in petrosal
FMC	Fossa for middle concha within external nares
FOV	Foramen ovale, transmits mandibular branch of trigeminal nerve
FR	Frontal bone
FRC	Frontal crest .
FRO	Foramen rotundum, transmits maxillary branch of trigeminal nerve
FRS	Frontal suture
FVE	Vestibular fenestra, dorsal vestibular opening in petrosal
GF	Glenoid fossa, articular surfaces for the dentary condyle
IIF	Interincisive fossa
INC	Inferior nasal crest
IOA+LAN	Groove for great infraorbital artery and lacrimal nerve
IOC	Infraorbital canal
IOF	Infraorbital foramen
ITC	Infratemporal crest
JMS	Jugal-maxillary suture
JUG	Jugal
LAC	Lacrimal bone
LAT	Lacrimal tuberosity
MAP	Maxillary portion of masseteric or zygomatic process
MAS	Mastoid bone
MAX	Maxillary bone
MEN	Margin of external nares
MNS	Median ventral sulcus of narial aperture
MOF	Median occipital foramen
MPP	Median premaxillary process or eminence
NAP	Aperture of the external nares
NAS	Nasal bone
NPP	Nasal articular surface of premaxilla
NPS	Nasopremaxillary suture
ORB	Orbit
PAL	Palatine bone
PAR	Parietal bone
PGP	Postglenoid process
PGT	Pterygoid bone
PHC	Pharyngeal crest of palatine bone

PMP Paroccipital-mastoidprocess
PMS Premaxillomaxillary suture
PPP Premaxillary process of palate
Rcl Fossa for rectus capitus lateralis muscle
Rcpma Fossa for rectus capitus major muscle
Rcpmi Fossa for rectus capitus minor muscle
SAC Sagittal crest
SAS Squamosal-alisphenoid suture
SFN Emissary foramina in supraoccipital
SOC Median crest of supraoccipital
SOF Sphenorbital foramen (optic nerve+ophthalmic artery)
SOT Suborbital tuberosity
SPF Sphenopalatine foramen
SSP Septal process of premaxilla
SQS Squamosal suture
SQ Squamosal bone
SZN Subzygomatic notch
VII Facial nerve groove, foramen or stylomastoid foramen

Neurocranium and endocasts:

α–α' Rostral-most sulcps separating prefrontal from parietofrontal lobes
β Sulcus separating parietofrontal and temporal lobes
μ Sulcus separating occipital lobefromtemporal lobe
δ Short sulcus in temporal lobe
ν' Sulcus separating parietofrontal lobe from occipital lobe
CH Cerebellar hemisphere
ECA Endocranial cavity
ETS Epitympanic sinus
FMA Foramen magnum
HYC Hypoglossal canal
IAM Internal auditory meatus (acoustic+facial nerves)
IB Interbrachial sulcus
IN Inner table or internal capsule of braincase
J Jugular sulcus
L Labial sulcus
LSS Lateral sinus of squamosal bone
OA-ON Opthalmic artery+optic nerve
OPC Optic pole of cerebrum
OUT Outer table of neurocranium
PFL Paraflocculus
PSM Parietal septum
RF Rhinal fissure
SMV Superficial middle cerebral vein
SS+TS Confluence of sagittal and transverse sinuses
SSI Squamosal sinus in the zygomatic root
SSU Squamosal sulcus
TPC Temporal pole of cerebrum
TS Transverse sinus
V Vermis of cerebellum

Basicranium and ear region:

ACR Attachment of anterior crus of ectotympanic bone
AEM Articular eminence of glenoid fossa
ATP Alisphenoid tympanic process
ATT Attic of tegmen tympani
BTP Basioccipital tympanic process or wing
CAG Groove for carotid artery
COF Condylar foramen
CTY Crista tympanica
ECT Ectotympanic
EGE Entoglenoid eminence
ENC Canal for internal carotid artery
ETF Epitympanic fenestra
ETS Epitympanic sinus
FLF Floccular fossa of periotic bone
FCO Fenestra cochlearlis
FOV Foramen ovale
FOV+EUS Mandibular nerve+eustacian tube
FVE Fenestra vestibularis
GF Glenoid fossa
HTS Hypotympanic sinus
ICF Incudal fossa
IJF Internal jugular foramen (posterior lacerate foramen)
ITY Incisura tympanica
MAS Mastoid bone
PCP Paroccipital-mastoid proces,s
PCR Attachment for posterior crus of ectotympanic bone
PET Petrosal
PGP Postglenoid process
PLF Posterior lacerate foramen
POC Paroccipital bone
PSI Petrosal sinus
PTF Pterygoid fossa
PYF Pyriform fenestra (middle lacerate foramen)
SAS Squamosal-alisphenoid suture
SIS Sigmoid sinus
STF Stapedial fossa
SUF Supratympanic fossa orrecess
TCA Tympanic cavity
VII Facial nerve foramina, grooves or stylomastoid foramen

Dentary:

ANG Angular process
DIC Diastemal crest
DIF Digastric fossa
DIP Digastric process
FOP Fovea pterygoidea
GEP Genial pit
ICS Intercoronoid sulcus
MAF Masseteric foramen
MEF Mental foramen
MFO Masseteric fossa
MNF Mandibularforamen
MNO Mandibular or coronoid notch
NCO Condylar neck
PDS Postdigastric sulcus
PME Postmasseteric eminence
PMF Posteriormental lornmen
PTF Pterygoid fossa
SLF Sublingual fossa
SMC Submasseteric crest
SYM Symphysis
TRT Transverse torus

Postcranial Structures:

ACP	Acromion process
ADS	Adductor muscle scar
AIL	Alaof ilium
APX	Apex of sacrum
ASF	Astragalar facet
ASP	Articular surfacc pecten pubis
BAS	Basis sacrum
CAB	Caudal border scapula
CAH	Humeral head
CAN	Anterior crest
CAP	Capitulum humerus
CFE	Femoral head
COF	Coronoid fossa
COP	Coracoid process
CPI	Conical process of inner condyle
CRB	Cranial bordcr scapula
CRI	Interosseous crest
CSU	Sipinator crest
DTP	Deltopcctoral tuberosity
ECB	Entepicondylar bridgc
ENF	Entepicondylar foramen
EPI	Epiphyseal line
FIF	Fibular facet
FIS	Infrascapular fossa
FSS	Suprascapular fossa
GLF	Glenoid fossa (scapula)
GRS	Groove bctwcen rotular surface and ectepicondyle
GRT	Greater trochanter
ICE	Intercondylar eminence
ICO	Intercondylar notch
IFT	Iliofemoral tuberosity
INS	Incisura scapulae
IPE	Iliopectineal eminence
IRA	Radial incisure
ITU	Ischial tubcrosity
LCO	Lateral condyle
LEC	Lateral epicondyle
LIT	Lateral intercondylar tubercle
LPO	Popliteal line
LTR	Lesser trochantcr
MCO	Medial condyle
MEC	Medial epicondyle
MIT	Medial intercondylar tubercle
MSC	Median sacral spine
OBC	Obturator crest
OBF	Obturator foramen
OLF	Olecranon fossa
OLP	Olecranon proccss
OTR	Origin triceps muscle
PCO	Coronoid process ulna
PEC	Pectcn
PER	Pectoral ridge
PRT	Pit (radial tuberosity) brachialis muscle scar
RAF	Radial fossa
RPS	Ridgc popliteal surface femur
RSU	Rotular surface femur
SAF	Sacral foramen
SAP	Superior articular process sacrum
SAR	Articular process for sacrum
SAT	Sacral tuberosity
SCA	Sacral canal
SFT	Shaft of epipubic bone
SLI	Semilunar notch ulna
STP	Styloid process
SSP	Scapular spine
SUS	Subscapular fossa
TEC	Teres muscle crest (humerus)
TMA	Major tubcrosity humerus
TMI	Minor tuberosity humerus
TRF	Trochanteric fossa
TTU	Tibial tuberosity
VEB	Vertebral border scapula

Museum and university collection prefixes:

CPC	Commonwealth Palaeontological Collection, Bureau of Mineral Resources, Canberra
NMV	Museum of Victoria (formerly National Museum of Victoria)
NTM	Northern Territory Museum (Museums and Art Galleries of the N.T.)

REFERENCES

Anderson, J., Hall-Martin, A. & Russell, D. 1985, 'Long-bone circumference and weight in mammals, birds and dinosaurs', *Journal of Zoology London (A)*, vol. 207, pp. 53–61.

Archer, M. 1977, 'Origins and subfamilial relationships of Diprotodon (Diprotodontidae, Marsupialia)', *Memoirs of the Queensland Museum*, vol. 18, pp. 37–39.

Archer, M. 1984, 'The Australian Marsupial radiation', in *Vertebrate zoogeography and evolution in Australasia*, eds M. Archer & G. Clayton, Hesperian Press, Carlisle, WA, pp. 633–808.

Archer, M. & Bartholomai, A., 1978, 'Tertiary mammals of Australia: a synoptic review', *Alcheringa*, vol. 2, pp. 1–19.

Archer, M., Hand S. J. & Godthelp, H. 1991, *Riversleigh. The story of animals in ancient rainforests of inland Australia*, Reed Books Pty Ltd, Sydney, 264 pp.

Black, K. 1997, 'Diversity and biostratigraphy of the Diprotodontoidea of Riversleigh, northwestern Queensland', *Memoirs of the Queensland Museum*, vol. 41, no. 2, pp. 187–92.

Flannery, T. 1992, 'New Pleistocene marsupials (Macropodidae, Diprotodontidae) from subalpine habitats in Irian Jaya, Indonesia', *Alcheringa*, vol. 16, pp. 321–31.

Flannery, T. & Plane, M. 1986, 'A new Late Pleistocene diprotodontid (Marsupialia) from Pureni, Southern Highlands Province, Papua New Guinea', *BMR Journal of Australian Geology and Geophysics*, vol. 10 no. 1, pp. 65–76.

Gill, T. 1872, 'Arrangement of the families of mammals with analytical tables', *Smithsonian Miscellaneous Collection*, no. 11.

Haight, J. & Murray, P. 1981, 'The cranial endocast of the Early Miocene marsupial, *Wynyardia bassiana*: an assessment of taxonomic relationships based upon comparisons with recent forms', *Brain, Behavior and Evolution*, no. 19, pp. 17–36.

Hand, S., Archer, M., Rich, T. & Pledge, N. 1993, '*Ninbadon*, a new genus and three species of Tertiary zygomaturines (Marsupialia, Diprotodontidae) from northern Australia, with a reassessment of *Neohelos*', *Memoirs of the Queensland Museum*, vol. 33 no. 1, pp. 193–210.

Illiger, C. 1811, *Prodromus systematis mamulian et aviun additus terminus zoographicis utriudque classis*, C. Salfield, Berlin.

Luckett, W. P. 1993, 'An ontogenetic assessment of dental homologies in therian mammals', in *Mammal phylogeny: Mesozoic differentiation, multituberculates, monotremes, early eutheriaus, and marsupials*, eds F. S. Szalay, M. J. Novacek, & M. C. McKenna, Springer-Verlag, New York, pp. 182–204.

Marshall, C. R., Raff, E. C. & Raff, R. A. 1994, 'Dollo's law and the death and resurrection of genes', *Proceedings of the National Academy of Science*, U.S.A., no. 91, pp. 12283–87.

Murray, P. 1986, '*Propalorchestes novaculacephalus* gen. et sp. nov., a new palorchestid (Diprotodontoidea: Marsupialia) from the middle Miocene Camfield Beds, Northern Territory', *The Beagle, Occasional Papers of the Northern Territory Museum of Arts and Sciences*, vol. 3 no. 1, pp. 195–211.

Murray, P. 1990a, '*Alkwertatherium webbi*, a new zygomaturine genus and species from the late Miocene Alcoota Local Fauna, Northern Territory (Marsupialia: Diprotodontidae)', *The Beagle, Records of the Northern Territory Museum of Arts and Sciences*, vol. 7 no. 2, pp. 53–80.

Murray, P. 1990b, 'Primitive marsupial tapirs (*Propalorchestes novaculacephalus* Murray and *P. ponticulus* sp. nov.) from the mid-Miocene of northern Australia', *The Beagle, Records of the Northern Territory Museum of Arts and Sciences*, vol. 7 no. 2, pp. 39–52.

Murray, P. 1992, 'The smallest New Guinea zygomaturines—derived dwarfs or relict plesiomorphs?', *The Beagle, Records of the Northern Territory Museum of Arts and Sciences*, vol. 9 no. 1, pp. 89–110.

Murray, P. & Megirian, D. 1992, 'Continuity and contrast in middle and late Miocene vertebrate communities from the Northern Territory', *The Beagle, Records of the Northern Territory Museum of Arts and Sciences*, vol. 9 no. 1, pp. 195–218.

Murray, P., Megirian, D. & Wells, R. 1993, '*Kolopsis yperus* sp. nov. (Zygomaturinae, Marsupialia) from the Ongeva Local Fauna: new evidence for the age of the Alcoota Fossil Beds of Central Australia', *The Beagle, Records of the Northern Territory Museum of Arts and Sciences*, vol. 10 no. 1, pp. 155–72.

Owen, R. 1859, 'On some outline drawings and photographs of the skull of *Zygomaturus trilobus*, Macleay (Nototherium, Owen?)', *Quarterly Journal of the Geological Society of London*, no. 15, pp. 168–76.

Owen, R. 1866, *On the anatomy of Vertebrates. 11, Birds and Mammals*, Erxleben, London.

Plane, M. 1967, 'Two new diprotodontids from the Pliocene Otibanda Formation, New Guinea', in *Tertiary Diprotodontidae from Australia and New Guinea*, eds R. Stirton, M. Woodburne, & M. Plane, *Bureau of Mineral Resources, Geology and Geophysics, Australia, Bulletin*, no. 85, pp. 107–228.

Plane, M. & Gatehouse, C. 1968, 'A new vertebrate fauna from the Tertiary of Northern Australia', *Australian Journal of Science*, no. 30, pp. 272–3.

Randal, M. A. & Brown, M. C. 1967, 'The geology of the northern part of the Wiso Basin', *Bureau of Mineral Resources, Geology and Geophysics, Australia, Record* 1967/110.

Rich, T. H. 1976, 'Recent fossil discoveries in Victoria. Five Late Cenozoic fossil Marsupial sites in Victoria: a progress report', *The Victorian Naturalist*, vol. 93 no. 5, pp. 198–206.

Rich, T., Archer, M., & Tedford, R. 1978, '*Raemeotherium yatkolai* gen. et sp. nov., a primitive diprotodontid from the medial Miocene of South Australia', *Memoirs of the National Museum of Victoria*, no. 39, pp. 85–91.

Stirton, R. 1967a, 'A diprotodontid from the Miocene Kutjamarpu Fauna, South Australia', in *Tertiary Diprotodontidae from Australia and New Guinea*, eds R. Stirton, M. Woodburne, & M. Plane, *Bureau of Mineral Resources, Geology and Geophysics, Australia, Bulletin*, no. 85, pp. 45–51.

Stirton, R. A. 1967b, 'The Diprotodontidae from the Ngapakali Fauna, South Australia', in *Tertiary Diprotodontidae from Australia and New Guinea*, eds R. A. Stirton, M. O. Woodburne, & M. Plane, *Bureau of Mineral Resources, Geology and Geophysics, Australia, Bulletin*, no. 85, pp. 129–50.

Stirton, R., Woodburne, M. & Plane, M. 1967, 'A phylogeny of the Tertiary Diprotodontidae and its significance in correlation', in *Tertiary Diprotodontidae from Australia and New Guinea*, eds R. Stirton, M. Woodburne, & M. Plane, *Bureau of Mineral Resources, Geology and Geophysics, Australia, Bulletin*, no. 85, pp. 151–60.

Woodburne, M. 1967, 'Three new diprotodontids from the Tertiary of the Northern Territory, Australia', in *Tertiary Diprotodontidae from Australia and New Guinea*, eds R. Stirton, M. Woodburne, & M. Plane, *Bureau of Mineral Resources, Geology and Geophysics, Australia, Bulletin*, no. 85, pp. 55–103.

Woodburne, M. 1969, 'A lower mandible of *Zygomaturus gilli* from the Sandringham Sands, Beaumaris, Victoria, Australia', *Memoirs of the National Museum of Victoria*, no. 29, pp. 29–39.